POST-FIRE ASSESSMENT OF UNBONDED POST-TENSIONED CONCRETE SLABS: STRAND DETERIORATION AND PRESTRESS LOSS

by

Kevin J.N. MacLean

A thesis submitted to the Department of Civil Engineering

in conformity with the requirements for

the degree of Master of Science in Engineering

Queen's University

Kingston, Ontario, Canada

December 2007

Dedicated to

Natalie

for putting up with me

ABSTRACT

Unbonded post-tensioned concrete slabs have been widely used in Canada and the United States since the 1960s, as they allow increased span-to-depth ratios and excellent control of deflections compared to non-prestressed reinforced concrete flexural members. The satisfactory fire performance of unbonded post-tensioned concrete slabs in North America was established by a series of standard fire tests performed in the United States during the 1960s. However, there is a paucity of data on the effect of elevated temperatures on cold-drawn prestressing steel, both in terms of post-fire residual mechanical properties and high-temperature stress relaxation, which can lead to significant prestress loss both during and after a fire.

A detailed and comprehensive literature review is presented that provides background on the residual mechanical properties of prestressing steel, as well as on the creep-relaxation behaviour experienced at elevated temperatures under stress. The results of two test series are discussed; the first examining the effects of elevated temperatures on the residual mechanical properties of prestressing steel exposed to elevated temperatures. The second test series examines the irrecoverable and significant loss of prestress force that results from steel relaxation and other thermal effects experienced during heating. A preliminary analytical model is presented, capable of predicting the change in prestress force experienced by a stressed strand under transient heating. The model is then compared with experimental elevated temperature relaxation data.

Finally, the analytical model developed and residual mechanical properties obtained through experimentation are used along with a pre-existing finite difference heat transfer model (developed for concrete slabs) to examine the effect of elevated

temperature exposure on the residual flexural capacity of a typical unbonded post-tensioned example slab. Several parameters, such as heated length and concrete cover, are examined using the example structure. From this it was observed that, after one hour of exposure to a standard fire (ASTM E119), significant losses in effective prestress and moment capacity occurred even with the appropriate amount of concrete cover. This is a finding which is of the utmost practical importance to engineers engaged in the evaluation of fire damaged unbonded post-tensioned structures.

ACKNOWLEDGMENTS

My time at Queen's afforded me the great pleasure of meeting unique and interesting colleagues, faculty, and staff, as well as forming close friendships with a great number of extraordinary people. To these individuals a great deal of thanks is owed.

Specifically, I would like to express my sincere gratitude to my supervisor Dr. Colin MacDougall for allowing me the freedom to pursue a collaborative and interesting project which combined areas of unique expertise within the Department of Civil Engineering. To that end, many thanks are extended to my co-supervisor Dr. Luke Bisby, whose intense sense of curiosity and knowledge of all things fire kept me motivated during this work. Further appreciation is due my supervisors for their patience with the preparation of this document, and their support with my decision to begin full-time employment prior to its completion.

Special thanks are extended to Dr. T. Ivan Campbell for his financial support of this work, as well as affording me the distinct pleasure of being one of his teaching assistants.

I would also like to thank the laboratory technicians, administrative staff, and fellow graduate students, including: Neil Porter, Dave Tryon, Paul Thrasher, Jaime Escobar, Lloyd Rhymer, Stan Prunster, Fiona Froats, Maxine Wilson, Cathy Wagar, Michael Ranger, Yazan Qasrawi, Sarah Foster, Sarah Howard, Ershad Chowdhury, and Alex Caspary.

For their technical expertise and equipment support I would like to express my gratitude to Charlie Cooney and the staff in the Department of Mechanical and Materials

Engineering materials laboratory, and to the staff and faculty in the Department of Civil Engineering at the Royal Military College of Canada.

To Natalie, Perry, Josh, Millman, Jordan, Brad, Travis, Neal, and my fellow staff members at Clark Hall, thank you keeping my spirits high for the better part of six years at Queen's.

Finally, the financial support provided by Natural Sciences and Engineering Research Council of Canada, and the Department of Civil Engineering at Queen's University, were greatly appreciated.

TABLE OF CONTENTS

LIST OF TABLES

LIST OF FIGURES

NOTATION

A	=	Arrhenius equation rate coefficient (function of stress) also shown as $A(\sigma)$
A_s	=	Area of bonded non-prestressed tension reinforcement
A_{ps}	=	Area of unbonded prestressed reinforcement
A'_s	=	Area of bonded non-prestressed compression reinforcement
b	=	Width of concrete compression face
b_c	=	Tendon depth as measured from slab soffit, depth of concrete cover
b_w	=	Width of beam web
c	=	Depth of neutral axis at nominal strength
cv	=	Coefficient of variation
c_y	=	Neutral axis depth assuming ($f_{pr} = f_{py}$)
d_{elem}	=	Depth of constant temperature tendon element from slab soffit
d_s	=	Depth of non-prestressed reinforcement from extreme compression fibre
d'_s	=	Depth of non-prestressed compression reinforcement from extreme compression fibre
d_p	=	Depth of prestressed reinforcement from extreme compression fibre
E	=	Elastic Modulus
E_T	=	Residual elastic modulus
$E_{20℃}$	=	Elastic Modulus; no exposure to elevated temperatures
f	=	Tensile stress
f'_c	=	Concrete cylinder compressive strength
f_{pe}	=	Effective stress in prestressed reinforcement (after all losses)
$f_{pe,T}$	=	Residual effective stress in prestressed reinforcement

$f_{pe,20°C}$ = Effective stress in prestressed reinforcement; no exposure to elevated temperatures

f_{pr} = Stress in prestressed reinforcement at nominal strength

$f_{pr,T}$ = Residual stress in prestressed reinforcement at nominal strength

$f_{pr,20℃}$ = Stress in prestressed reinforcement at nominal strength; no exposure to elevated temperatures

f_{pu} = Ultimate tensile strength of prestressed reinforcement

$f_{pu,T}$ = Residual ultimate tensile strength of prestressed reinforcement

$f_{pu,20℃}$ = Ultimate tensile strength of prestressed reinforcement; no exposure to elevated temperatures

f_{py} = 0.2% offset yield strength of prestressed reinforcement

$f_{y,T}$ = Residual 0.2% offset yield strength of prestressed reinforcement

$f_{y,20℃}$ = 0.2% offset yield strength of prestressed reinforcement; no exposure to elevated temperatures

f_s = Stress in bonded non-prestressed tension reinforcement

f'_s = Stress in bonded non-prestressed compression reinforcement

$f_u(T)$ = Ratio of residual ultimate tensile strength to unheated ultimate tensile strength ($= f_{pu,T} / f_{pu,20℃}$)

h_f = Thickness of beam flange, for slabs equal to t

k = Ratio between the minimum and maximum value of the material property (Hertz Equation)

l = Total tendon length (taken to be the length of floor plate in the direction of analysis) or specimen length

l_e = Effective tendon length

l_{elem} = Length of constant temperature tendon element

l_h = Heated length, taken to be summation of heated bay lengths

M_r = Factored moment of resistance

$M_{r,T}$ = Residual factored moment of resistance

$M_{r,20℃}$ = Factored moment of resistance; no exposure to elevated temperatures

n = Number of typical interior spans (bays)

n_{hl} = Heated length ratio (= l_h / l)

R = Universal gas constant

R^2 = Square of residuals; statistical measure of a function's fit to discrete data

s = Standard deviation

s_1 = Standard deviation of residual properties; heated without stress

s_2 = Standard deviation of residual properties; heated with stress

T = Temperature in degrees Celsius or absolute temperature in Kelvin

T_{crit} = Critical value below which no outliers existing for a given α in a T-test

T_1 = Fitting constant in Hertz Equation or ASTM E178-01 T-test parameter (= $|\bar{x}_2 - x_{min}| s_2^{-1}$)

T_2 = Fitting constant in Hertz Equation

T_8 = Fitting constant in Hertz Equation

T_{64} = Fitting constant in Hertz Equation

t = Elapsed time or slab thickness

x = Longitudinal distance from a supporting column to tendon location

$\bar{x}$ = Statistical mean

x_{min} = Minimum data value (residual mechanical properties)

$\bar{x}_1$ = Statistical mean of residual properties; heated without stress

$\bar{x}_2$ = Statistical mean of residual properties; heated with stress

Z = Zener-Hollomon parameter, slope of secondary creep phase (= ε / θ)

α = Significance level in analysis of variance or T-test

β_1 = Ratio of depth of equivalent rectangular stress block to depth of neutral axis

ΔH = Activation energy for creep

Δf_{pr} = Increase in tendon stress created by member deflection

Δl = Change in length, l (specifically due to thermal expansion)

ε = Strain

$\dot{\varepsilon}$ = Creep rate

ε_{cr} = Creep strain also shown as $\varepsilon_{cr}(\sigma, T, t)$

$\varepsilon_{cr,\,0}$ = Dimensionless creep parameter (see Figure 2.12)

ε_{exp} = Experimental uncertainty

ε_T = Strain due to thermal expansion (=Δl / l)

ε_u = Strain at Rupture

ε_t = Residual strain at rupture

ε_{tot} = Total strain

$\varepsilon_{20\,°C}$ = Strain at Rupture; no exposure to elevated temperatures

ε_σ = Strain due to applied prestress and gravity load

ϕ_c = Material reduction factor for concrete (= 0.6)

ϕ_p = Material reduction factor for prestressed reinforcement (=0.9)

ϕ_s = Material reduction factor non-prestressed reinforcement (=0.85)

η = Tensile viscosity of Newtonian fluid

σ = Stress

θ = Temperature compensated time

ρ_p = Prestressed area reinforcement ratio (= A_{ps} / bd_s)

CHAPTER 1 – Introduction

1.0 General

Concrete has a compressive strength which is many times higher than its tensile strength. Where concrete members are utilized in compression, such as columns, this shortcoming is of little concern. However, when concrete is used in the construction of flexural members, such as beams and slabs, tensile stresses are created at the extreme fibre opposite the applied loading. To combat concrete's weakness in tension, steel reinforcement is used to carry tensile forces.

Under working load, concrete on the tension side of a reinforced concrete beam is typically cracked as it is unable to carry significant tensile stresses and cannot conform to the longitudinal strain in the steel reinforcement. In addition, the flexural rigidity and resulting service deflections of floors are controlled by the depth of members. It is thus difficult to achieve large span-to-depth ratios with conventional reinforced concrete.

Prestressing of concrete is a popular technique used to increase the efficiency of concrete members subject to flexure. It involves the application of an initial compressive stress to a concrete member which offsets tensile stresses created under service loading.

1.1 Evolution of Prestressed Concrete

The idea of inducing compressive stress on concrete members to overcome their shortcomings when subject to flexure had been known for some time. However, it was not until the pioneering work of French engineer Eugene Freyssinet in the late 1920s that prestressing became a viable construction technology (Lin and Burns 1981; Schupack 2001).

Previous attempts had utilized normal strength steel, with little success. After precompression, concrete continues to shorten over time in a process referred to as creep. In addition, the loss of moisture in concrete associated with curing causes shortening called drying shrinkage. The combined effect of creep and shrinkage losses precluded the effective use of normal strength steel in prestressing. Freyssinet initiated the use of high strength cold-drawn steel wires, overcoming the problem of excessive losses in prestressing force due to creep and shrinkage of concrete.

Subsequent developments in prestressing reinforcement included the introduction of stress-relieved and low relaxation strand. Both techniques are utilized to provide a more bilinear stress-strain profile than standard cold-drawn wires, which serves to further reduce relaxation losses at high levels of prestress, as seen Figure 1.1.

1.2 Pretensioning and Post-Tensioning

There are two different techniques for applying prestressing force to a concrete flexural member: pretensioning and post-tensioning. In pretensioning, steel strand is tensioned between two stressing abutments and concrete cast around it. Once the concrete has cured the requisite amount, the strand is cut from the abutments and prestressing force is applied to the member through bond development. In post-tensioning, concrete is cast around hollow ducts containing the strands. After the concrete reaches its specified strength, the strands are gripped with mechanical anchorages and stressed against the cured concrete. Ducts containing the strand may be grouted to create a bonded post-tensioned tendon, or may contain grease for an unbonded assembly.

Of particular interest in this investigation are continuous multiple bay floor slab assemblies containing unbonded post-tensioned tendons.

The primary reinforcement in an unbonded post-tensioned structure is monostrand tendons, which consist of cold-drawn high-strength steel strands coated with grease and enclosed in a thin plastic (or in some cases paper) sheath as shown in Figures 1.2 and 1.3. The strand itself is comprised of six outer wires that are helically wound around a straight core wire. Each tendon is encased in concrete during floor construction and the strand is tensioned using a hydraulic jack after the concrete has cured. Finally, the strand is locked-off using a mechanical anchorage. These anchorages transfer the tensile force stored in the tendon to the floor as seen in Figure 1.2.

The amount of stressing force applied is crucial to the performance of all prestressed concrete members. The magnitude of the force applied controls the depth of the concrete compression zone, and in the case of harped or draped tendons, the amount of uplift force counteracting service loads (see Figure 1.4). Utilizing uplift forces created by eccentrically placed tendons to counteract all or part of service loads is commonly referred to as load-balancing.

1.3 Susceptibility of Prestressed Structures to Fire Damage

In most countries there exist technical specifications and guidelines for structural fire protection contained in building codes and bylaws. Much of this design is performed by project architects or independent consultants, rather than the engineer. Recent events in the United States, Venezuela, and Spain demonstrate that fire is a critical structural design scenario (ARUP 2005; Hampton 2004; Gilvary and Dexter 1997; Soules 2004).

Until recently, most fire design has been based on *prescriptive* building code provisions aimed at ensuring adequate structural performance to allow for occupant egress and the protection of firefighters (Buchanan 2001). However, prescriptive codes do not provide the engineer much insight into the performance of structures subject to fire conditions, nor do they aid in the assessment and repair of fire damaged structures (Holmes et al. 1982; Schneider 1990).

One recent example illustrating the need for information on the post-fire assessment and repair of fire damaged structures was the dispute over the structural integrity of Meridian Plaza in Philadelphia. The 38 storey office building suffered severe fire damage between the 22nd and 30th floors in 1991, and remained empty for over five years while its safety was assessed, only to eventually be demolished (Gilvary and Dexter 1997).

Increasingly, the engineering and insurance communities are recognizing the value of a *performance-based* approach to fire-safety design. This is a shift from standard fire ratings (in hours) and empirical testing to *rational design*. Due to the extreme cost associated with full-scale fire testing and the advancement of modern heat-transfer and structural simulation, accurately quantifying the elevated-temperature and residual material properties of both conventional and emerging building materials is an essential first step in rational fire-safety design. As such, one must recognize the inherent weaknesses of different structural components and assemblies during and after exposure to elevated temperatures.

1.3.1 Cold-drawn Prestressing Steel

Of particular importance to the fire performance of prestressed concrete structures are: the maximum temperature reached at the level of the prestressed reinforcement; the temperature-induced degradation of bond between concrete and strand; the relaxation of strand in unbonded construction; and the change in in-plane loading due to the combined effects of thermal expansion and restraint. It is important to note that, in continuous construction, strand relaxation can affect adjacent bays not exposed to elevated temperatures. In fact, while prestressed concrete was still in its infancy, Hill and Ashton (1957) noted that prestressed concrete members of a given configuration, span, and capacity, would be more susceptible to fire effects than their reinforced concrete equivalent because:

1) prestressed members have a smaller section and therefore have less thermal mass;
2) cold-drawn wire used in prestressing is more susceptible to the effects of elevated temperatures than mild steel; and
3) prestressing steel usually carries a higher proportion of its ultimate tensile strength under service conditions.

These defects have also been identified in more recent publications, most notably by Buchanan (2001).

In addition to the aforementioned concerns, in the case of unbonded post-tensioned concrete members exposed to fire, an appreciable permanent loss in prestress may occur upon cooling as a result of irrecoverable creep deformations (Collins and Mitchell 1987; Hill and Ashton 1957; Malhotra 1982; Schneider 1990). As will be discussed later, the magnitude of tendon stress present in an unbonded member at the

formation of plastic hinges has a significant influence on its flexural strength. This prestress loss is thus significant for the post-fire ultimate limit states of these types of members.

To compensate for the susceptibility of post-tensioned slabs exposed to fire, it is often suggested that the engineer can still achieve design economy while increasing nominal concrete cover; thereby thermally protecting prestressing reinforcement from elevated temperatures (Gustaferro 1973a; Hill and Ashton 1957). Unfortunately, in practice many existing unbonded post-tensioned structures are found to lack the specified concrete cover intended by the original designers (Chacos 1988; Freyermuth 1991; ACI Committee 423 1998). As a result, in fires the strand might be subjected to significantly higher temperatures than envisioned. Therefore there is a crucial need to understand cold-drawn prestressing steel at a material level, and then apply this knowledge through rational evaluation methods for the reinstatement of fire damaged unbonded post-tension floor slabs.

1.3.2 Normal Strength Concrete

Concrete strength, both at elevated temperatures and after cooling, is affected by many different parameters, including: aggregate type; mix proportions; curing conditions; heating and cooling rates; the presence of steel or polymer fibres; and applied stresses (Khoury 2000; Schneider 1988; Xiao and König 2004). As such, certain distinctions and generalizations must be applied to a typical fire-damaged post-tensioned floor.

In common practice, post-tensioned floors are constructed using normal strength concrete mixes, as large amounts of prestress are not required to counterbalance live load deflections. It has been demonstrated that exposure to elevated temperatures reduces the

compressive strength of both normal and high strength concrete mixes. However, high strength concretes are particularly susceptible to failure by explosive spalling, which is often attributed to the inability of moisture to escape during heating as a result of the relatively low permeability of these mixes (Khoury 2000; Phan and Carino 1998; Phan and Carino 2000; Schneider 1988).

The effect of fire on concrete's properties will be discussed further in Chapter 2 of this thesis, where it is shown to have a less significant effect on the reinstatement of unbonded floors than fire damage to the prestressed reinforcement.

1.4 Rehabilitation of Fire Damaged Unbonded Post-tensioned Slabs

Given the creativity of the engineer and the skill of the contractor, the rehabilitation of damaged structures can take many forms. As many unbonded post-tensioned buildings have experienced corrosion damage, the engineering community has identified several common, cost effective methods of repairing damaged tendons. A general repair scheme is proposed below for fire-damaged slabs:

1) determine the amount of residual material strength of prestressing steel using the data presented herein;
2) estimate the amount of prestress force remaining in the tendon using the model herein or other applicable methods such as Deflectometer Testing (CMHC 2002);
3) assess the potential to re-stress existing tendon based on 1 and 2; and
4) assess the potential to repair fire damaged concrete if required (Schneider 1990).

Where irreparable damage to the tendon is determined, other strengthening options, such as: tendon replacement; external post-tensioning; and steel subframing are presented at length in ACI 423.4R-98 (1998).

1.5 Research Objectives

It is widely known that the physical degradation of cold-drawn steel's mechanical properties occurs at elevated temperatures. The degree to which heating affects these properties is crucial in the formulation of a rational approach to investigating fire damaged prestressed concrete structures.

The objective of the research presented herein is to gain a better understanding of the changes observed in commonly used 1860 Grade, low-relaxation prestressing strand both during and after exposure to simulated fire damage, and the consequences for unbonded post-tensioned concrete slabs in fire. The specific objectives treated in the current document are:

1) to experimentally determine the residual strength and mechanical properties of unstressed-while-heated cold-drawn prestressing strand for various levels of simulated fire damage;
2) to develop and/or apply analytical expressions describing the variation in residual strength and mechanical properties based on the test data mentioned previously;
3) to illustrate through metallographic analysis the changes in microstructure caused by various levels of heating;

4) to experimentally determine the loss of prestress that occurs during heating for an unbonded tendon under a representative service load and the amount of prestress remaining after heating to various temperatures; and

5) to develop and validate a numerical model using available elevated temperature creep parameters for prestressing steel in order to analytically predict loss of prestress with heating for an unbonded post-tensioned concrete slab during fire (subject to realistic thermal exposure scenarios).

Finally, residual mechanical properties and prestress levels are used, along with a pre-existing finite difference heat transfer model, in the rational assessment of a typical unbonded post-tensioned concrete floor slab exposed to the ASTM E119 Standard Fire (ASTM 2001d). Additionally, the influence of different amounts of concrete cover on prestress loss during and after fire exposure is explored.

1.6 Outline of Thesis

This thesis is formatted according to the "Traditional Format" described in Queen's University School of Graduate Studies General Forms of Theses. A summary of each chapter is provided below:

CHAPTER 2 – Literature Review provides background information on the manufacture and material properties of cold-drawn wires and prestressing strand for concrete, and on previously published studies about the residual mechanical properties of prestressing steel after exposure to elevated temperatures. Previously presented creep parameters and elevated temperature relaxation behaviour are discussed. Finally, existing fire endurance tests and fire test methods, and the factors influencing the flexural capacity of unbonded post-tensioned concrete slabs are discussed.

CHAPTER 3 – Residual Properties of Cold-Drawn Prestressing Steel after Exposure to Elevated Temperatures discusses the test program performed to study the residual mechanical properties of prestressing steel after exposure to elevated temperatures. The design, fabrication, and operation of the high-temperature electric tube furnace used in the current study are presented. The procedures used for specimen preparation and tension testing are given. Finally, a metallographic analysis is presented and discussed, as are the experimental residual mechanical properties determined through testing.

CHAPTER 4 – Transient Stress Relaxation of Cold-Drawn Prestressing Steel at Elevated Temperatures outlines the experimental setup, instrumentation, and procedures used to determine the loss of prestress experienced due to thermal expansion and creep at high temperatures in an isolated unbonded prestressing tendon with a particular ratio of heated length to total length. The formulation of a transient relaxation model using known creep parameters available in the literature is presented and compared with the experimental data for validation. Finally, the residual mechanical properties of the stressed-while-heated prestressing strand used in relaxation tests are discussed.

CHAPTER 5 – Consequences for the Post-Fire Performance of Unbonded Post-Tensioned Members presents the formulation of a pre-existing validated finite difference heat transfer model created for use in the fire analysis of concrete structures. The model is then used to apply the ASTM E119 standard fire to a typical unbonded post-tensioned concrete slab with varying heated lengths and different amounts of concrete cover to the prestressed reinforcement. Residual prestressing tendon ultimate tensile strength and remaining prestress force are approximated based on the findings and analytical models presented previously in Chapters 3 and 4. The remaining flexural

capacity of the example structure is examined as a function of concrete cover to the reinforcement; concrete cover being the primary design parameter currently used to provide fire endurance in unbonded post-tensioned reinforced concrete slabs. The significance of the results for the post-fire evaluation of fire damaged structures is discussed.

CHAPTER 6 – Conclusions and Recommendations highlights the important findings of the study presented herein, and recommends areas of significance for future research.

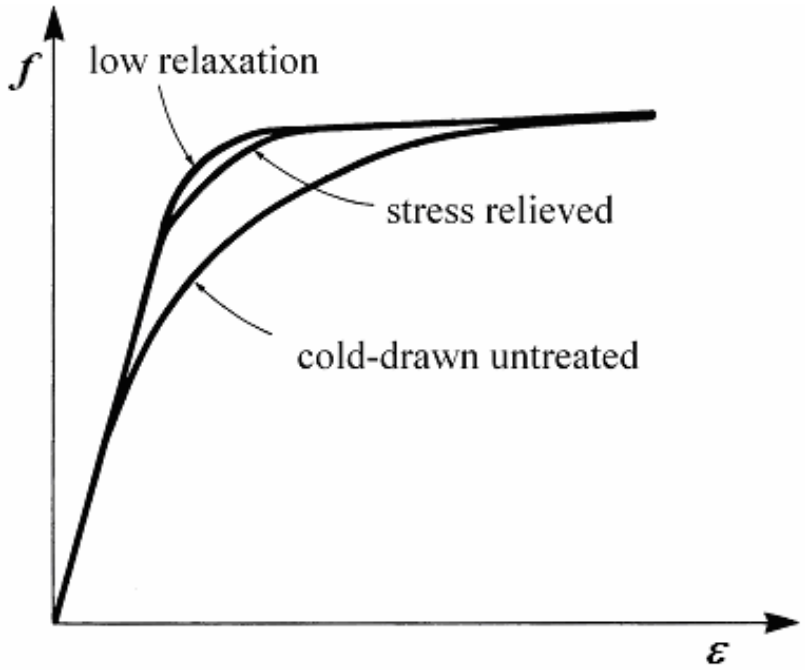

Figure 1.1: Improvement of Stress-strain Response of Cold-Drawn steel; adapted from Collins and Mitchell (1987)

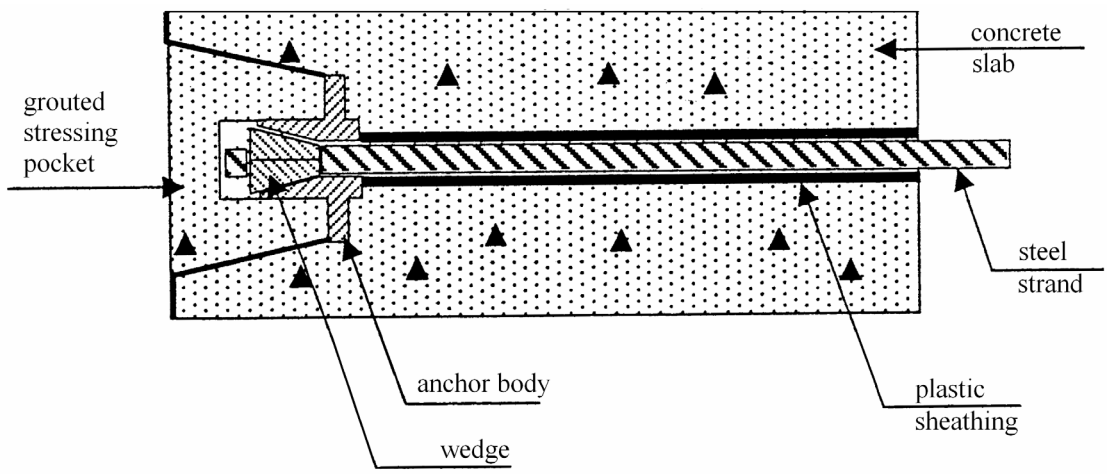

Figure 1.2: Monostrand Mechanical Anchorage Detail

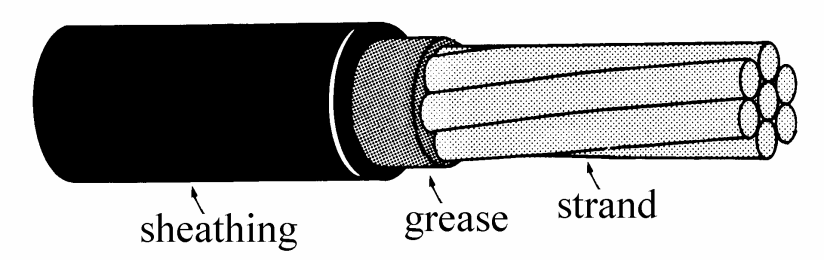

Figure 1.3: Grease Filled Plastic Sheath Containing Unbonded Monostrand; adapted from Collins and Mitchell (1987)

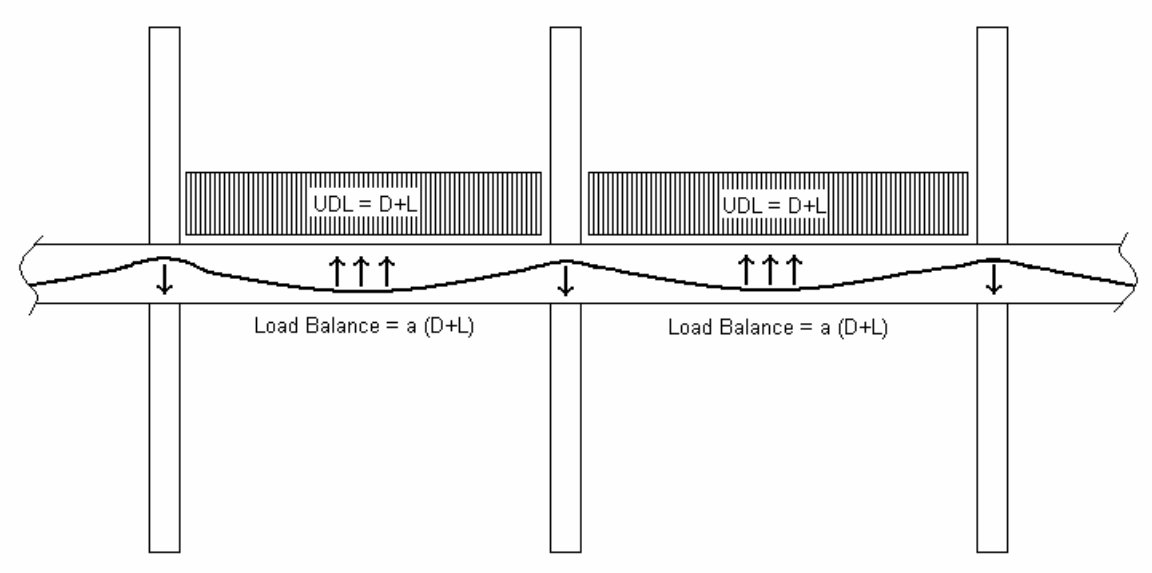

Figure 1.4: Load Balancing Effect Created by Draped Tendon Profile

CHAPTER 2 – Literature Review

2.0 General

Previous work relating to the high temperature residual strength and relaxation properties of prestressing steels is outlined in this chapter. An historical approach is taken, which highlights the parameters varied in each study. This is followed by a discussion of how high temperature residual strength and relaxation properties affect the ultimate strength of post-tensioned floors and of how structural elements are assessed fire endurance ratings. The effect of fire on other important properties, such as concrete compressive strength, is also briefly discussed.

2.1 Properties of Cold-drawn Prestressing Steel

2.1.1 General

Prestressing strand obtains its high strength from large amounts of cold-working performed on steel wires of a specific alloy. Thermomechanical treatments are then used to improve relaxation properties and to create a more bilinear stress-strain curve. Understanding the basic metallurgical concepts used in the manufacture of prestressing strand is crucial in any discussion of fire effects on these materials.

2.1.2 Manufacturing of Seven-Wire Strand

The manufacture of prestressing strand begins by passing high-carbon steel bars, with eutectoid composition, through three stages of controlled heating in a long furnace. The bars are then allowed to cool slowly to ambient temperature. This process of heating and slow cooling is commonly referred to as ‘patenting’ in the wire making industry.

Patenting utilizes a common solid state transformation called a eutectoid reaction to create a metal mixture containing two distinct solid phases. In the case of steels, defined as iron-carbon alloys having less than 2% carbon, the eutectoid point is found at 0.8% carbon by weight on the iron-iron carbide phase diagram shown in Figure 2.1. Heating to a temperature of approximately 720°C or greater followed by slow cooling creates 'pearlite,' a very fine mixture of cementite (F_3C) lamellae in a ferrite (pure iron) matrix (see Figure 2.2). As a result, the patenting process creates a homogenous micro-composite, whose platelike grains are ideally suited for large amounts of cold-working (Anderson 1964; Avner 1974; Lankford et al. 1985). It should be noted that, for equal amounts of cold working, more strain hardening occurs in a fine grained metal than in a coarse grained metal.

A basic literature review on the manufacture of prestressing strand highlights an important point with regard to its post-fire properties; if the temperature of the reinforcement exceeds 720°C during a fire, its microstructure will revert to pearlite when cooled isothermally (slowly). The typical properties of pearlite are: a tensile strength of approximately 830 MPa; a strain at ultimate of approximately 20%; and a hardness of Rockwell C20 (Avner 1974).

The patented bars are run through a series of dies which serve to reduce the bar's diameter to the required size. The bar is then referred to as 'cold-drawn wire'. This cold-working of steel increases hardness, stiffness and tensile strength, but reduces ductility. These changes in material properties are brought on by the alteration of grain structure caused by the pressure applied during the drawing process. This serves to further elongate and narrow microstructure elements along the wire's length, to such a degree

that it becomes difficult to distinguish individual grains under optical microscopy (Lankford et al. 1985) and can be seen in Figure 2.3.

Finally, six smaller cold-drawn wires are helically wound around a slightly larger core wire to form a seven-wire prestressing strand (see Figure 1.3). Residual internal stresses caused by drawing and stranding are removed by exposing the seven-wire strand to temperatures of about 350°C for a specific duration (Anderson 1964; Collins and Mitchell 1987; Lankford et al. 1985).

2.1.3 Stress Relieving vs. Strain Tempering

During the final stage of manufacture, a distinction must be made between stress-relieved and low-relaxation prestressing steel. While both techniques involve heating strand or individual wires to approximately 350°C, in the strain tempering process used to create low-relaxation products, tensile stress is applied to the strand during heating.

Currently in North America, low-relaxation seven-wire strand adhering to ASTM A416-01 is regarded as the standard type and is used in most applications (ASTM 2001b). Two different grades, Grade 1725 [250] and Grade 1860 [270], are available, having minimum ultimate tensile strengths of 1725 MPa [250 000 psi] and 1860 MPa [270 000 psi] respectively. Strand is normally available in nominal diameters of 9 mm, 11 mm, 13 mm, and 15 mm. In unbonded post-tensioned floor slabs, 13 mm strand is most commonly used (Chacos 1988; Schupack 1994; Schupack 2001). As such, the specimens selected for this thesis research were 13 mm diameter Grade 1860 ASTM A416-01 low-relaxation seven-wire strand.

Older structures containing unbonded tendons may have used individual wires, grouped together in a duct, which adhere to ASTM Standard A421 for stress-relieved

wire (ASTM 2001c). These materials were often produced with lower minimum ultimate tensile strengths than today's grades.

It should be noted that stress relieving and strain tempering do not markedly affect the strength of cold-drawn wires, but rather improve their relaxation properties and create a raised and better defined yield point (Collins and Mitchell 1987; Schupack 2001). As such, the effect of fire exposure on the residual ultimate tensile strength of the material should presumably be the same for prestressing strand manufactured by either process.

2.1.4 Chemical Composition of Cold-Drawn Wire

Because the formation of pearlite is crucial to the manufacture of cold-drawn wire, prestressing steel must contain the characteristic eutectoid chemical composition. Therefore, its percent weight of carbon is universally approximately 0.8%. Other elements such as manganese and silicon are varied in small amounts to help obtain desirable mechanical properties and, on occasion, sulphur and phosphorus contents may be increased to improve drawability (Glodowski 1990). A summary of various chemical compositions observed in prestressing steels is presented in Table 2.1.

2.1.5 Young's Modulus

At room temperature, the modulus of elasticity for cold-drawn wire is assumed to be approximately 200 GPa for design purposes. This value is often slightly reduced for seven-wire strand to account for the twisting of the helical outer wires during stressing operations and is assumed to be 193 GPa (ACI-ASCE Committee 423 2005). As temperature is increased, a subsequent decrease in elastic modulus is exhibited in metals as they soften under heating. Lie (1972) summarizes the influence of temperature on the elastic modulus of various grades of mild steel, showing noticeable differences in the rate

of decrease in modulus for each. These differences could be attributed to the rate of loading utilized in each study, since modulus of elasticity is known to be relativity insensitive to the microstructure of steel (Harmathy and Stanzak 1970).

Holmes et al. (1982) present an upper and lower limit of decrease in modulus with temperature for mill coil wire, stress-relieved wire, and seven-wire strand. These data were normalized to elastic modulus values of 203.3 GPa, 204.1 GPa and 199.5 GPa respectively. Similarly, a study by Ruge and Winkelmann, cited in Anderberg (1983), presents modulus data normalized to stress-relieved wire with a modulus of 214 GPa at 20°C (see Figure 2.4). Finally, upon cooling from elevated temperatures the residual modulus of elasticity of prestressing steel wires has, as expected, been observed not to change (Fan 2004).

2.1.6 Tensile Strength

Both the 0.2% offset yield strength and the ultimate tensile strength of prestressing steels have been observed to decrease significantly at elevated temperatures and have also been shown to be more sensitive to high temperatures than mild steels (Anderberg 1983; Harmathy and Stanzak 1970; Holmes et al. 1982; Lie 1992). Additionally, the residual 0.2% offset yield strength and the ultimate tensile strengths of various prestressing steels have been shown to decrease significantly at between 400°C and 500°C (Abrams and Cruz 1961; Abrams and Erlin 1967; Hertz 2004; Neves et al. 1996). Because residual material strength is crucial in the post-fire evaluation of structures, and is the focus of this thesis, it is discussed in detail in Section 2.2.

2.1.7 Thermal Expansion

Thermal expansion is of particular interest for unbonded construction since tendons in these structures are free to elongate within a slab. The coefficients of linear expansion for prestressing steel are lower than those determined for mild (ferrite) steels (Lie 1992). The thermal expansion behaviour of prestressing steel can be defined by:

$$\Delta l / l = -2.016 \times 10^{-4} + 1.0 \times 10^{-5} T + 0.4 \times 10^{-8} T^2 \quad 20°\text{C} < T < 1200°\text{C} \qquad (2.1)$$

where l represents specimen length and T represents temperature in Celsius, as found in Rigberth (2000).

2.1.8 The Physical Effect of Heat Treatment on Cold-Worked Metals

During the manufacture of cold-worked metals, a portion of the mechanical energy used in the plastic deformation of the material is stored in the specimen. This energy is stored within the crystalline structure of the metal in the form of point defects, dislocations, and stacking faults. As a result, a cold-worked specimen maintains a higher state of energy than its undeformed counterpart, and is thereby thermodynamically unstable. When cold-worked metals are thermally activated through annealing (heat-treatment), the specimen is able to transform to a state of lower energy, which is accompanied by microstructural changes (Avner 1974; Hu 1985).

The annealing process can be divided into three stages: recovery, recrystallization and grain growth. Recovery is a low temperature process in which microstructural changes are not appreciable. Its main effect is the relief of internal stresses caused by cold working and is the mechanism used to provide a higher and better defined yield plateau in low-relaxation and stress-relieved prestressing steels. During recrystallization, minute new crystals having the same composition and structure of undeformed grains

begin to appear. These grains are not elongated and have approximately uniform dimensions, contributing to a decrease in the tensile strength of the material. Finally, grain growth occurs at temperatures nearing the eutectoid transformation temperature (720°C for 0.8% carbon steel), and results in a more pronounced loss of tensile strength (Avner 1974; Hu 1985).

2.2 Prestressing Steel after Exposure to Elevated Temperatures

2.2.1 General

Several studies of the effect of elevated temperature exposure on the mechanical properties of cold-drawn prestressing steel are available in the literature. Pertinent literature spans the entire lifespan of modern prestressing and has been authored in several different countries and languages. However, no recent validation of residual properties for current North American prestressing steels has evidently been performed. As well, investigations referenced herein fail to cite findings from other previously published studies. The compilation of data presented in this chapter provides, for the first time, a comprehensive review of the post-fire residual mechanical performance of prestressing steels. It should also be noted that much of the literature reviewed does not provide a measure of the variation within each data set.

2.2.2 Historical Review

The earliest known tests of prestressing strand under heating were conducted in France in the 1940s and were cited by Guyon (1953). Residual strength data were obtained by heating individual wires (not seven wire strand), since early prestressed concrete relied on bundled parallel wires for prestressed reinforcement.

Tests were performed on cold-drawn steel wires 5.1 mm and 2.5 mm in diameter, having nominal tensile strengths of 1475 MPa and 2000 MPa respectively. The chemical composition of the wires was not reported, nor was any standard designation. Furthermore, the number of specimens tested and the variability in values were not provided.

Unheated wires were reported to exhibit a rounded stress-strain profile and no discrete yield point prior to failure. This behaviour is common to cold-drawn wires which have not been stress relieved or strain tempered, and is consistent with known wire making practices at that time. Additionally, an attempt was made to simulate the service stress of the strand during heating. This was done by applying to the tested steels, at room temperature, an initial tension estimated to be approximately equal to the tension to which the steel would be stressed in a beam at high temperature. Initial stress levels were maintained during heating through load control. From Tables 2.2 and 2.3 it can be seen that the tension applied to the strand was reduced (mechanically) as temperatures increased, implying an unbonded system. However, in unbonded structures, where thermal expansion is restrained, tendons maintain a condition of constant elongation, not constant stress as tested.

In general it can be observed that heating has adverse effects on the strength of cold-drawn steel. However, inconsistencies in test procedures and reporting, coupled with changes in wire making procedures over time, necessitated further investigation. Abrams and Cruz (1961) performed several series of tests to better understand the effect of elevated temperature on cold-drawn prestressing steel. Residual strength tests were performed on 9.53 mm diameter seven-wire stress-relieved strand with a specified ultimate tensile strength equivalent to that of Grade 1725 prestressing steel. Specimens

were heated at 10°C / min. and held at a particular temperature for 30 minutes (and in one test for 90 minutes). Hold temperatures were varied between 450°C and 750°C. The effect of different cooling regimes, slow ambient cooling and water jet cooling, were examined. It was shown that different rates of cooling did not markedly affect residual ultimate tensile strength; refer to the discussion provided later in this section.

Later, Abrams and Erlin (1967) examined changes in material residual strength and other properties such as hardness, as well as made note of changes in grain structure due to heating. Specimens were heated in an electric tube furnace at 10°C / min. and held at a particular temperature for various time periods. Two different series of tests were performed using Grade 1860 ASTM A416-65 seven-wire strand; note that strand chemical composition is provided in Table 2.1. In the first series, samples were heated to a set point for one, four, or eight hours, and then allowed to cool under ambient conditions for 24 to 48 hours. Note that all specimens in this series were unstressed during heating. The results of this analysis are shown in Figure 2.5.

At 400°C, no appreciable difference and little decrease in residual ultimate tensile strength was observed for the one, four, and eight hour specimens, indicating that only the recovery phase of annealing had been achieved. At 600°C, the one and four hour specimens differed by approximately three percent and metallographic analysis depicted a general reduction in grain elongation indicating that recrystallization had begun. The slight variation of residual ultimate tensile strength to exposure time results from the recrystallization process being far more sensitive to changes in temperature than to variations in time at a constant temperature (Avner 1974).

Abrams and Erlin (1967), in a second series of tests, considered the effects of stress during heating by applying an initial stress, typical of that found in service, and fixing grips at a corresponding elongation. The results are summarized in Table 2.4. This approach better simulates actual fire conditions for unbonded tendons as it allows the strand to relax as it heats. The effect of stress at a relatively high temperature of 540°C was found to have little effect on the residual strength of prestressing steel. Finally, microhardness (DPH) was examined as a function of temperature and time as shown in Figure 2.6. As expected, hardness decreased with temperature and prolonged exposure lead to increased softening.

Holmes et al. (1982) investigated the effect of elevated temperatures on mild and prestressing steels of varying sizes to determine the relative susceptibility of cold-worked steels to heating. As was commonplace for elevated temperature structural materials testing, a temperature range of 20°C to 700°C was examined. Both individual wires (5 mm in diameter) and seven-wire strand (9.3 mm in diameter) were tested at high temperatures and after cooling. The chemical composition was stated to be in accordance with British Standards.

Four specimens of each type were placed in an electric tube furnace and the ends of the furnace were lightly packed with ceramic fibre. The temperature was then raised to the desired set-point and held for a soak time of 30 minutes. The specimens were then allowed to cool within the furnace to room temperature prior to tension testing. Additionally, a series of tension tests were performed at elevated temperatures. The elastic modulus data from these tests was discussed earlier (see Figure 2.4).

As expected, heavily cold-worked prestressing steel exhibited a more drastic reduction in strength after heating than did mild steel specimens. It was also determined that size had little effect on residual strength since the reinforcement cross-section reached a uniform temperature relatively quickly. Results of the aforementioned test series are shown later in a comprehensive review of currently published data (see Figure 2.9).

Neves et al. (1996) obtained residual ultimate tensile strength and strain at rupture data by heating seven-wire strand to various temperatures. Once cooled, the 5.5 mm diameter core wire was removed and a 230 mm length tested. Although the specific grade of strand used in each of the tests was not reported, the chemical composition of the prestressing steel was provided and is shown in Table 2.1.

Specimens were heated in an electric tube furnace at a rate of 10°C / min. and held at a particular temperature for one hour. Temperature control was achieved using a thermocouple suspended in the interior of the furnace, not on the specimen surface. Changes in material residual strength and other properties such as brittleness were determined as a function of different cooling methods meant to simulate conditions experienced by structures as fires are extinguished, for example concrete spalling. As such, specimens were subjected to air cooling and cooling by water jet. A total of 80 residual tension tests were performed; five specimens for each temperature-cooling combination. Finally, metallographic analysis was performed.

Both the air-cooled and the water jet cooled specimens demonstrated a similar decrease in residual tensile strength between 400°C and 700°C. After 700°C both specimens retained some strength; with the water jet cooled specimen observing a sharp

decrease in residual strength after 800°C (see Figure 2.7). This rapid loss of strength was attributed by the authors to the formation of micro-cracks resulting from rapid cooling. Metallographic analysis served to confirm micro-cracking as the cause of rapid strength loss at 800°C for the water jet cooled specimens, as the formation of martensitic structures was identified at high-temperatures after rapid cooling. Martensitic structures are characterized by larger and coarser grains distributed throughout the microstructure. The manner in which these grains are oriented serves to promote brittle rupture of steel due to increased ease of off-axis crack propagation (Krauss 1989). As expected, for temperatures below 700°C, the cooling method used did not markedly affect the residual ultimate tensile strength of cold-drawn prestressing steel since the eutectoid transformation temperature was not achieved (and solid state reactions markedly altering microstructure did not occur).

Finally, Neves et al. (1996) examined the strain at rupture for the aforementioned test series (see Figure 2.8). As expected at the higher temperatures associated with recrystallization, the material exhibited a softening characterized by increased strain at rupture and a large reduction in strength as previously described.

Similar to Neves et al. (1996), Fan (2004) obtained residual strength data by heating cold-drawn steel in an electric furnace and cooling the samples under ambient conditions and with water jets. Because this study contained significantly less detail than those previously mentioned, residual strength results are shown in a summary of the state-of-the-art later is this chapter. The authors do, however, present residual modulus of elasticity data. As expected different levels of subcritical annealing (heating below the eutectoid transformation temperature) do not have a marked affect on modulus.

2.2.3 Models Describing the Residual Strength of Cold-Drawn Prestressing Steel

In an effort to increase the application of rational design methods for fire safety, Danish researchers proposed a sigmoid (S-shaped) curve in Hertz (2004) capable of predicting the reduction in strength of various building materials both at elevated temperatures and upon cooling. It is demonstrated that the equation can be used to represent a straight-line reduction, a variety of S-shaped reductions, and a sudden drop in strength, all as functions of temperature. The curve is given by:

$$\xi(T) = k + \frac{1-k}{1+\left(T/T_1\right)+\left(T/T_2\right)^2+\left(T/T_8\right)^8+\left(T/T_{64}\right)^{64}} \tag{2.2}$$

where ξ is the ratio of material strength at a given temperature to the same property at 20°C and T is temperature in Celsius. Fitting parameters T_1 to T_{64} are used to describe curve behavior and are specific to the type of material examined. Finally, k represents the ratio between the minimum and maximum value of the material property. Note that k is often zero, except when examining residual properties, which occur after fire-exposure and subsequent cooling.

Parameters for Equation 2.2 were derived by Hertz (2004) using the data from a number of different fire tests at and post high-temperature conducted on various building materials. Of interest for the development of this review is that its author used test data presented in an internal submission to develop coefficients used to describe the residual strength of 1600 MPa cold-drawn prestressing steel. These data were not readily available to the Author; however, the coefficients provided (and summarized in Table 2.5) were used to plot Equation 2.2 against all available data, as summarized in Figure 2.9.

Figure 2.9 shows that Equation 2.2 is indeed well suited for use in the examination of fire damaged cold-drawn prestressing steel. It offers a lower, and therefore conservative, boundary for most of the collected data. Those points which fall on or just below the lower boundary, such as the eight hour exposure reported in Abrams and Erlin (1967), represent extreme amounts of elevated temperature exposure and would likely not be found in structures suitable for rehabilitation. It should also be noted that, at a temperature of approximately 700°C, Equation 2.2 predicts that the residual tensile strength becomes asymptotic at 20% of the tensile strength at room temperature. This is a result of the selection of 0.2 for the parameter *k*. Because this parameter represents the ratio between the minimum and maximum value of a given material property, the ratio of tensile strength of pure pearlite (approximately 830 MPa as previously presented) to cold-drawn prestressing steel would be appropriate for use where temperatures exceed 720°C. This would suggest a *k* coefficient closer to 0.40 and thus raise the asymptote (seen in Figure 2.9) to a more realistic level.

2.2.4 Summary

It has been demonstrated that the physical degradation of cold-drawn steel's microstructure occurs at elevated temperatures. Several different test series, summarized in Table 2.6, were used to illustrate this phenomenon. Variables such as cooling rate, hold time, and applied stress have been investigated and found to have little effect. As expected, it was found that the single most important factor affecting the residual mechanical properties of cold-drawn prestressing steel, after exposure to simulated fire damage, is the peak temperature experienced.

Using the summary of data provided, the Hertz equation for post-fire residual strength in cold-drawn steel was examined. It was found that this expression offered good correlation to these data collected, and represented a lower boundary useful for the rehabilitation of fire-damaged structures. However, since no recently published North American residual strength data is currently available, and because little research has been conducted on the elevated temperature relaxation properties of prestressing steel, particularly as relevant to prestressing steel encased in concrete, further investigation is required in order to adequately evaluate fire damaged unbonded prestressed concrete slabs.

2.3 Relaxation of Seven-Wire Strand as a Result of Elevated Temperatures

2.3.1 General

The flexural strength of unbonded post-tensioned concrete floor slab assemblies relies on both the strength and proportioning of constituent materials such as concrete, mild reinforcement, and prestressed reinforcement, as well as on the magnitude of the applied prestress. Consequently, understanding the elevated temperature relaxation properties of cold-drawn steel is crucial in the post-fire assessment of such floors.

Since unbonded tendons are free to expand and contract within the slab, two significant effects of fire can cause changes in prestress force to occur. As the temperature of the reinforcement is raised during a fire, the tendon will experience thermal expansion. This process, in accordance with Equation 2.1 and other known expressions, is reversible upon tendon cooling. In addition, at a temperature particular to the metal being examined, high temperature creep will be initiated under stress. The resulting creep-related relaxation of the tendon is irrecoverable and results in a permanent

loss in prestress force (Collins and Mitchell 1987; Hill and Ashton 1957; Malhotra 1982; Schneider 1990).

2.3.2 Elevated Temperature Relaxation Tests

Although many authors, as mentioned previously, have identified the elevated temperature relaxation of unbonded tendons as being significant to the fire performance of post-tensioned floors, there is a worrying paucity of experimental data or analytical modeling describing this phenomenon.

Hill and Ashton (1957) studied 16 simply supported unbonded post-tensioned rectangular and T-beam sections exposed to fire in some of the earliest fire endurance tests conducted on prestressed concrete members. The authors noted significant irrecoverable deflections and cited an 'appreciable loss' of prestress upon cooling but did not provide any numerical data illustrating this observation.

Abrams and Cruz (1961) performed two series of tests to investigate the elevated temperature relaxation of cold-drawn prestressing steel. In the first series of tests, strand was tensioned to 40%, 56% or 71% of ultimate, heated to approximately 540°C [1000°F] and then allowed to cool slowly to room temperature. In the second series of tests strand was stressed to 60% of ultimate and heated to predetermined temperatures ranging from approximately 93°C [200°F] to 650°C [1200°F] and allowed to cool slowly. It should be noted that all specimens were stress-relieved 9.4 mm diameter seven-wire strand (see Table 2.6). It was shown that a gradual loss of prestress occurs up to approximately 315°C, followed by a more drastic decrease above this temperature (see Figure 2.10). This drastic change in rate of prestress loss is a result of creep-related relaxation being activated above 315°C, which is consistent with other tests conducted by the author and

discussed in Chapter 4. It was also noted that a small portion of load lost at 650°C was recovered upon cooling, indicating the presence of a small amount of recoverable thermal strain (thermal expansion).

2.3.3 Elevated Temperature Creep Behaviour

The physical mechanisms which cause time dependent deformations under constant stress, or *creep*, differ markedly from one material to another. Furthermore, for any given material, different creep mechanisms may act at various combinations of stress and temperature. The creep phenomena is typically divided into three distinct phases: primary, over which the rate of creep diminishes; secondary, where the rate of creep is constant and at a minimum; and tertiary, where the rate of creep increases as a result of necking, which ultimately leads to failure (see Figure 2.11). This failure behaviour is commonly referred to as *creep-rupture*.

The same distinctions can be made at elevated temperatures; however, here the effects of temperature on creep rate must also be incorporated. This is most often accomplished by the inclusion of a *temperature-time parameter*; such as the Sherby-Dorn or Larson-Miller Parameters (Dowling 1998). Previous publications specific to the elevated temperature performance of steels used in the building industry have focused on the approach proposed by Dorn (1955) (Anderberg 1983; Anderberg 1988; Harmathy 1967; Harmathy and Stanzak 1970).

The approach proposed by Dorn (1955) idealizes creep behaviour as being analogous to the flow of a Newtonian liquid with very high viscosity. At elevated temperatures the average oscillation of atoms about their equilibrium point increases, resulting in more frequent stress-driven molecular rearrangements. These rearrangements

contribute to the creep phenomenon, and the entire process is said to be *thermally activated*. The rate of a thermally activated process is governed by the Arrhenius equation:

$$\dot{\varepsilon} = Ae^{\frac{-\Delta H}{RT}} \tag{2.3}$$

where $\dot{\varepsilon}$ represents creep rate, ΔH is activation energy (and is a measure of the amount of energy required to cause molecular motion), R is the universal gas constant, and T is the absolute temperature.

When applied to a Newtonian fluid with tensile viscosity as follows:

$$\eta = \frac{\sigma}{\dot{\varepsilon}} \tag{2.4}$$

the Arrhenius equation can be rewritten in a form which describes the effects of both stress and temperature:

$$\dot{\varepsilon} = A(\sigma)e^{\frac{-\Delta H}{RT}} \tag{2.5}$$

where the new coefficient A is a function of stress and depends mainly on the material being examined (Dowling 1998; Dorn 1955). It should be noted that a key assumption utilized in Dorn's approach is that the activation energy of creep (ΔH) is constant. In general this assumption is valid only at temperatures above half the melting point of a metal; however, Harmathy (1967) asserts that for carbon steels the assumption is valid in the range of 400°C to 700°C.

By writing Equation 2.5 in differential form and integrating both sides it can be seen that creep strains (engineering strain) can be represented in terms of so called *temperature-compensated time* as shown below:

$$\varepsilon = A(\sigma)\int e^{\frac{-\Delta H}{RT}} dt \quad \text{for } \sigma \text{ constant} \tag{2.6}$$

where temperature-compensated time is:

$$\theta = \int_0^t e^{\frac{-\Delta H}{RT}} dt \tag{2.7}$$

or for constant temperature as:

$$\theta = te^{\frac{-\Delta H}{RT}} \tag{2.8}$$

Elevated temperature creep parameters can only be experimentally determined in a steady-state test. In such a test a specimen is heated to a predetermined temperature and a constant load is then applied. In plotting experimental strain data versus temperature-compensated time, one is able to quantify the well known Zener-Hollomon parameter, Z, and the dimensionless creep parameter, $\varepsilon_{cr,\,0}$, as defined in Figure 2.12.

By determining these parameters for different stress levels and temperatures, Harmathy (1967) proposed the expression:

$$\varepsilon_{cr} = \frac{\varepsilon_{cr,0}}{\ln 2}\cosh^{-1}\left(2\exp\left(Z\theta/\varepsilon_{cr,0}\right)\right) \quad \text{for } \sigma \text{ constant} \tag{2.9}$$

to describe elevated temperature primary and secondary creep as a function of temperature and time at a given stress level.

Experimentally determined values of ΔH, Z, and $\varepsilon_{cr,\,0}$ for structural steel and mild reinforcement are available in the literature and are summarized in Anderberg (1983). However, to date there has only been one study known to have experimentally examined the creep parameters of cold-drawn prestressing steel.

Harmathy and Stanzak (1970) performed elevated temperature creep tests on ASTM A421 1725 grade prestressing steel (ASTM 2001c), with chemical composition

shown in Table 2.1. In these tests a single wire was removed from a seven-wire strand, heated in an electric tube furnace to a predetermined temperature, and constant load was then applied. Creep curves plotting strain against temperature compensated time were used to calculate values of Z and $\varepsilon_{cr,0}$ for temperatures and stress levels ranging from 370°C to 650°C and 6.9 MPa to 690 MPa respectively (see Table 2.7). It should be noted that the values of Z presented take the general form proposed by Dorn (1955), in which the creep rate at a low stress levels is defined by power function, and at a high stress levels is defined by an exponential. Additionally, the value of ΔH divided by the gas constant R was also determined and is presented in Table 2.7.

The authors note a great deal of scatter in these data discussed, which is not uncommon in creep and elevated temperature testing. They cite differential heating of high-temperature extensometer arms and inconsistent application of stress as possible sources of error. As well, the creep theory utilized does not account for physiochemical changes in the microstructure which occur due to recrystallization at high temperatures (approximately 600°C and above).

2.3.4 Elevated Temperature Relaxation Behaviour

As shown previously, the steady state creep behaviour of cold-drawn prestressing steel can be defined using creep theory proposed by Dorn (1955) and modified by Harmathy (1967). However, this is of little use for unbonded post-tensioned slabs exposed to fire unless steady-state creep predictions can be incorporated into a *transient* description of strand relaxation. Note that a transient process incorporates varying temperatures and a simultaneously varying applied load.

According to Anderberg (1983; 1988) the relaxation process experienced in an unbonded tendon can be found analytically by using instantaneous stress-related strain determined in steady-state creep tests. As the total strain of an unbonded tendon is approximately constant, the sum of all strains must also be a constant. Therefore, an increase in creep strain must be followed by a proportional decrease in strain resulting from applied loading (prestress force and gravity loads). The total strain (engineering strain) in the tendon can be described as:

$$\varepsilon_{tot} = const = \varepsilon_{\sigma}(\sigma) + \varepsilon_{T}(T) + \varepsilon_{cr}(\sigma, T, t) \tag{2.10}$$

where ε_{σ} represents the strain due to prestress and applied loading, ε_{T} represents strain resulting from thermal expansion / contraction, and ε_{cr} represents creep strain.

A comprehensive relaxation model is used and discussed in greater detail in Chapter 4, which uses Equation 2.9 to predict the change in strain at a particular stress level as a result of (elevated temperature) creep. The predicted creep strain and computed thermal elongation are then used in Equation 2.10, along with elevated temperature elastic modulus (based on data available in the literature) to update tendon stress. The process is then repeated for the new stress level. A time step approach, where step size is selected to minimize the temperature difference between steps, is used herein to simplify the calculation of temperature compensated time.

2.4 Fire Endurance

2.4.1 General

In the most basic sense, fire safety engineering is concerned with the protection of human life and property from the effects of fire (Buchanan 2001; Lie 1992). During a fire, significant changes in building materials, member behaviour, and applied loading

occur. Although fire scenarios are extreme and less common than other load events, it is still necessary to prevent structural collapse for a sufficient amount of time to allow for occupant egress and to protect the lives of fire-fighters. Design for fire safety is complex and incorporates many disciplines as: containment (physical barriers); suppression (sprinklers and extinguishers); smoke propagation (exhaust fans); egress (signage and building layout); and structural integrity (prevention of collapse) are all important factors in design.

Understanding the principles used to define structural fire endurance is crucial to the development of this thesis as it serves to illustrate that a member may survive a fire but upon cooling may not be adequate for the original design loads.

2.4.2 Post-Tensioned Slabs

Fire endurance requirements are generally contained in regional or national building codes such as the National Building Code of Canada (NRC 1995) or the American Concrete Institute (ACI) Building Code Requirements for Structural Concrete (ACI 2002) and are typically applied on a prescriptive basis. In the case of concrete slabs, a predetermined amount of concrete cover is associated with different fire endurance times for various types of slab assemblies (see Table 2.8).

Gustaferro (1973b) summarizes the results of 18 full scale tests on concrete slabs reinforced with post-tensioned tendons. The failure criteria used were that:

1) the specimen must sustain the load applied and not collapse (structural end point);
2) holes, cracks, or fissures through which flames or gasses hot enough to ignite cotton waste must not form (containment end point);

3) the temperature increase on the unexposed surface of the slab could not exceed an average of 121°C or a maximum of 162°C at any one point (heat transmission end point); and

4) the temperature of reinforcement could not exceed 426°C for cold-drawn prestressing steel and 593°C for mild rebar;

when exposed to the ASTM E119 standard fire (which is essentially the same as the Canadian Standard CAN/ULC S101), whose thermal profile is summarized in Figure 2.13. It should be noted that the reinforcement temperatures specified above were selected on the basis that they represent a loss of approximately half the material strength at room temperature which corresponds to a high likelihood of failure in flexure under service loads (Gustaferro and Lin 1986).

In comparison to standard fires, real fires often exhibit a longer and slower growth phase, which may be associated with higher overall temperatures. In an actual fire the peak temperature achieved is rarely sustained due to frequent temperature fluctuations. Consequently, design fires constitute a severe fire, but not the most severe fire (Khoury 2000).

Flexural members (simply supported) generally fail a standard fire test as a result of an unacceptable rise in reinforcement temperature, not as a result of inability to carry applied loads (Khoury 2000). Continuous construction, reduced occupancy live loads, thermal restraint, membrane action, and the availability of alternative load paths all allow for even better performance (i.e., resistance to collapse) of real concrete slabs when compared to fire test results (Buchanan 2001; Gustaferro and Lin 1986; Khoury 2000). Thus, the reinforcement temperature in a real fire may reach critical levels without

significant outward signs (i.e., structural distress) being apparent. This makes the diagnosis of strand deterioration and creep related relaxation paramount in the post-fire evaluation and repairability of fire damaged unbonded post-tensioned floor slabs.

Restrained flexural members are known to have markedly better fire performances than unrestrained members (Buchanan 2001; Gustaferro 1973a; Lim et al. 2004). A restrained flexural member is one whose thermal expansion is prevented by surrounding structural elements. In the case of a continuous slab, the bottom of a heated bay tends to expand along the slab's length. Where adjacent bays are not heated, the surrounding rigid diaphragm and columns contain thermal expansion of the heated slab. Because a temperature gradient exists through the concrete slab, the line of thrust created by thermal restraint can often fall below the member's centroid, causing an upward arching action or thrust. This effectively induces a prestress force in the concrete at the edge of the fire affected bay which normally further enhances fire endurance.

Once a fire has been extinguished, the effects of reduced loading and restraint likely no longer exist. Furthermore, the damage to continuous tendons is not contained to a fire exposed bay alone. Therefore, extreme care is needed in evaluating unbonded post-tensioned slabs exposed after fire.

2.5 Residual Strength of Concrete

As mentioned previously, elevated temperatures can cause a reduction in the residual strength of concrete. The degree to which the concrete is affected depends on many factors including: aggregate type; mix proportions; curing conditions; heating and cooling rates; and applied stresses. Since post-tensioned slabs do not generally make use

of high-strength mixes, the discussion herein is limited to the effect of elevated temperatures on the residual material properties of normal strength concrete.

Several different mechanisms have been identified which contribute to the loss of compressive strength in concrete both at high temperatures and after cooling. In the range of 530°C to 600°C a marked increase in the *basic creep* of Portland cement occurs resulting in a drastic loss in compressive strength (Khoury 2000). In the range of 400°C to 500°C calcium hydroxide in the cement paste dissociates, creating CaO which expands as it is cooled and rehydrated, creating microcracks (Khoury 2000; Schneider 1988). This phenomenon results in the residual compressive strength of concrete being lower than its compressive strength at high temperatures. The final mechanism resulting in decreased compressive strength of concrete as a result of elevated temperatures is a physical degradation of aggregates, which can occur from 350°C, for flint, up to 600°C, for granite and gabbro (Khoury 2000).

In general it has been suggested that concrete exposed to temperatures up to 300°C will experience little loss in strength, both at temperature and after cooling (Phan and Carino 2000). As well, concrete exposed to temperatures greater than 300°C often exhibits a distinctive deep pink colour caused by a reaction in ferrous salts in sand and aggregate (Khoury 2000; Schneider 1990). This phenomenon is useful as it can aid engineers in locating areas of damaged concrete within slabs.

Fortunately in flexural members, concrete in positive moment regions is typically in tension and merely acts to protect reinforcement from fire effects. In negative moment regions, temperatures exceeding 300°C within a section are generally limited to the first few centimeters of the slab. Consequently, elevated temperature exposure has a much

more pronounced effect on the residual moment capacity of unbonded floor slabs (when compared to concrete slabs with bonded mild reinforcement) through the susceptibility of post-tensioned tendons to elevated temperature damage and subsequent loss of prestress forces (rather than through damage to the concrete in compression).

2.6 Moment Capacity of Unbonded Slabs

2.6.1 General

Flexural deformations in unbonded post-tensioned slabs lead to an increase in tendon stress. Compatibility of deformation between the concrete at the level of the tendon and the tendon cause an increase in strain in the tendon as the slab deflects under gravity loads (Allouche et al. 1998). This increase in strain along the entire length of the tendon leads to an increase in tendon stress.

Determining the amount of stress increase caused by applied loading is required in order to calculate the moment of resistance (M_r) of a given slab cross-section. Investigations into the factors affecting tendon stress serve as the basis for most modern design codes. Although more advanced methods for computing the bending resistance of unbonded members exist (Allouche et al. 1999), the discussion herein will be limited to the application of common North American code equations.

2.6.2 Moment Capacity

For a partially prestressed (having both mild and prestressed reinforcement) beam or slab strip, the moment capacity at ultimate limit states can be defined as:

$$M_r = \phi_s A_s f_s \left(d_s - \frac{\beta_1 c}{2} \right) + \phi_{ps} A_{ps} f_{pr} \left(d_p - \frac{\beta_1 c}{2} \right) - \phi_s A'_s f'_s \left(d'_s - \frac{\beta_1 c}{2} \right) \qquad (2.11)$$

where c represents the depth to the neutral axis and can be determined from equilibrium of forces at a section as follows:

$$c = \frac{\phi_s A_s f_s + \phi_{ps} A_{ps} f_{pr} - \phi_{ps} A'_s f'_s}{0.85 \phi_c f'_c b \beta_1} \tag{2.12}$$

All of the terms in Equation 2.11 are known or can be determined directly, with the exception of tendon stress, f_{pr}. As mentioned previously, this value is partially dependent on the amount of strain in the concrete at the level of the tendon caused by member deflection.

Tendon stress in an unbonded member consists of two components: the stress created by prestressing operations after all loses (effective prestress force), f_{pe}, and the increase in stress created by member deflection, Δf_{pr}. Therefore, tendon stress can be defined as:

$$f_{pr} = f_{pe} + \Delta f_{pr} \tag{2.13}$$

where f_{pe} is again a known quantity. The determination of Δf_{pr} is a slightly more complicated process and has been shown to depend on many factors, including: patterned loading; span-to-depth ratio; and the amount of bonded reinforcement present (Allouche et al. 1998).

Both the Canadian A23.3 (CSA 1994) and American ACI 318 (ACI 2002) codes utilize data from laboratory experimentation to provide an empirical equation defining tendon stress at ultimate in an unbonded post-tensioned concrete flexural member. Since other approaches have not become widely accepted for design, and because this thesis is focused on assessing existing strength, moment capacity will be calculated in accordance

with existing code standards, rather than with more complicated research-level procedures.

2.6.3 Tendon Stress ACI 318-02

Based on tests of full-scale fully prestressed simply supported beams, the ACI (2002) equation for tendon stress, which has been found to be conservative for span-to-depth ratios of 35 or less, is defined as:

$$f_{pr} = f_{pe} + 70 + \frac{f'_c}{100\rho_p} \quad \text{(MPa)} \tag{2.14}$$

where ρ_p is the ratio of prestressed reinforcement in the section. It has been found that Equation 2.14 overestimates tendon stress in members with higher span-to-depth ratios (ACI-ASCE Committee 423 2005). For members with span-to-depth ratios greater than 35, tendon stress is defined as:

$$f_{pr} = f_{pe} + 70 + \frac{f'_c}{300\rho_p} \leq f_{pe} + 200 \quad \text{(MPa)} \tag{2.15}$$

2.6.4 Tendon Stress CAN/CSA A23.3

Initially A23.3 (CSA 1994) adopted the same equations as the ACI Code. However, to address some of the deficiencies recognized in the American code, an approach based on the formation of plastic hinges is now used. Tendon stress is defined by the CSA as:

$$f_{pr} = f_{pe} + \frac{8000}{l_e}(d_p - c_y) \leq f_{py} \quad \text{(MPa)} \tag{2.16}$$

where l_e is the total tendon length between anchorages divided by the minimum number of plastic hinges required to create a failure mechanism in the span being designed, and c_y is determined assuming a stress of f_{py} in tendons, as follows:

$$c_y = \frac{\phi_p A_{ps} f_{py} + \phi_s A_s f_s - \phi_s A'_s f'_s - 0.85\phi_c f'_c h_f (b - b_w)}{0.85\phi_c \beta_1 f'_c b_w} \tag{2.17}$$

for a generic T-beam section (with all the terms in the equation being known or determined easily). It should be noted that the selection of coefficient value (i.e., 8000) in Equation 2.16 was still based mainly on tests performed on simply supported members.

2.7 Summary

It can be seen from the code equations presented previously that the strength of unbonded post-tensioned slabs is affected both by the ultimate strength of the strand itself and also by the amount of stress in the tendon. As elevated temperatures have been shown to reduce both the strength of cold-drawn steel and the magnitude of prestress in the strand, the evaluation of unbonded slabs exposed to fire becomes less straight forward than for bonded members. Additionally, it is important to note that these reductions in material strength and prestress will affect adjacent bays which may not have been exposed to fire. As a result, being able to estimate material strength and prestress loss is crucial in assessing the reusability of such structures.

Table 2.1: Chemical Composition of Various Prestressing Steels (in wt.%)

Study	MacLean	Neves et al.	Harmathy and Stanzak	Abrams and Erlin[1]	Cahill[2]
Country	Canada	Portugal	Canada	USA	UK
Year	2006	1996	1970	1967	1965
Standard	ASTM A416	-	ASTM A421	ASTM A421	-
C (%)	0.800	0.824	0.794	0.740 to 0.830	0.78
Cr (%)	0.040	0.237	-	-	-
Mn (%)	0.868	0.712	0.780	0.450 to 0.600	0.630
P (%)	0.023	0.020	0.012	0.010 to 0.014	0.024
Si (%)	0.450	0.235	0.187	0.260 to 0.340	0.210
S (%)	0.012	0.013	0.031	0.026 to 0.049	0.022

[1] Abrams and Erlin present composition of five different series of specimens
[2] Cahill is cited in Anderberg (1983)

Table 2.2: Residual Strength of Cold-drawn 5.1 mm Wire (Guyon 1953)

Initial Tens. (MPa)	Temperature (°C)	Duration (min.)	$f_{pu,20°C}$	$f_{pu,T}$	$f_{pu,T}/f_{pu,20°C}$
787.4	200	60	1476.9	1489.3	1.01
491.6	400	60	1420.3	1223.8	0.86
0.0	600	60	1489.3	1000.4	0.67
0.0	600	20	1447.9	1028.7	0.71

Table 2.3: Residual Strength of Cold-drawn 2.5 mm Wire (Guyon 1953)

Initial Tens. (MPa)	Temperature (°C)	Duration (min.)	$f_{pu,20°C}$	$f_{pu,T}$	$f_{pu,T}/f_{pu,20°C}$
787.4	200	60	2069.8	2089.1	1.01
491.6	400	60	2069.8	1686.5	0.81
0.0	600	60	2069.8	991.5	0.48
0.0	600	20	2089.1	1118.3	0.54

Table 2.4: Effect of Stress on Residual Strength ASTM A416-65 Strand (Abrams and Erlin 1967)

Applied Stress % f_{pu}	Temperature (°C)	$f_{pu,T}$ (MPa)	$f_{pu,T}/f_{pu,20°C}$
0	540	-	0.61-0.66
40	540	1206.6	0.64
56	540	1165.2	0.62
71	540	1179.0	0.63

Table 2.5: Recommended Parameters for Strength Reduction with Temperature of Cold-Drawn Prestressing Steel (Hertz 2004)

Residual Stress	k	T_1	T_2	T_8	T_{64}
f_{py}	0.20	100 000	750	550	650
f_{pu}	0.20	100 000	950	550	650

Table 2.6: Summary of Materials and Methods used in Residual Ultimate Strength Tests

Study	Country	Year	Standard	Thermomechanical Treatment	Strand / Wire	Diameter (mm)	Applied Stress	Cooling Regime
Guyon[1]	France	1953	-	none	wire	2.5, 5.1	yes	slow cooling in furnace
Abrams and Cruz	US	1961	-	stress relieved	strand	9.53	no	slow cooling in furnace and water
Abrams and Erlin	US	1967	A421-65	stress relieved	both	various	yes	slow cooling in furnace
Holmes et al.	UK	1982	BS 2691 BS 3617	stress relieved	both	5, 9.3	no	slow cooling in furnace
Neves et al.	Portugal	1996	-	-	wire	5.5	no	slow cooling in furnace and water
Fan	China	2004	-	-	-	-	no	slow cooling in furnace and water
Hertz	Denmark	2004	-	-	-	-	-	-

[1] Guyon citing previous publications

Table 2.7: Elevated Temperature Creep Parameters for ASTM A421 Prestressing Steel (Harmathy and Stanzak 1970)

$\Delta H / R$ (°K)	Z (h^{-1})	$\varepsilon_{cr,\,0}$ (mm / mm)
30 556	$Z = 195.27 \times 10^{6}\ \sigma^{3}$ if $\sigma \leq 172$ MPa $Z = 8.21 \times 10^{13}\ e^{0.0145\ \sigma}$ if $172 < \sigma \leq 690$ MPa	$\varepsilon_{cr,\,0} = 9.262 \times 10^{-5}\ \sigma^{0.67}$

Table 2.8: Concrete Cover (mm) for Fire Endurance Ratings of Post-Tensioned Slab Assemblies (PTI 1990)

Restraint	Aggregate	1 Hour	1.5 Hour	2 Hour	3 Hour	4 Hour
Unrestrained	Carbonate	19	27	35	48	-
Unrestrained	Siliceous	19	32	38	54	-
Unrestrained	Lightweight	19	25	32	41	-
Restrained	Carbonate	19	19	19	25	32
Restrained	Siliceous	19	19	19	25	32
Restrained	Lightweight	19	19	19	19	25

As per ACI 318 (ACI 2002)

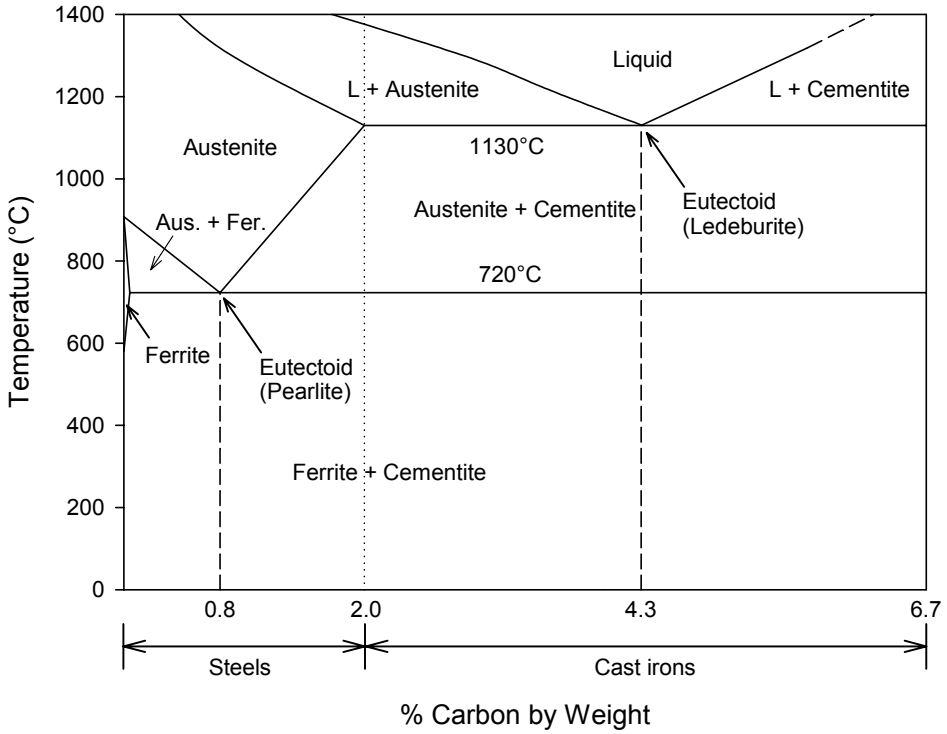

Figure 2.1: Iron-Iron Carbide Phase Diagram (adapted from Avner 1974)

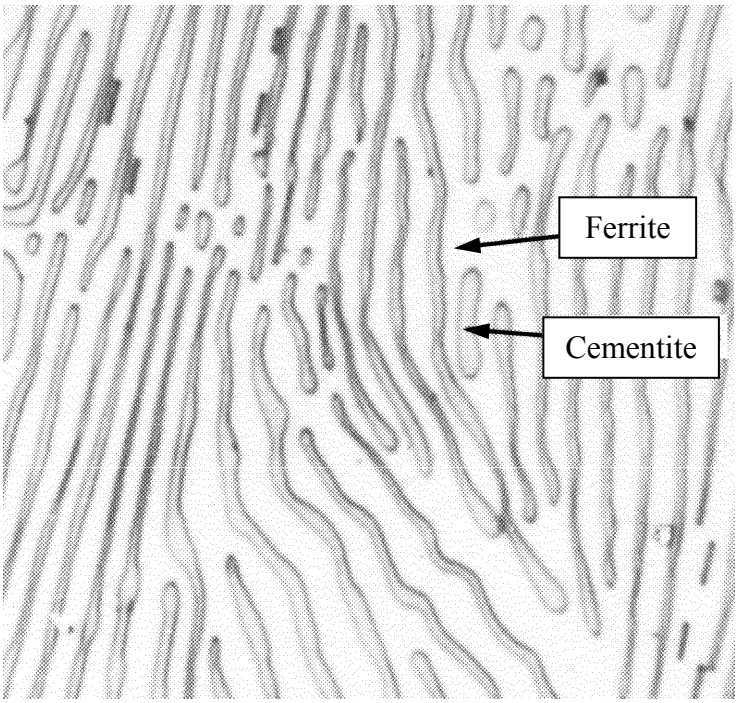

Figure 2.2: Pearlite 2500x, Enlarged 1.9x in Printing; Courtesy of U.S. Steel Corporation Research Laboratory (Avner 1974)

Figure 2.3: Cold-Drawn Prestressing Steel (Longitudinal) 1070x, Nital Etch (current study)

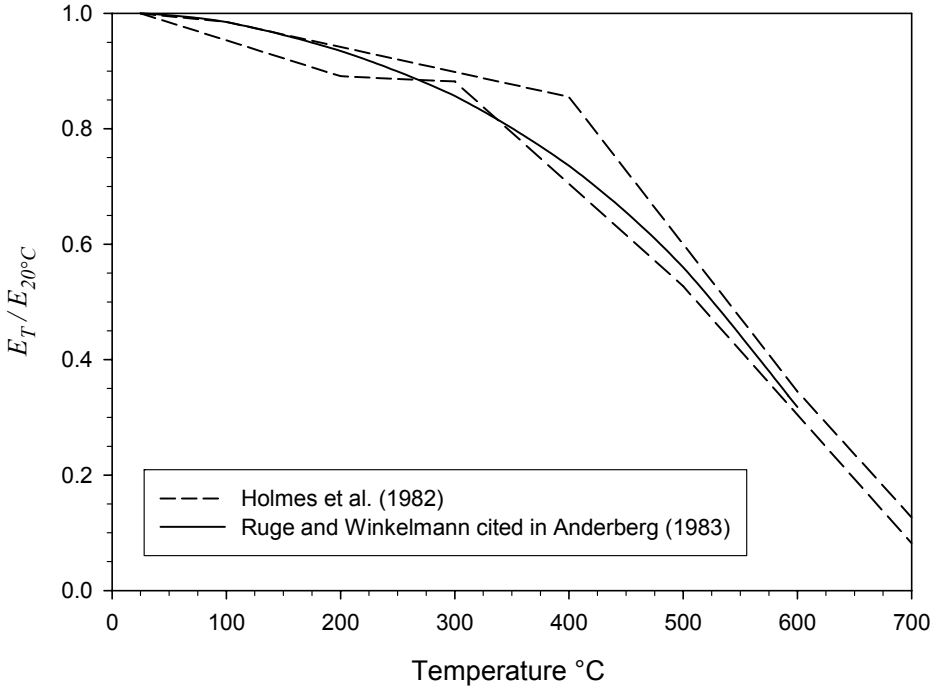

Figure 2.4: Reduction of Elastic Modulus in Cold-Drawn Steel at Elevated Temperatures (Anderberg 1983; Holmes et al. 1982)

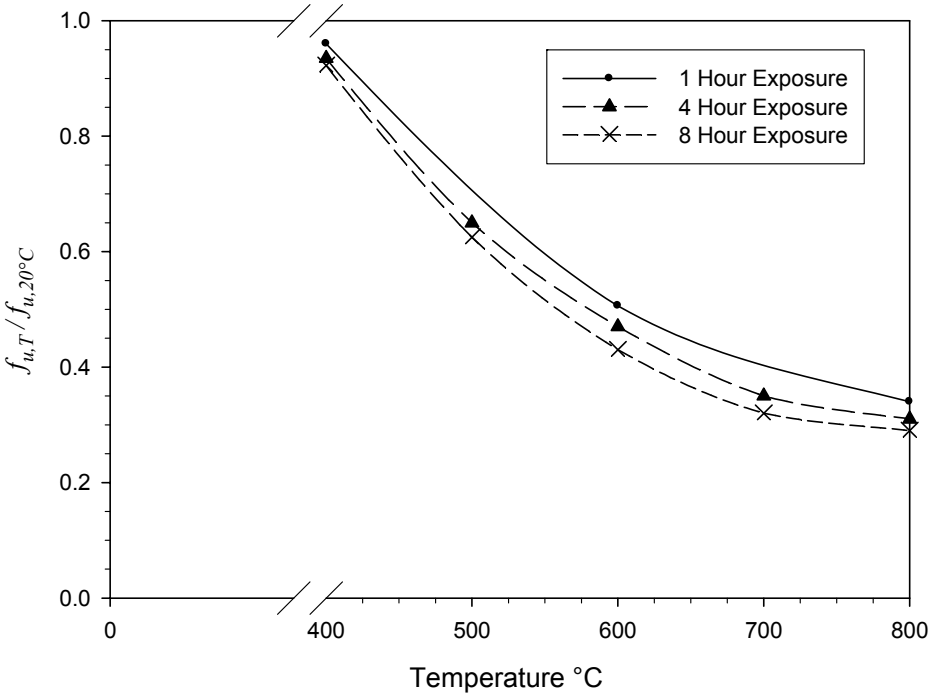

Figure 2.5: Variation of Residual Ultimate Tensile Strength in Prestressing Steel as a Function of Exposure Time (Abrams and Erlin 1967)

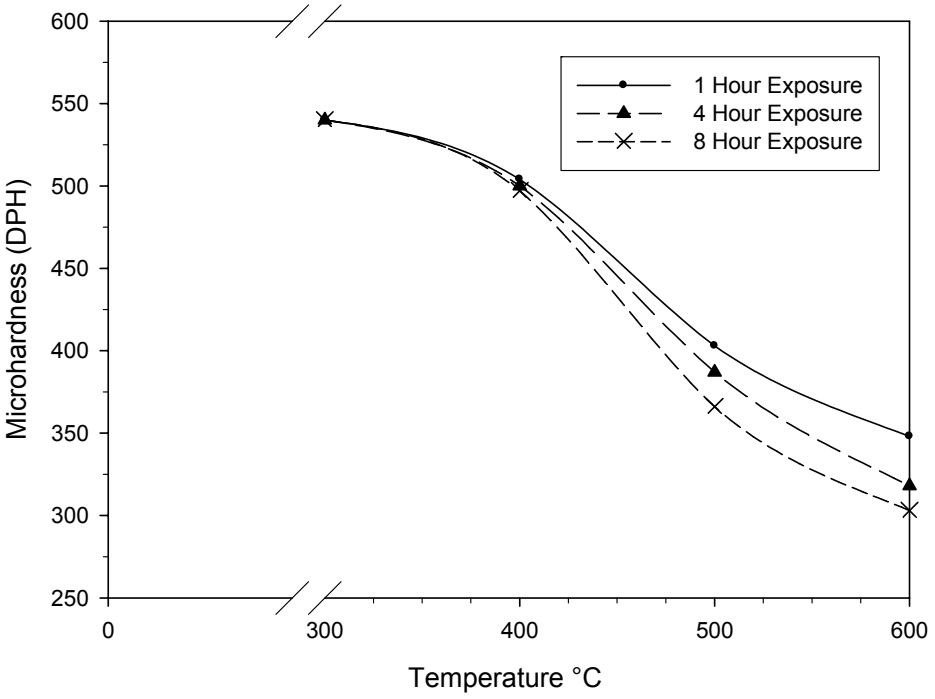

Figure 2.6: Variation of Residual Hardness in Prestressing Steel with Temperature (Abrams and Erlin 1967)

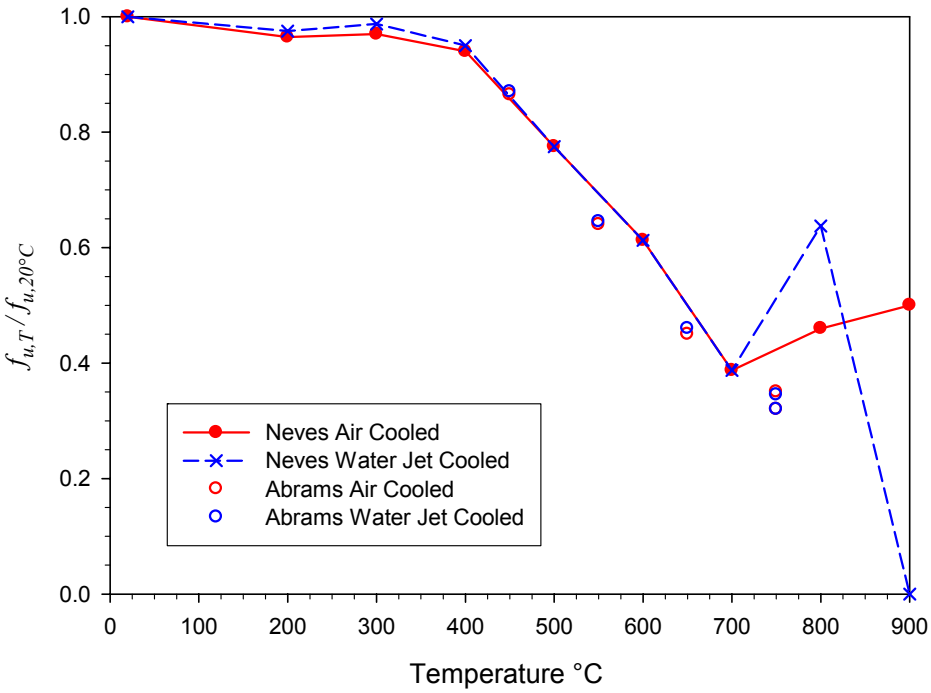

Figure 2.7: Variation of Residual Ultimate Tensile Strength in Prestressing Steel as a Function of Cooling Regime (Abrams and Cruz 1961; Neves et al. 1996)

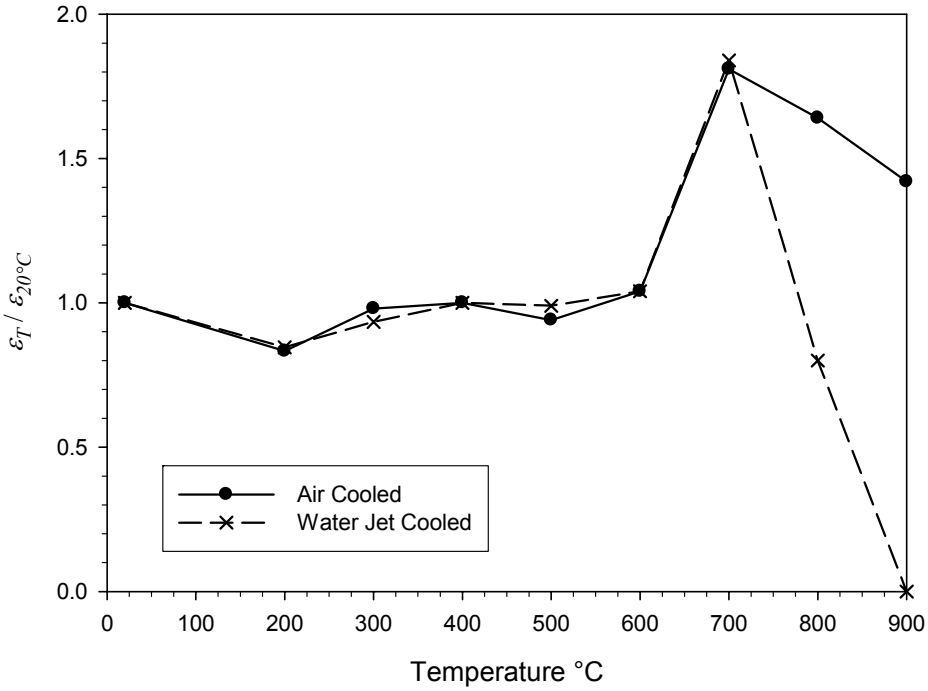

Figure 2.8: Variation of Residual Strain at Rupture in Prestressing Steel as a Function of Cooling Regime (Neves et al. 1996)

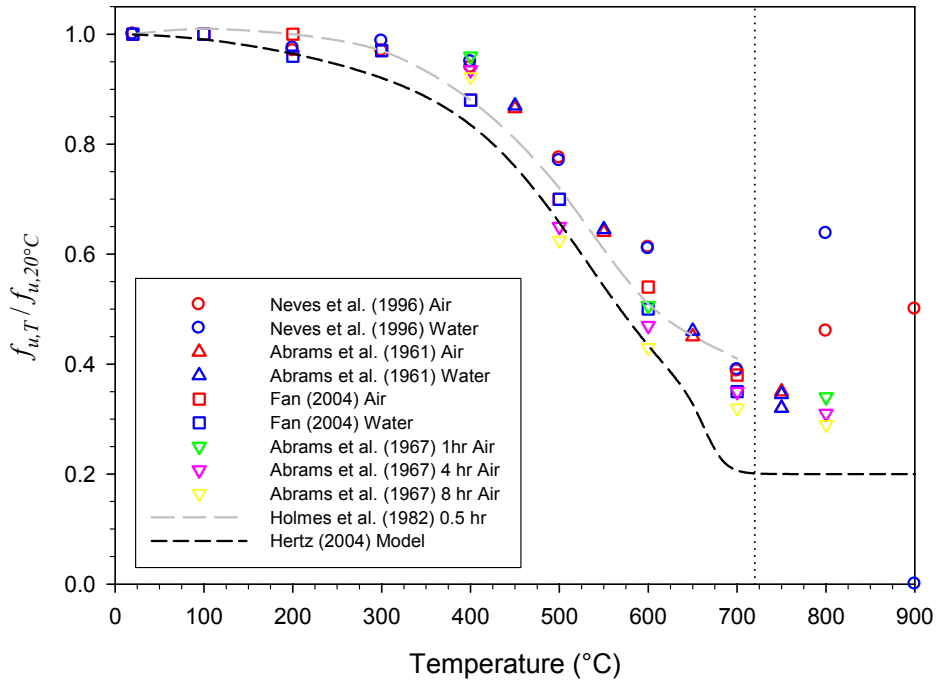

Figure 2.9: Summary of Residual Ultimate Tensile Strength in Prestressing Steel as a Function of Temperature

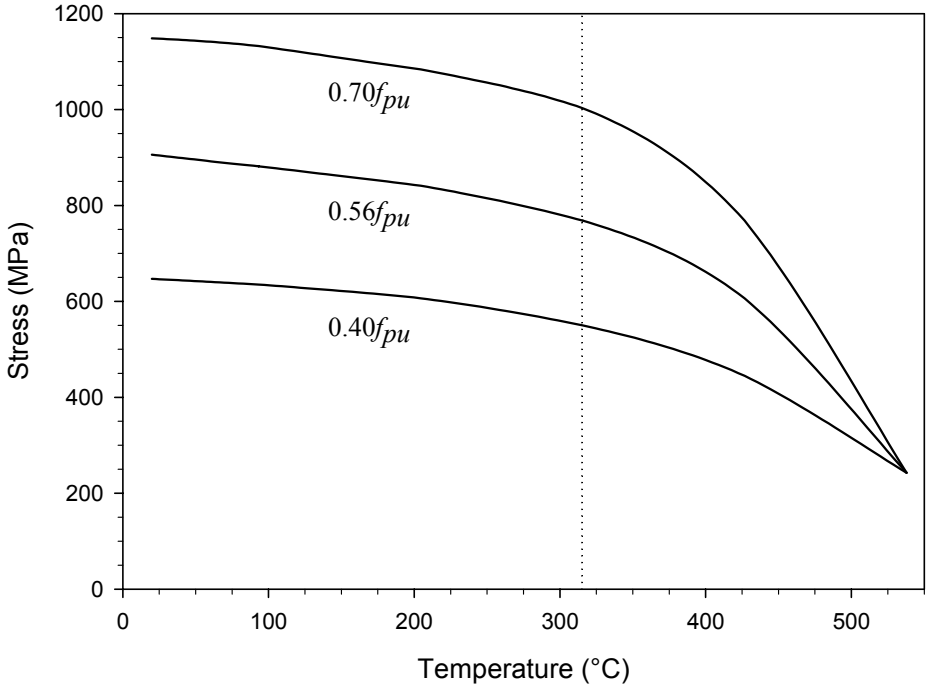

Figure 2.10: Reduction in Prestress as a Function of Temperature and Level of Prestress (Abrams and Cruz 1961)

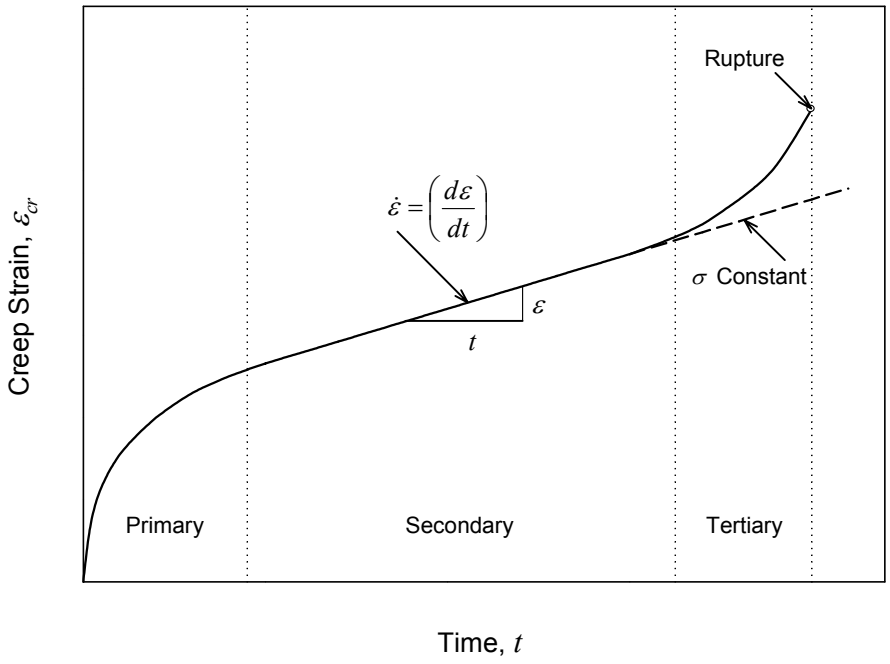

Figure 2.11: Typical Creep Behaviour under Constant Load (Dowling 1998)

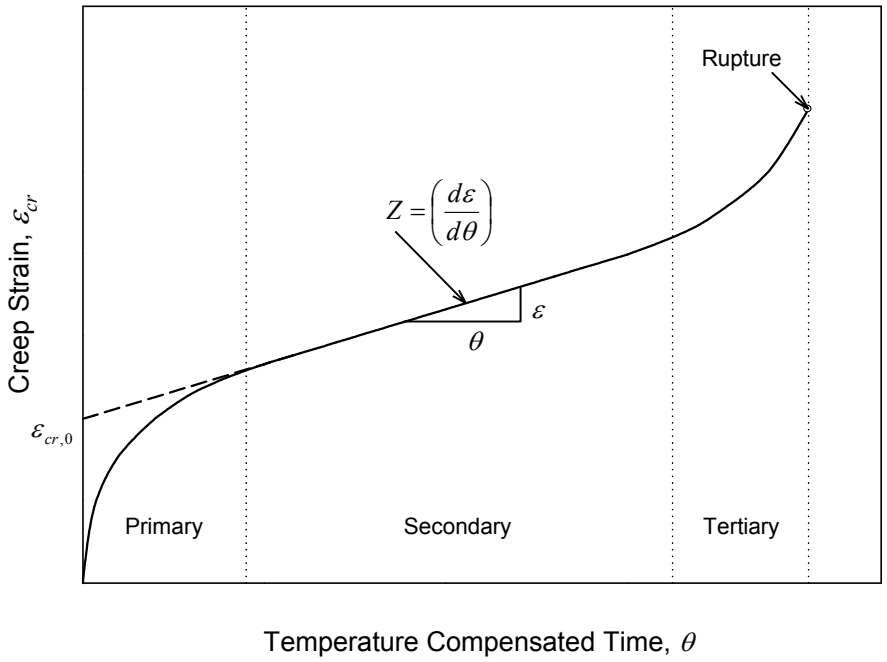

Figure 2.12: Elevated Temperature Creep Behaviour under Constant Load (Anderberg 1988)

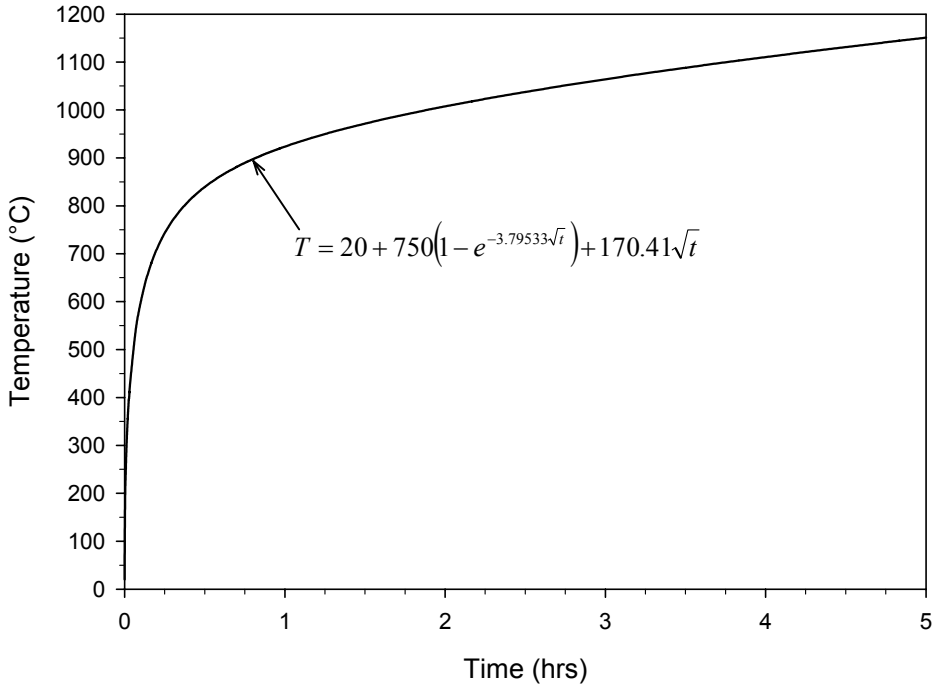

Figure 2.13: ASTM E-119 (ASTM 2001d) / CAN/ULC S101 (ULC 1989) Standard Fire Curve

CHAPTER 3 – Residual Properties of Cold-Drawn Prestressing Steel after Exposure to Elevated Temperatures

3.0 General

The comprehensive review of literature presented in Chapter 2 of this thesis indicated that little recent data exist which describe the residual strength and relaxation behaviour of cold-drawn prestressing steel exposed to elevated temperatures. In this chapter, the design of a high-temperature electric tube furnace, capable of integration within an existing prestressing bed, is described. This furnace allowed for up to six unstressed seven-wire strand specimens to be heated to temperatures in excess of 700°C. When used in conjunction with the rigid frame of the prestressing bed, a single seven-wire strand could be stressed to service load levels and heated while stressed, as described in detail in Chapter 4 of this thesis.

The current chapter provides an overview of the furnace operation, followed by a description of individual wire removal from seven-wire strands and of testing procedures to obtain data on the residual material properties of the prestressing steel after exposure to elevated temperatures.

3.1 Materials and Test Methods

3.1.1 Materials

Currently, unbonded post-tensioned slabs in North America typically utilize 13 mm nominal diameter ASTM A416 (ASTM 2001b) Grade 1860 low-relaxation seven-wire strand (Chacos 1988; Schupack 1994; Schupack 2001). A continuous coil of this material was acquired from Precon Inc., a precasting company in Brampton ON, and was used for all test series discussed herein. The chemical composition of the strand was

determined by an independent testing laboratory (Bodycote Testing) and is presented in Table 2.1. In addition, the ultimate tensile strength of the strand was determined at room temperature prior to elevated temperature exposures.

3.1.2 Heat Treatment Procedure

The heat treatment of all specimens tested in the unstressed-while-heated testing series was comprised of three distinct phases: ramp; soak; and cooling (see Figure 3.1). In the ramp phase, the surface temperature of specimens was increased at a rate of approximately 10°C / min. from room temperature (taken to be 20-25°C) to a predetermined set-point temperature. This heating rate was selected in order to prevent thermal shock in the specimen and is consistent with previous studies of the residual material properties of cold-drawn prestressing steel (Abrams and Cruz 1961; Abrams and Erlin 1967; Neves et al. 1996). Furthermore, it should be noted that in the case of a real fire in a post-tensioned concrete building (with adequate concrete cover to the reinforcement) concrete cover insulates the reinforcement, thus preventing direct exposure to rapid increases in ambient temperature which are observed during standard fires (ASTM 2001d). Indeed, a heating rate of 10°C / min. is roughly representative of expected heating rates for steel reinforcement protected by 20 mm to 40 mm of concrete cover when exposed to a standard fire, as would be the case in most building applications (see Table 2.8).

Once the predetermined set-point for each thermal treatment batch of specimens was reached, the temperature was held constant for a soak time of 90 minutes. This duration of elevated temperature soak exposure time was selected to ensure even temperature distribution within the furnace, and also corresponds to typical fire endurance

ratings of restrained unbonded floor slabs with minimum concrete cover (19 mm), as presented in Table 2.8. The soak time selected also falls within the range of those investigated in similar studies (Abrams and Cruz 1961; Abrams and Erlin 1967; Fan 2004; Holmes et al. 1982; Neves et al. 1996).

Finally, the cooling rate of specimens was not controlled and was governed by the insulating characteristics of the furnace used. In all cases the rate of cooling observed was much lower than the 10°C / min. heating ramp rate used (see Appendices A and B). As none of the specimens tested achieved peak temperatures above the eutectoid transformation point for 0.8% carbon by weight steel (as studied herein), no significant quenching affects (i.e., the formation of martensitic grain structures upon rapid cooling) were expected (Krauss 1989). Therefore, as noted in Chapter 2, the effects of cooling rate are reasonably assumed not to have caused any observable variation in residual mechanical properties.

3.1.3 Design and Fabrication of High-Temperature Electric Furnace

Since no furnaces in the Department of Civil Engineering were large enough to encase lengths of strand appropriate for standard tension testing, and because shorter available muffle furnaces could not achieve the precision of temperature control desired, a custom strand heating unit was designed and fabricated for the current study.

The furnace constructed was a radiant-type electric ceramic tube furnace utilizing two semi-cylindrical units having helically wound ribbon resistance coils vacuum formed in low mass ceramic fibre. Both semi-cylindrical units were purchased from Omega Scientific (model CRRS-247/240-A) and were placed together to form a complete cylinder (see Figure 3.2). The ceramic cylinder was then surrounded by approximately

50 mm of Unifrax Durablanket-S ceramic fibre blanket and clamped to a steel base-plate with two large steel rings. A rectangular steel casing with two openings approximately 230 mm in diameter was then bolted to the base-plate, and voids between the cylindrical furnace and rectangular steel enclosure were packed with additional ceramic fibre blanket for further insulation and to prevent heating of the outside surface of the steel casing (see Figure 3.3). The 50 mm space between the end of the heating cylinders and the ends of the steel casing was plugged with ceramic blanket, packed tightly against specimen ends. Finally, electric leads were drawn through two openings in the sides of the furnace casing and into two electrical panels bolted to the case's exterior. With the two coil units wired together, a heavily insulated cord with cabtie (twist-lock) type connector was used to attach the furnace to a high-voltage control panel located on an adjacent column in the laboratory (see Figure 3.4).

Temperature regulation was achieved using a custom control panel containing an Omega Scientific model SSRL240DC50 solid state relay (SSR). This relay was driven by a 10V direct current pulse output from a digital control box, integrated with a personal computer. The control panel was also equipped with 50 amp fast blow fuses, to protect from electrical short-circuits, and a solenoid and switch driven by an alarm output from the digital control box. Note that in the event that the SSR failed in a closed position, the solenoid and switch would de-energize the system after receiving a high-temperature alarm from the controller. A complete schematic of the control panel is shown in Figure 3.5.

An Omega Scientific model CNi3243-C24 programmable proportional-integral-derivative (PID) controller was used to drive the solid state relay through a 10 V direct current pulse output. The controller was connected to the serial port of a personal

computer, allowing for settings to be programmed using software provided by the manufacturer. The process variable (temperature) was monitored using a Type-K thermocouple mounted on the surface of one of the specimens. Specimen layout and instrumentation within the furnace are discussed in detail in the following section.

With all of the components in working order, the programmable controller was manually tuned to minimize overshoot and droop at the transition from ramp to soak modes for a set-point of 400°C. This temperature was selected as it constitutes the approximate midpoint of the temperatures being examined (200°C to 700°C). A physical representation of overshoot and droop is shown in Figure 3.6.

Once appropriate control parameters were selected, a series of preliminary tests were conducted to quantify the longitudinal thermal profile of the heating chamber. In these tests a single instrumented strand was placed along the centerline of the furnace, with the surface-mounted controller thermocouple at its midpoint. Additional thermocouples were positioned along the length of the strand and temperature readings recorded during ramp, soak, and cooling phases. It was found that the temperature along the 200 mm gauge length used in tension testing could be adequately controlled given the current furnace configuration and controller settings (see Appendix A).

Note that the functioning furnace unit, as designed and fabricated by the Author, can achieve maximum temperatures in the range of 900°C, and has been certified for use up to 800°C. The maximum power output of the unit was rated at 6400 W which draws 31 amps nominally at 210 VAC. To ensure safety, all fuses and relays used were rated for 50 amps.

3.1.4 Specimen Preparation – Heat Treatment

A total of 41 test samples were prepared and were divided into several batches for this test series. Six specimens were heated simultaneously for each of the (six) elevated soak temperatures investigated. An additional five specimens were not heat treated and were used as a control group.

For each elevated temperature exposure two standard NIST Type-K thermocouples, of precision ± 1.7°C at 427°C (as provided by the manufacturer), were placed on five of the specimens; one at the midpoint and the other at a distance of 100 mm ± 5 mm from the midpoint. These thermocouples provide a measure of the difference in temperature from the midpoint to end of each specimen's gauge length, assuming symmetry about the centerline of the furnace (as was verified in characterization testing on the furnace described in the previous section and as noted in Appendix B). The thermocouples were continuously monitored using a 16-bit digital data acquisition system (Vishay Measurements Group System 5000) recording data at a frequency of 1 Hz. The remaining (sixth) specimen had one standard NIST Type-K thermocouple placed at its midpoint, which was used to control the process variable by providing feedback to the furnace controller. The tip of each thermocouple was pressed between two of the individual wires comprising the seven-wire strand through clamping pressure exerted by a stainless-steel hose clamp attached to a bend in the insulated portion of the thermocouple wire. This configuration had the effect of spring loading the thermocouples to each specimen to prevent loss of surface contact during heating.

The strand specimens were subsequently positioned in the furnace using an adjustable jig and centered on the heating coils (shown in Figures 3.3 and 3.4). Once

positioned, the outer edge of each specimen was approximately 45 mm ± 5 mm away from the heating coils. This configuration was selected in order to maximize the spacing between each specimen, to allow for even heating, yet maintain a reasonable distance from the heating coils to prevent localized hot-spots. Finally, all specimens were rotated such that each thermocouple was diametrically opposite the inner surface of the furnace (see Figure 3.7).

With specimens instrumented and properly positioned, the furnace temperature was increased at a rate of 10°C / min. to one of six predetermined set points of 200°C, 300°C, 400°C, 500°C, 600°C, or 700°C, and the temperature was held constant for 90 minutes. The furnace was then turned off to allow slow cooling to room temperature. Temperature-time profiles of five of the six specimens were recorded simultaneously using the digital data acquisition system. Experimental temperature-time data (maxima and minima within gauge length) for each specimen is provided in Appendix B.

Once controlled heating and slow cooling were complete, the core wires from each of the five specimens having designations S1, S2, S3, S4 and S6, as defined in Figure 3.7, were removed and tested in tension to failure in accordance with ASTM A370-01 A4 (ASTM 2001a). The remaining (sixth) specimen, having designation S5 and whose thermocouple was attached to the model CNi3243-C24 controller, was used to prepare a standard metallographic mount to examine any microstructural changes resulting from each heat treatment.

3.1.5 Tension Testing – Gripping

Tension testing of seven-wire strand is difficult as the ultimate tensile strength of the material is much higher than that of mild steel (i.e., 1860 MPa as opposed to

400 MPa), but the diameter of helically wound outer wires is only a third of the overall strand diameter. As a result, deep notching in the specimen caused by the use of standard serrated mechanical wedge grips can lead to high stress concentrations and premature failure of the strand within the grips. ASTM A370-01 A7 addresses the difficulty of testing multi-wire strand by suggesting the use of smooth bore mechanical grips or by incorporating conventional standard V-grips with cushioning material, soft metal, or high-strength epoxy to reduce indentations (ASTM 2001a).

It was initially hoped that it would be possible to conduct tension tests on intact strands. However, because of inherent difficulties in testing seven-wire strand a series of gripping tests were performed using special cylindrical wedge grips with smooth, semi-cylindrical grooved faces. The grips were comprised of two tapered wedges with a smooth semi-cylindrical bore of constant diameter. With the strand in place, the wedges were forced into a large tapered cylinder (mechanically) by pretensioning bolts to adjust an end plate bearing on the wedges. Once the wedges were embedded (seated) in the cylinder, a corresponding clamping force was exerted on the strand.

In each of the tests (eight trials in total), pullout of the strand occurred at load levels between 25% and 40% of the strand's specified ultimate tensile strength. An insufficient amount of gripping friction between the strand and wedges was likely the cause of pullout at such low load levels. To correct this problem, ASTM (2001a) suggests the use of high friction slurry such as aluminum oxide mixed with water or glycerin to coat the strand-grip interface. However, due to the inherent inconsistency in applying such a coating from one specimen to another it was decided that standard wedge action V-grips would be attempted to be used.

Three tension tests were performed on 13 mm diameter seven-wire strand using standard V-grips (wedge action) with serrated teeth (fitted into a screw driven universal test frame). An integrated load cell having a known precision of ± 0.7% in the range of 100 kN to 200 kN was used to monitor load at rupture.

In the first test, no cushioning material was applied. In the second and third tests, an increasing amount of aluminum tape was used as cushioning material. All of the specimens failed prematurely within the grips. The largest load carried at rupture by any of the specimens was 181 kN ± 1.3 kN, which is below the minimum acceptable ultimate tensile load for 13 mm diameter Grade 1860 strand of 183.6 kN (CPCI 1996). Upon removal of the strand samples from the grips, heavy notching was observed in close proximity to the rupture path. It was concluded that tension testing using seven-wire strand could not be performed reliably given the available testing facilities (specifically grips).

Finally, the approach used by Neves et al. (1996) was adopted, wherein straight core wires were removed from seven-wire strand and tested in tension using small standard wedge action V-grips with fine serrated teeth. Tests were performed in accordance with ASTM A370-01 A4 with a 200 mm gauge length (ASTM 2001a). The reader should note that it appears from literature that previous studies regarding effects of temperature on prestressing strand have also performed tests on core wires in isolation for the same reasons cited above.

Five tension tests were performed on 4.4 mm nominal diameter core wires using standard wedge action V-grips (with fine serrated teeth fitted) in a screw driven 45 kN maximum capacity universal testing frame. An integrated load cell having a known

precision of ± 1.0% in the range of 0 kN to 45 kN was used to monitor load. Rupture of all five core wire specimens occurred within the middle third of the specimen well away from the grips. The average stress at rupture was 1953.5 MPa with a standard deviation of 9.8 MPa. Since the results of these preliminary tests were deemed to be consistent with expected ultimate tensile strength of the material used, and since they were shown to be repeatable, the core wire testing method was utilized in all further tensile coupon tests. Note that neither the test frame nor the load cell used were the same as those used in the previously mentioned trials of large diameter V-grips for seven-wire strand.

3.1.6 Tension Testing – Procedures

As mentioned previously, a total of 35 seven-wire strand specimens were prepared for tension testing and an additional six specimens were used to fabricate metallographic mounts. With the predetermined amount of heat treatment provided as described previously in Section 3.1.4, helical outer wires were removed and the core wire was cut to create a coupon approximately 430 mm in length. This enabled a 200 mm gauge length to be used with a clear space of one grip length between the edge of the gauge length and the 25 mm long wedge grips used, as specified by ASTM A370-01 A4 (ASTM 2001a). An additional 13 mm of the core wire coupon was allowed to protrude from the unloaded end of each grip to allow for potential slippage during seating of the wedges.

The grips were fitted into the same screw driven 45 kN universal testing frame described previously. Again an integrated load cell having a known precision of ± 1.0% in the range of 0 kN to 45 kN was recorded continuously using a 16-bit digital data acquisition system (Vishay Measurements Group System 5000). An externally mounted

Novotechnik model TRS 100 linear potentiometer, having a precision of ± 0.08 mm, was used to monitor crosshead speed and grip slippage.

With the specimen positioned in the grips, a 200 mm MTS series 632 electronic extensometer, having a precision of ± 0.05 mm, was attached to specimen surface using mounting springs and knife edges. Note that two drops of quick set epoxy were placed on the specimen surface to help seat extensometer knife edges and to prevent slippage (see Figure 3.8).

Finally, a crosshead speed of 2 mm / min. was selected and applied to the specimen throughout the duration of the test (based on ASTM A370-01). The extensometer was removed after yielding and prior to specimen rupture to prevent damage to the equipment. In all cases, a minimum extension of 6 mm (representing a strain 0.03 mm/mm) was achieved before removal of the extensometer.

3.1.7 Metallographic Analysis

Upon the completion of each level of heat treatment, a standard metallographic mount was prepared by encasing in bakelite thermoplastic a short length of specimen removed from directly below the tube furnace's control thermocouple (specimen S5 in Figure 3.7). Using coarse abrasives, the mount thickness was reduced such that the specimen's centre cross section in the longitudinal direction was exposed (ground until longitudinal and transverse specimens on each mount approximately the same width). A series of increasingly fine abrasives were subsequently used to polish the specimen in preparation for etching. Several different etches were used; however, it was found that the best results were obtained with a 3% Nital solution. Grain structure images were captured using a charge-coupled device (CCD) digital camera integrated with an optical

microscope; several different magnifications were investigated: 107x; 215x; 430x; and 1070x. The atypical magnification increments used resulted from the interplay between the CCD camera's lens and the microscope lens.

Upon the completion of microscopy, the Rockwell C hardness of each specimen was determined using the metallographic mounts. These hardness tests were performed using a Wilson 150 Rockwell C tester.

3.2 Results

3.2.1 General

Through experimentation, exposure of cold-drawn prestressing steel to elevated temperatures above 300°C was shown to affect the steel's mechanical properties. This section reports the results of post high temperature standard tension tests to demonstrate the effect of heating on the residual ultimate tensile strength, modulus of elasticity, 0.2% offset yield strength, and strain at rupture of heavily cold-worked eutectoid prestressing steel. Additionally, residual Rockwell C hardness data and metallographic analysis, showing corresponding changes in grain structure, are reported.

3.2.2 Ultimate Tensile Strength

Tension tests of prestressing wire coupons exposed to varying levels of elevated temperature exposure indicate that no appreciable loss of ultimate tensile strength occurred below a temperature of 300°C (see Figure 3.9). After exposure to a temperature of 400°C, a seven percent reduction in average ultimate tensile strength was observed, signifying the onset of microstructural changes in the material. After exposure to temperatures in excess of 400°C, ultimate tensile strength was shown to decrease rapidly

(see Table 3.1). After exposure to temperatures of 700°C (close to the eutectoid point of 720°C), ultimate tensile strength was reduced to approximately 770 MPa, or approximately 38% of the unheated ultimate tensile strength. It is widely known that pearlitic steels which have not been strain hardened typically have ultimate tensile strengths of approximately 830 MPa (Avner 1974). Therefore, as expected, heating the prestressing steel specimens near to the eutectoid transformation temperature apparently results in significant recrystallization effects as the grain growth phase is initiated. This results in tensile strengths comparable to pearlite which has not been cold-worked.

The maximum standard deviation of ultimate tensile strength in any given batch of specimens was determined to be approximately 16 MPa for specimens heated to 400°C and 500°C (shown in Table 3.1). This results in a coefficient of variation (*cv*) of 1.03% for the residual ultimate tensile strength at 500°C. Furthermore, the remaining experimental values of ultimate tensile strength were found to have a maximum coefficient of variation of 1.00%. These results indicate little variation in experimental results; see Appendix C for further discussion and analysis of variance (ANOVA) between different heat treatments.

3.2.3 Modulus of Elasticity

The elastic modulus of each specimen was determined by isolating a portion of data from the linear elastic region of the stress-strain curve (between 15% and 85% of the specimen's 0.2% offset yield strength) as described in detail in Appendix C. It was found that the temperature to which the prestressing steel was exposed, up to a maximum of 700°C, had little effect on the steel's post-heated residual modulus of elasticity (see Table 3.2). This is as expected given the relative insensitivity of tensile elastic

modulus to grain structure for metals of similar chemical composition, as resistance to stretching is known to be heavily influenced by atomic bond strengths rather than grain structure (Dowling 1998).

Note that, the variation exhibited in modulus data was found to fall within the maximum experimental uncertainty calculated (see Table 3.2). Therefore the slight increase in modulus exhibited after heating could not be demonstrated to be significant (see Appendix C for ANOVA).

3.2.4 Offset Yield

The previously calculated elastic modulus of each specimen was used to graphically determine the 0.2% offset yield. As was found for ultimate tensile strength, no significant loss of yield strength occurred for exposure temperatures below 300°C (see Appendix C for ANOVA). After exposure to 400°C, a 9% reduction in average 0.2% offset yield strength was observed, while after exposure to temperatures greater than of 400°C, residual offset yield strength decreased rapidly (see Table 3.3). The relative amount of offset yield strength loss at each temperature was observed to decrease at a similar rate as ultimate tensile strength (see Figure 3.10). When examining the discrete stress-strain relationship for a particular specimen (S2 in Figure 3.11 for example), it is clear that an increase in exposure temperature shifts both the yield plateau and ultimate tensile strength downward. Additionally, a flatter, more defined yield plateau, characteristic of steel with little cold-working, was exhibited with increasing exposure temperatures (see Figure 3.11). Recalling the information presented in Chapter 2 of this thesis, the observed behaviour is consistent with previous work in this area.

The maximum standard deviation for 0.2% offset yield strength in any given batch of specimens was determined to be 18.3 MPa for the specimens heated to 300°C (shown in Table 3.3). This results in a coefficient of variation of 0.98%. Furthermore, the remaining experimental values of 0.2% offset yield strength were found to have a maximum coefficient of variation of 1.01%. These results indicate little variation in experimental results (see Appendix C).

3.2.5 Strain at Rupture and Rockwell C Hardness

The tensile strain at rupture, as measured from overall elongation of failed specimens over their initial gauge length (200 mm), was observed to increase dramatically after temperature exposures of 700°C (see Table 3.4). This can be attributed to recrystallization and some new grain growth in the steel's microstructure at these temperatures, thus increasing its capacity for plastic deformation. It should be noted that the precision in measuring strain at rupture was low as a result of several factors as discussed in Appendix C. Consequently, less emphasis should be placed on specific values of residual strain at rupture, but rather on the overall trend shown (see Appendix C for ANOVA).

The initiation of recrystallization was also evident in the Rockwell C hardness data obtained from the specimens mounted for metallographic analysis. For specimens UH5, 200-5, and 300-5, hardness was determined to be RC54, with a slight decrease in hardness observed for specimens 400-5 and 500-5 to RC52 and RC50 respectively. At 600°C (600-5) hardness was seen to decrease drastically to RC41, and ultimately to RC26 for specimen 700-5.

3.2.7 Grain Structure

Finally, a series of metallographic photos were taken using an optical microscope in order to help illustrate microstructural changes caused by the application of heat energy. Examination of unheated specimens, and specimens experiencing relatively mild heat treatments (i.e., exposure temperatures 200°C, 300°C and 400°C) revealed long, well defined grains running parallel to one another across the field of view (see Figures 3.13 to 3.16). Specimens heated to 500°C and 600°C began to exhibit a finer structure having less well defined longitudinal grains (Figures 3.17 and 3.18), while the specimen heated to 700°C had a large fraction of fine grains, indicating the recrystallization and new grain growth (of pearlite) within the metal's microstructure (see Figure 3.19). The temperature exposures after which noticeable changes in grain structure occurred appeared to correlate well with exposure temperatures where the most significant increases in strain at rupture and the most significant decreases in Rockwell C hardness were observed. This further indicates that significant recrystallization and new grain growth had occurred.

It should be noted that all metallographic specimens shown in Figures 3.14 to 3.19 were removed from the core wire of strand coupons designated S5 as noted in Figure 3.7. As such, the longitudinal samples displayed in Figures 3.14 to 3.19 were extracted from a length of strand in direct contact with the PID controller thermocouple.

3.3 Discussion

The results discussed herein serve to demonstrate the reductions of the cold-working effects on a common grade of commercial prestressing steel strand with increases in short term exposure temperature. Degradation in the most important

mechanical properties occurred as a result of the well known thermodynamic instability of work hardened metals. For these types of metals, the application of heat allows the material to revert to a lower energy state with inferior mechanical properties.

A summary of residual ultimate tensile strength data consolidated from literature, in addition to the residual ultimate tensile strength data obtained in the current study, is shown in Figure 3.12 and illustrates a consistent trend in reduction of ultimate tensile strength with exposure temperature for a large variety of samples from around the world. This figure clearly indicates that currently used North-American prestressing steels such as that studied herein behave similarly to steel used in Europe (Hertz 2004; Neves et al. 1996), China (Fan 2004), and to steels used circa 1960 in the United States (Abrams and Cruz 1961; Abrams and Erlin 1967).

In further examining Figure 3.12 it should be noted that the only available predictive model for the residual ultimate tensile strength of prestressing steels, described by Hertz (2004), appears to be conservative with respect to the available data, particularly at higher temperature exposures (above 300°C). The Hertz expression would thus serve as an appropriate lower bound for engineers evaluating fire damaged post-tensioned slabs; however, it fails to accurately represent the data collected to date. As such, an alternate curve of simpler formulation is proposed below for use in predictive modeling of structural response to high temperature exposures:

$$f_u(T) = 0.25 + \frac{0.75}{1 + \left(T/550\right)^{6.5}} \tag{3.1}$$

where $f_u(T)$ is the ratio of ultimate tensile strength after a given temperature exposure to ultimate tensile strength at 20°C and T is temperature in Celsius. The remaining coefficients were determined using regression analysis of all data cited herein from 20°C

to 750°C with data points at 800°C omitted since this temperature is well above the eutectoid transformation temperature (i.e., large jump in tensile strength of some data above eutectoid point deemed erroneous). The resulting function is seen to exhibit a reasonable fit to the data analyzed (again, see Figure 3.12), and was found to have an R^2 parameter of 0.9824.

Figure 3.10 shows the results of the current study for residual ultimate tensile strength, residual 0.2% offset tensile yield strength, residual tensile modulus of elasticity, and residual strain at failure, with average data for each five-sample treatment normalized with respect to the room temperature average values and plotted versus exposure temperature. The data from the current study agree very well with the available literature (see Chapter 2), and indicate that no significant loss of either ultimate tensile or 0.2% offset yield strength occurred below an exposure temperature of 300°C (see Appendix C for ANOVA). After exposure to a temperature of 400°C, the data indicate a 7% reduction in the residual tensile ultimate/yield strength, signifying the beginning of thermally-induced microstructural changes in the cold-drawn metal. After exposures above 400°C, tensile ultimate strength and yield strength began to decrease rapidly with increasing exposure temperature. After exposures at 700°C (i.e., approaching the steel's eutectoid point), ultimate tensile strength was reduced to approximately 770 MPa, or about 38%, of the unheated values. As expected, heating specimens near to the eutectoid transformation temperature in the current study caused significant recrystallization effects as the grain growth phase is initiated, resulting in tensile strengths comparable to non-cold-worked pearlite.

Finally, it is widely known that correlation exists between the ultimate tensile strength of steel and its Rockwell C hardness. It may, therefore, be thought that in-situ hardness testing could serve to help determine the degree to which strand has deteriorated due to elevated temperature exposure after a severe building fire. However, due to the relative similarity in hardness exhibited at temperatures below 600°C, and the impracticality of performing hardness tests on small diameter wires (in an overhead inspection condition), it was deemed that this approach would offer little useful information to aid the engineer in inspection of fire damaged unbonded post-tensioned slabs.

3.4 Summary

Cold-drawn prestressing steel exposed to temperatures below 300°C exhibited no significant changes in mechanical properties, whereas specimens exposed to temperatures in excess of 400°C exhibited marked changes in both mechanical properties and grain structure. Consequently, it is recommend that unbonded tendons suspected to have experienced temperatures in excess of 300°C should be replaced or considered damaged when determining the remaining capacity of unbonded post-tensioned members after a fire. Finally, the good correlation exhibited by Equation 3.1 to available and currently presented ultimate tensile strength data will aid engineers in effectively evaluating the likely condition of prestressing steel exposed to elevated temperatures during a building fire, as the duration and intensity of a particular compartment fire can be estimated using common techniques. An approximate estimate of compartment peak temperature and duration of burn (from fire department) can be used along with a standard finite difference heat transfer model, to be discussed in Chapter 5, along with the known depth

of concrete cover, to estimate the peak temperature experienced by the tendon; thereby allowing engineers to determine the extent of tendon material damage. However, the following chapters will demonstrate that the amount of material ultimate tensile strength reduction is not necessarily the only important factor to consider in the post-fire evaluation of unbonded post-tensioned reinforced concrete structures, as it is shown that both creep and relaxation effects also play important roles.

Table 3.1: Residual Ultimate Tensile Strength (f_{pu}) of Prestressing Wire in MPa

Temp.	S1	S2	S3	S4	S6	$\bar{x}$	s	$f_{u,T}/f_{u,20℃}$
20 °C	2022.9	2008.3	2008.4	2031.7	2026.0	2019.5	10.6	1.00
200 °C	2015.8	1985.9	2001.3	1999.3	2005.0	2001.5	10.8	0.99
300 °C	2015.0	1998.1	2027.2	1996.4	1994.0	2006.1	14.4	0.99
400 °C	1879.3	1887.9	1918.3	1903.2	1884.0	1894.5	16.0	0.93
500 °C	1538.4	1539.7	1570.0	1571.4	1553.0	1554.5	15.9	0.77
600 °C	1132.6	1137.6	1154.5	1162.5	1137.9	1145.0	12.8	0.57
700 °C	763.4	763.3	773.8	774.9	760.1	767.1	6.8	0.38

Experimental Uncertainty ± 20.2 MPa (See Appendix C)

Table 3.2: Residual Elastic Modulus (E) of Prestressing Wire in MPa

Temp.	S1	S2	S3	S4	S6	$\bar{x}$	s	$E_T/E_{20℃}$
20 °C	212590	213030	214770	215140	214650	214036	1144	1.00
200 °C	220460	226430	217680	216650	216830	219610	4106	1.03
300 °C	217730	217600	217120	218180	218040	217734	415	1.02
400 °C	218780	230810	224310	218240	218780	222184	5423	1.04
500 °C	219940	220090	220300	220700	220160	220238	289	1.03
600 °C	222860	222610	221080	223570	222840	222592	919	1.04
700 °C	219600	225700	224710	218730	225640	222876	3424	1.04

Experimental Uncertainty ± 28 851 MPa (See Appendix C)

Table 3.3: Residual 0.2% Offset Yield Strength (f_{py}) of Prestressing Wire in MPa

Temp.	S1	S2	S3	S4	S6	$\bar{x}$	s	$f_{y,T}/f_{y,20℃}$
20 °C	1839.2	1836.3	1836.3	1857.6	1844.7	1842.8	8.9	1.00
200 °C	1830.0	1799.5	1806.9	1810.9	1817.5	1813.0	11.5	0.98
300 °C	1878.4	1849.7	1888.0	1852.3	1849.4	1863.6	18.3	1.01
400 °C	1666.0	1668.2	1703.1	1684.5	1662.0	1676.8	17.0	0.91
500 °C	1406.5	1404.4	1428.9	1427.2	1418.8	1417.2	11.4	0.77
600 °C	1082.6	1094.3	1102.9	1108.7	1083.4	1094.4	11.6	0.59
700 °C	692.8	691.4	704.7	706.1	690.7	697.1	7.6	0.38

Experimental Uncertainty ± 20.2 MPa (See Appendix C)

Table 3.4: Residual Strain at Rupture (ε_u) of Prestressing Wire in % Strain

Temp.	S1	S2	S3	S4	S6	$\bar{x}$	s	$\varepsilon_T/\varepsilon_{20℃}$
20 °C	5.1	-	4.7	4.7	5.3	5.0	0.3	1.00
200 °C	5.3	4.9	5.3	4.4	5.3	5.0	0.4	1.00
300 °C	4.7	5.1	5.4	5.1	4.7	5.0	0.3	1.00
400 °C	4.7	5.1	4.9	4.9	4.9	4.9	0.1	0.98
500 °C	5.1	4.7	4.4	5.3	4.9	4.9	0.3	0.98
600 °C	6.0	5.6	5.1	5.6	5.6	5.6	0.3	1.12
700 °C	11.1	11.3	10.9	11.3	11.1	11.1	0.2	2.20

Experimental Uncertainty ± 0.25% strain (See Appendix C)

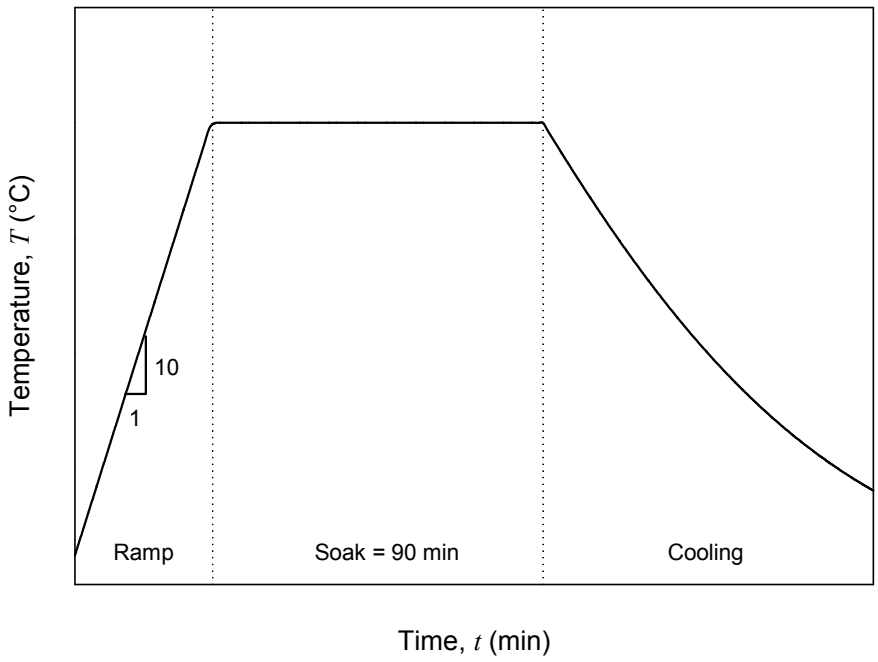

Figure 3.1: General Heat Treatment Temperature-Time Profile

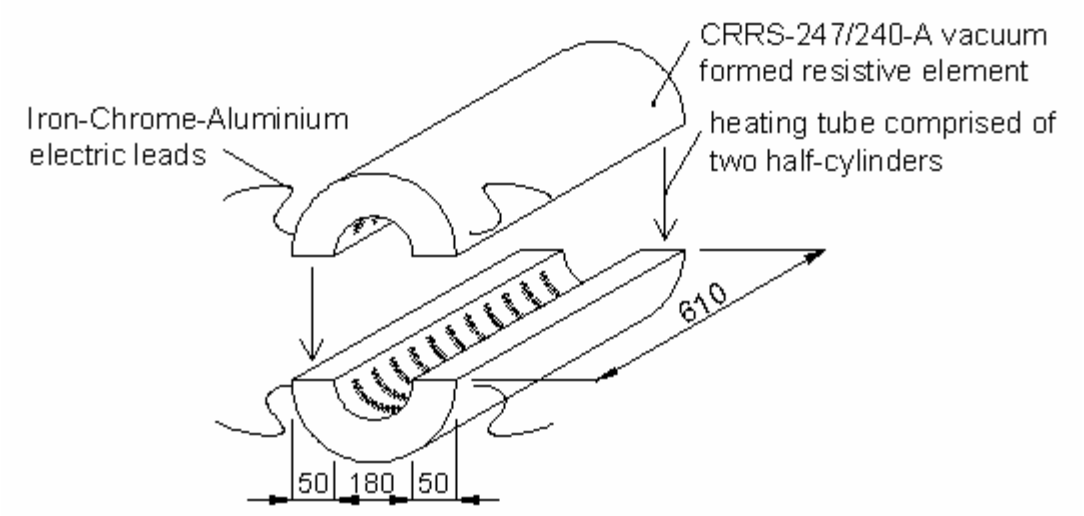

Figure 3.2: Omega Scientific CRRS-247-240-A Electric Resistance Elements (units in mm)

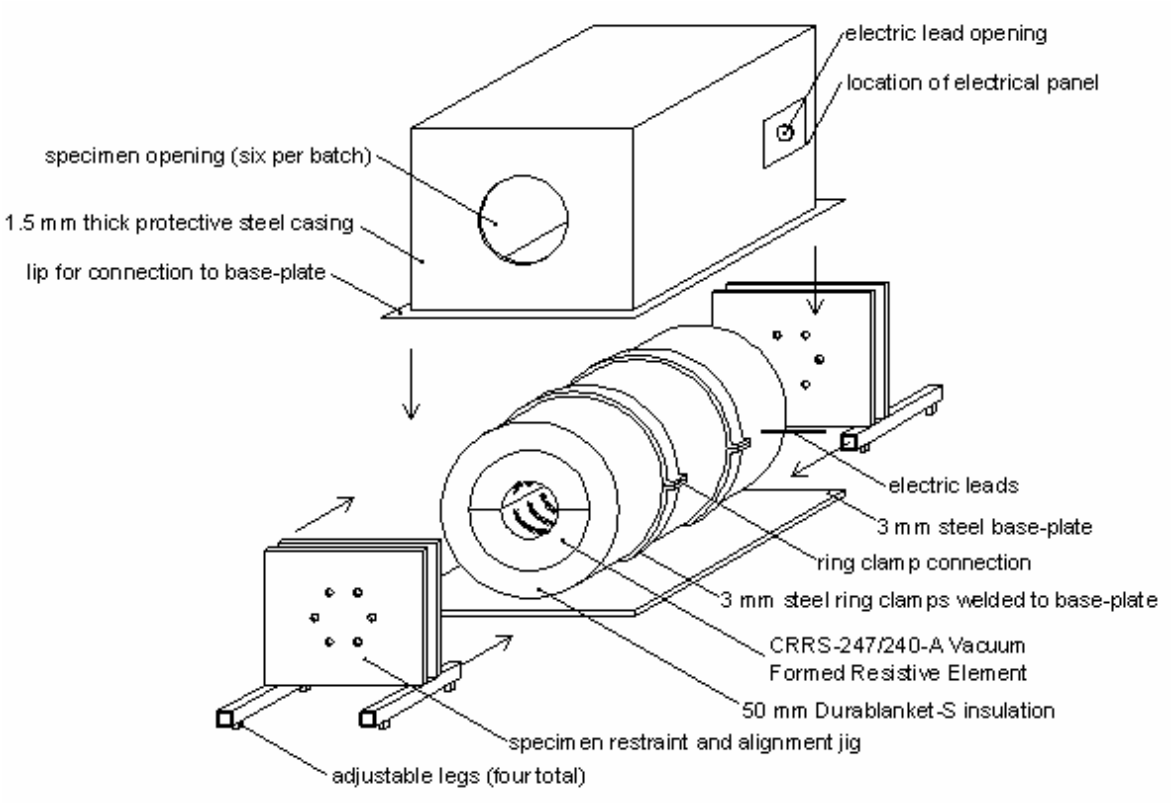

Figure 3.3: High-Temperature Electric Heating Unit with Specimen Adjustment Jigs

Figure 3.4: High-Temperature Electric Furnace in Working Condition

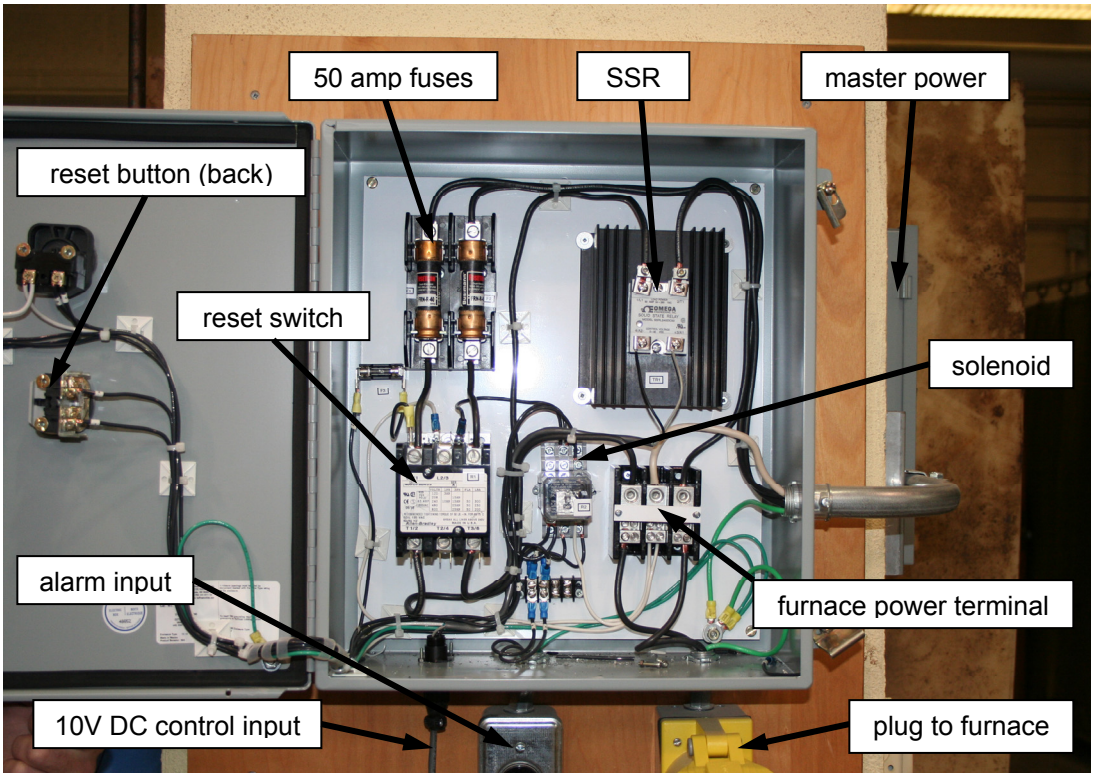

Figure 3.5: High-Voltage Furnace Control Panel

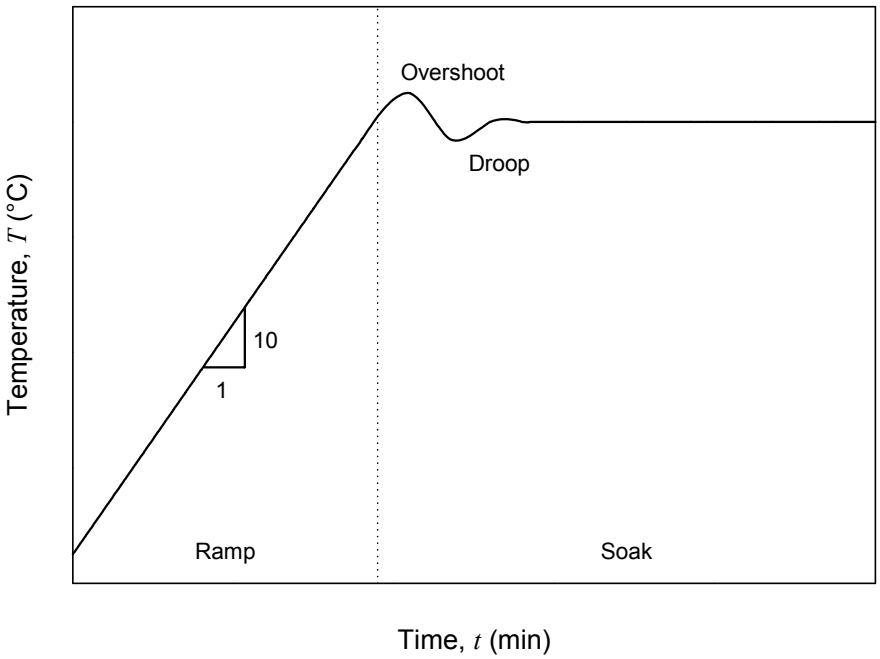

Figure 3.6: Characteristic Overshoot and Droop of a Manually Configured Controller

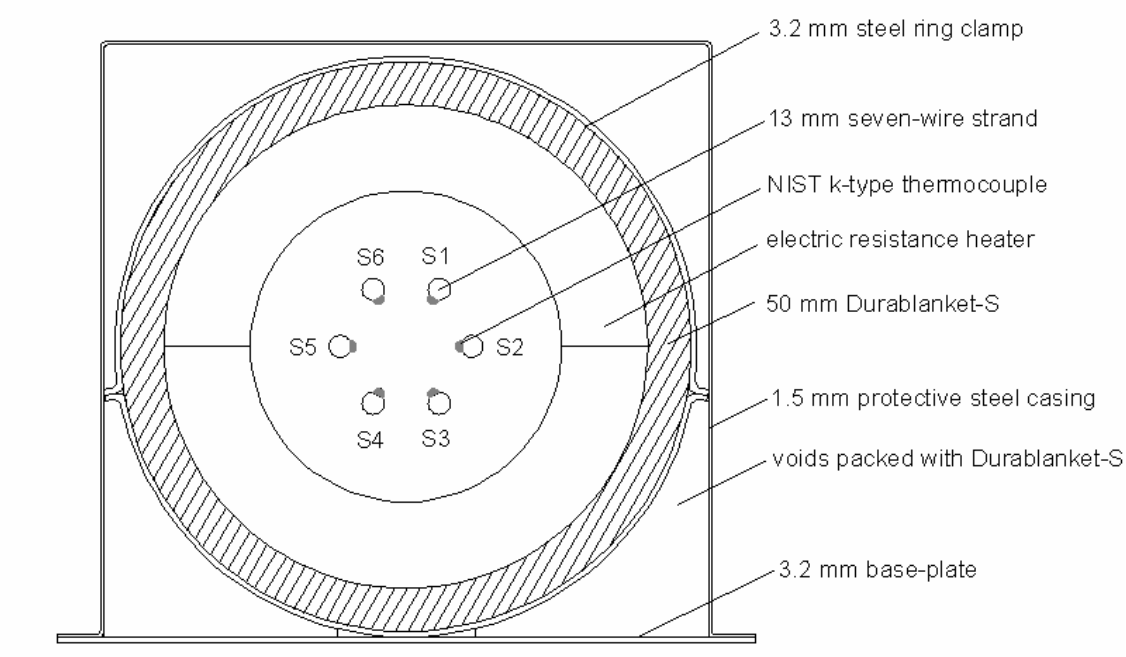

Figure 3.7: Schematic Cut through Furnace Centerline (Midpoint); approx. scale 1: 4.4

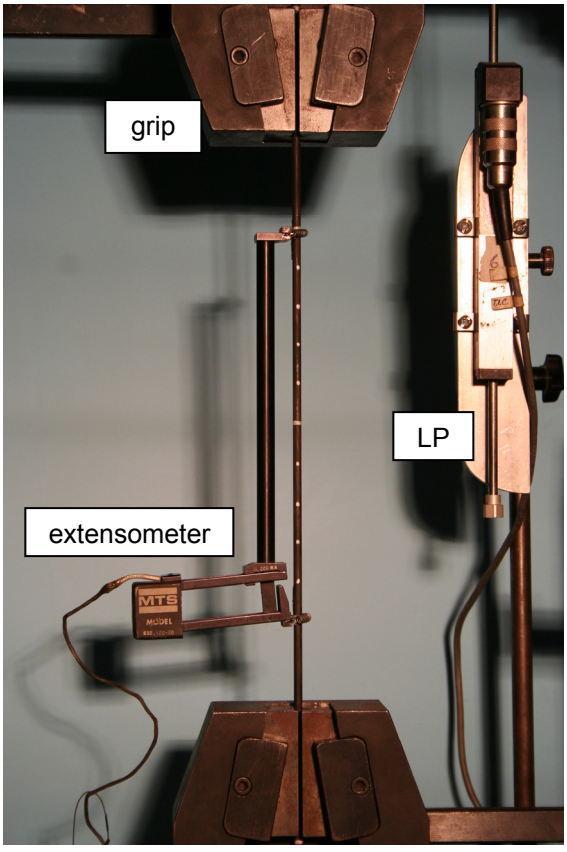

Figure 3.8: Typical Tension Test of Core Wire (in progress)

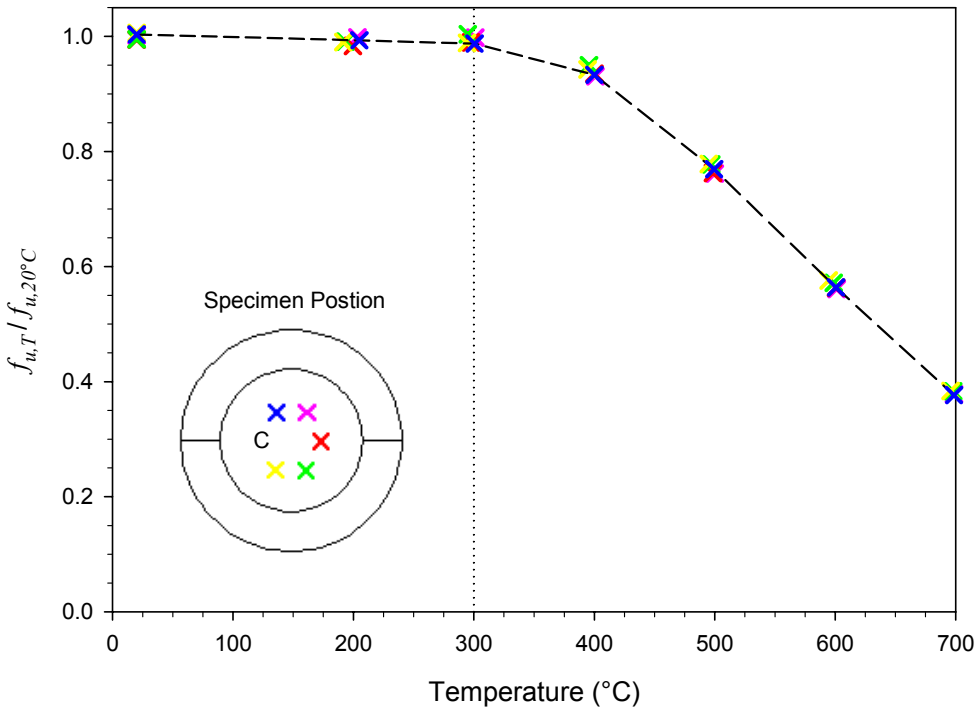

Figure 3.9: Residual Ultimate Tensile Strength of Cold-Drawn Prestressing Steel

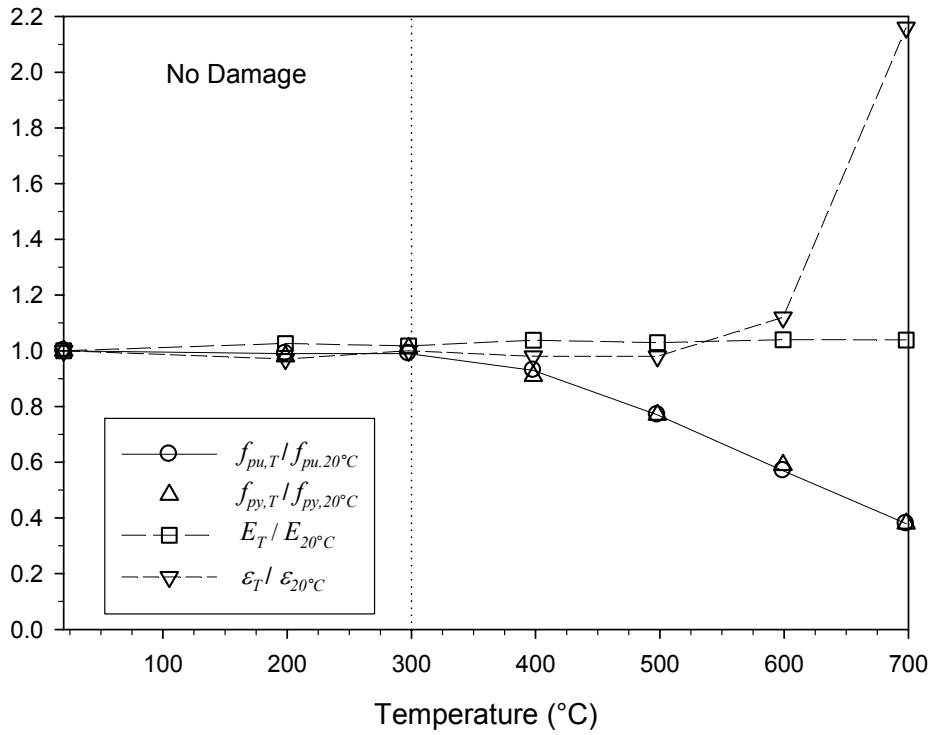

Figure 3.10: Summary of Changes in Residual Mechanical Properties with Temperature Exposure

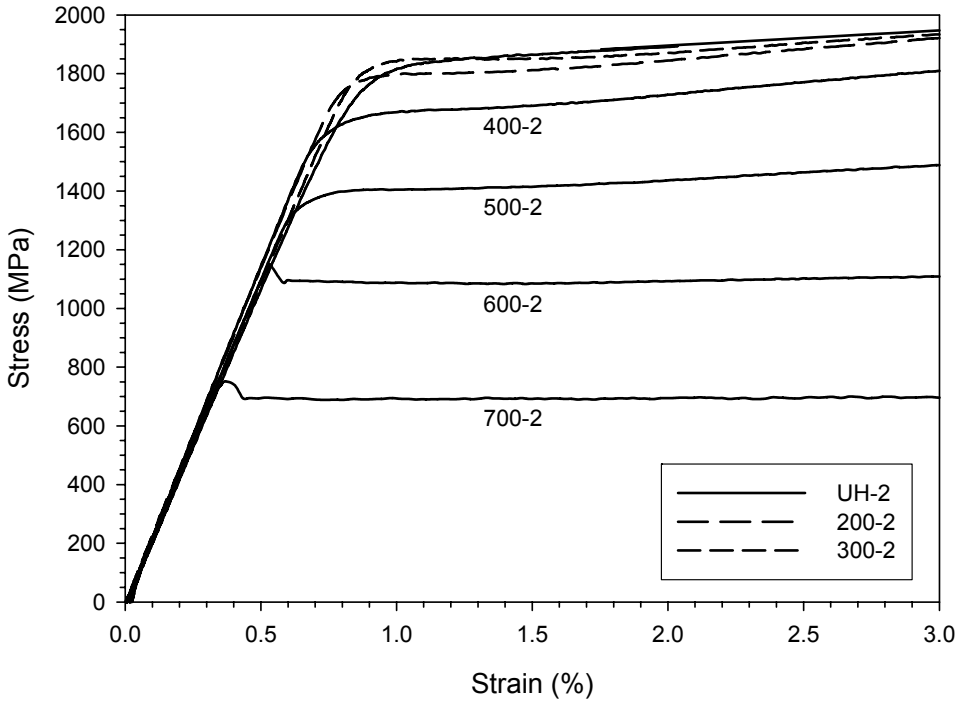

Figure 3.11: Variation of Residual Stress-Strain Profile (S2) with Heating

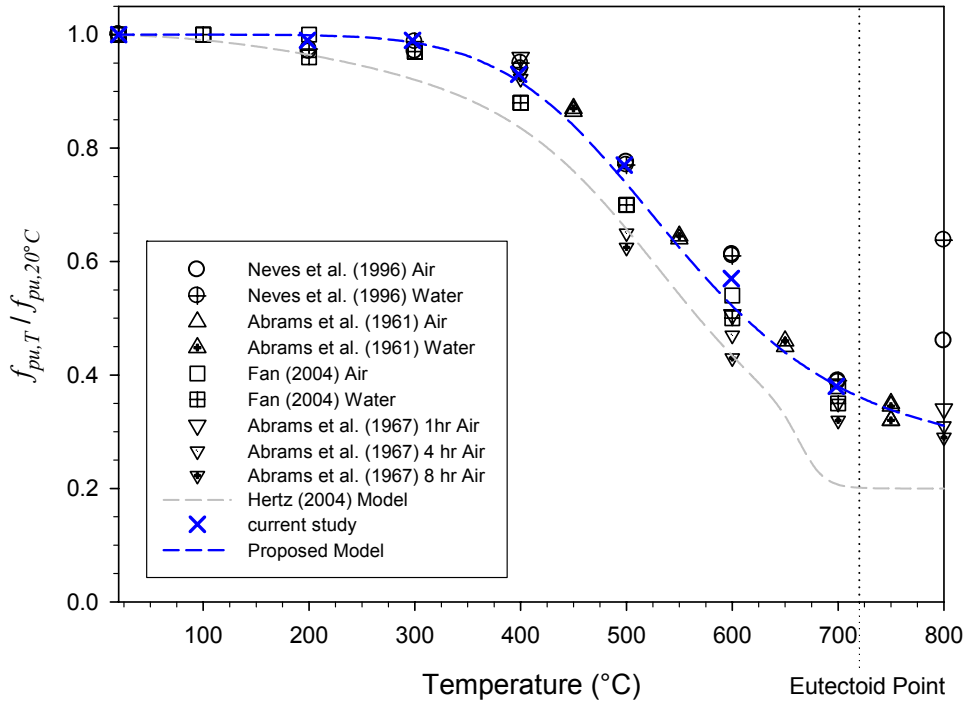

Figure 3.12: Summary of Residual Ultimate Tensile Strength Data

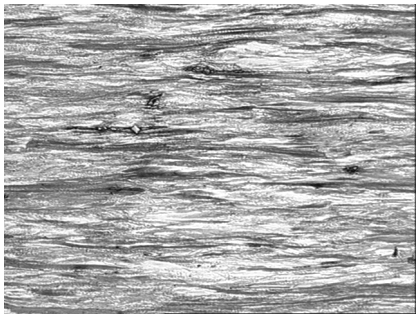

Figure 3.13: UH-5 1070X nital (reduced to 0.25 of original)

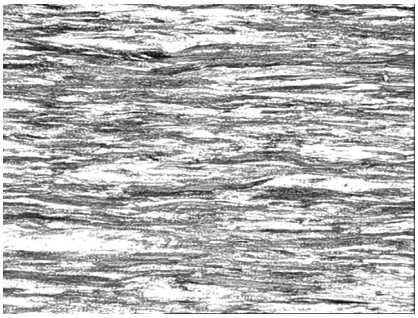

Figure 3.14: 200-5 1070X nital (reduced to 0.25 of original)

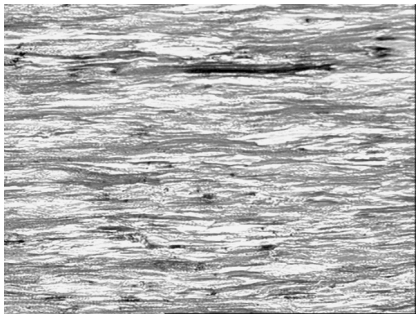

Figure 3.15: 300-5 1070X nital (reduced to 0.25 of original)

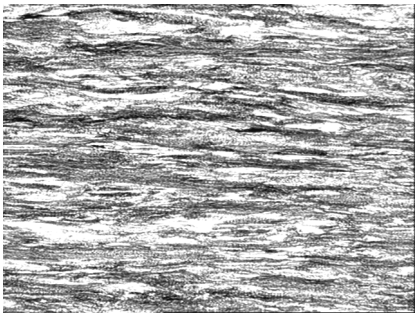

Figure 3.16: 400-5 1070X nital (reduced to 0.25 of original)

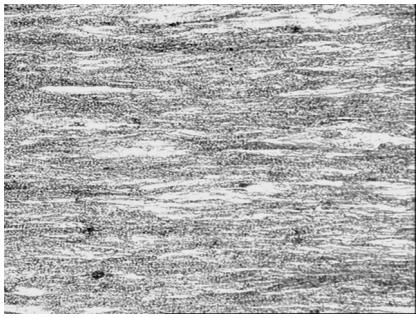

Figure 3.17: 500-5 1070X nital (reduced to 0.25 of original)

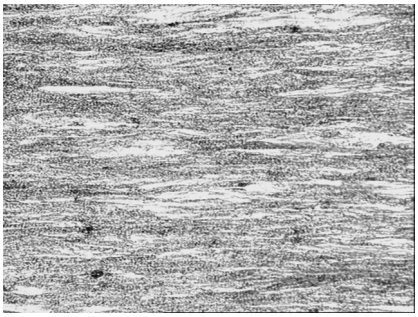

Figure 3.18: 600-5 1070X nital (reduced to 0.25 of original)

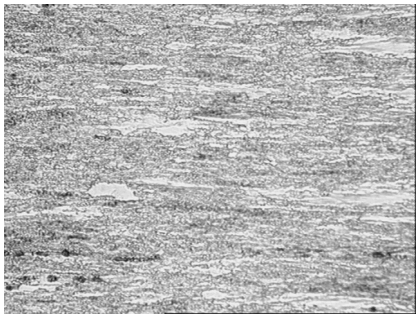

Figure 3.19: 700-5 1070X nital (reduced to 0.25 of original)

CHAPTER 4 – Transient Stress Relaxation of Cold-Drawn Prestressing Steel at Elevated Temperatures

4.0 General

As mentioned previously, the flexural strength of unbonded post-tensioned concrete floor slab assemblies relies on both the strength and proportioning of constituent materials such as concrete, mild reinforcement, and prestressed reinforcement, as well as the magnitude of the applied prestress (Allouche 1996). Consequently, the elevated temperature relaxation properties of cold-drawn prestressing steel are potentially critical in the post-fire assessment of these systems. Two significant effects of heating can cause changes in prestress force during fire: thermal expansion, and creep under stress at elevated temperature (other phenomena such as thermal bowing and restraint induce compression in slab diaphragms but do not directly affect tendon stress). As the temperature of prestressed reinforcement increases during a fire, the cold-drawn prestressing strand will experience thermal expansion, which, in the absence of stress, is reversible upon cooling. In addition however, at some temperature particular to the specific metal under consideration, high temperature creep will be initiated when the material is under stress, as is the case for an unbonded prestressing tendon (due to post-tension force and gravity loads). The resulting creep-related relaxation of the tendon is irrecoverable and results in a permanent loss of prestress (Malhotra 1982; Hill and Ashton 1957; Schneider 1990).

Although many authors have identified the elevated temperature relaxation of unbonded tendons as being significant to the fire performance of post-tensioned floors, there is a surprising paucity of experimental data or analytical modeling describing this

phenomenon. In 1957, Hill and Ashton (1957) reported the results of tests on 16 simply-supported unbonded post-tensioned rectangular and T-shaped sections under service loads and exposed to simulated fire. As mentioned previously, the authors noted significant irrecoverable deflections and appreciable loss of prestress upon cooling. Similarly, Abrams and Cruz (1961) performed two series of tests to investigate the elevated temperature relaxation of cold-drawn prestressing steel. In the first series, strand was tensioned to typical service levels, heated to approximately 540°C under constant total elongation and then allowed to cool slowly to room temperature. In the second series, strand was stressed to 60% of ultimate and heated to predetermined temperatures ranging from approximately 93°C to 650°C and allowed to cool slowly. It was shown that a very slight and gradual loss of prestress occurred up to approximately 315°C, followed by drastic decreases above this temperature (see Figure 2.10). This drastic change in the observed rate of prestress loss at high temperature is a result of creep-related relaxation of the cold-drawn prestressing steel, which is activated above 300°C as discussed later herein.

For any given material, different creep mechanisms may act at various combinations of stress and temperature. To date, there has apparently only been one study which has sought to quantify high temperature creep parameters of cold-drawn prestressing steel. Harmathy and Stanzak (1970) performed elevated temperature creep tests on Grade 1725 prestressing steel in which single core wires were removed from seven-wire prestressing strands, heated to a predetermined temperature, and loaded to a predetermined level (i.e., in load control). Creep curves plotting strain versus a temperature compensated time parameter, as shown in Figure 2.12, were used to

determine creep parameters for temperatures and stress levels ranging from 370°C to 650°C and 6.9 MPa to 690 MPa, respectively.

The steady state creep behaviour of cold-drawn prestressing steel can be defined using creep theory proposed by Dorn (1955) and modified by Harmathy (1967), as mentioned previously in Chapter 2. However, this is of little use for unbonded post-tensioned slabs exposed to fire, unless steady-state creep predictions can be incorporated into a *transient* description of strand relaxation during fire – a process which includes varying temperatures, simultaneously varying stress levels, and creep-stress dependency. According to Anderberg (1983; 1988), the relaxation process experienced in an unbonded tendon upon heating can be found analytically by using an instantaneous stress-related strain determined from steady-state creep test data. As such, if the total strain is constant (assuming that the total elongation, i.e., the tendon anchorage location, does not change significantly during heating) an increase in creep strain (or thermal strain) must be accompanied by a decrease in strain resulting from prestress and applied loading. Clearly, the result is a reduction in stress-related strain, and a corresponding loss of prestress. The reader will note that the assumption of constant tendon length is not strictly true for an unbonded post-tensioned slab in a fire, although this assumption is reasonable for initial studies. In reality, a complex interplay exists between thermally induced bowing occurring due to thermal gradients in the slab, overall thermal expansion of the slab, and both axial and flexural continuity and restraint in slabs post-tensioned over multiple bays. These factors will be studied in future work.

The above concepts have apparently never been used to study the prestress losses that could be expected in unbonded post-tensioned concrete members during fire events;

nor have they apparently been extended to predict the residual level of prestress (i.e. effective prestress) remaining in an unbonded post-tensioned reinforced concrete member after cooling. These concepts are used later in the current chapter to develop an analytical procedure capable of predicting prestress losses, both during heating and after high temperature exposure, for transient thermal regimes and realistic service prestress levels. This analytical model is then compared to the results of eight transient high temperature relaxation tests, also described in the current chapter.

It should be noted that for the relaxation testing described in this chapter, the same electric coil radiant heater, and similar heat treatments as those described in Chapter 3, were used. As such, a great deal of the testing methodologies and the logic behind specific test protocols and test parameters has been discussed previously.

4.1 Materials and Test Methods

4.1.1 Materials

Each specimen of prestressing strand used for the transient relaxation tests was extracted from the same continuous coil of 13 mm diameter ASTM A416 (ASTM 2001b) Grade 1860 low-relaxation seven-wire strand utilized in the test series previously described in Chapter 3. As such, the stress-strain behaviour, as well as other mechanical properties, are readily available in the preceding chapter and in Appendix C. As previously noted, the chemical composition of the strand was determined by an independent testing laboratory (Bodycote Testing) and is presented in Table 2.1.

4.1.2 Heat Treatment Required

As previously described, the heat treatment of all specimens tested in this series was comprised of three distinct phases: ramp; soak; and cool (see Figure 3.1). Again,

during the ramp phase the surface temperature of specimens was raised at a rate of approximately 10°C / min. from room temperature (taken to be 20°C) to a predetermined set-point ranging between 200°C and 700°C. Once the predetermined set-point for each specimen was reached, the temperature was held constant for soak times of 5 minutes, 45 minutes or 90 minutes, as described in Section 4.1.5.

Finally, the cooling rate of each specimen was accelerated by removing the ceramic fibre end plugs from the furnace and expelling heated air with a small cooling fan. The initial rate of cooling observed was much lower than the 10°C / min. ramp rate used and was seen to decay rapidly as the cooling process progressed (see Appendix B). Unlike the residual mechanical properties of cold drawn prestressing strand, strain relaxation is greatly affected by the duration of exposure to temperature (i.e. soak time); as such, specimen temperature was continuously monitored until room temperature was achieved.

4.1.3 High-Temperature Electric Furnace

As with the previous test series, no furnace in the Department of Civil Engineering could achieve the desired precision of temperature control nor allow for the application of stress during heating. As such, the design of the custom radiant-type electric tube furnace described in Chapter 3 was completed, ensuring its compatibility with an existing rigid prestressing bed already available in the laboratory for use in this test series.

4.1.4 Specimen Preparation – Elevated Temperature Relaxation

A total of eight test samples of seven-wire prestressing strand were prepared for use in the relaxation testing. Each specimen was approximately 6300 mm in length and was extracted from the same continuous coil of material used for all of the tests presented herein. The strand was cleaned of corrosion using a wire brush and an alcohol solution to ensure good surface contact of the installed thermocouples and to prevent slippage of the strand within mechanical chucks (used to anchor the specimen for stressing operations within the prestressing bed).

Each of the seven-wire strand specimens was instrumented with seven NIST Type-K thermocouples, having a precision of ± 1.7°C at 427°C (as provided by the manufacturer), to monitor surface temperatures and to provide control feedback for the tube furnace. Details of the furnace and thermocouple placement are shown schematically in Figure 4.1. Two thermocouples were positioned in the centre of the furnace unit; one to regulate temperature via the Omega Scientific model CNi3243-C24 controller, described in Chapter 3 (designated TCC), and the other to continuously record peak temperature on the surface of the specimen (TC1). Another thermocouple was placed halfway between the centre of the 610 mm long heating coils and a ceramic fibre end plug (TC2), approximately 150 mm from the furnace centre. The final two thermocouples located within the heating chamber were placed just inside the ceramic fibre plugs at each end, approximately 300 mm from the furnace centre (TC3 and TC5). An additional thermocouple was placed immediately outside the ceramic fibre plug at one end of the heating chamber, approximately 350 mm from the furnace centre (TC4). The remaining two thermocouples were positioned well outside the furnace unit, one affixed

to the specimen and the other monitoring the ambient temperature of the stressing bed; see Figure 4.1 and Table 4.1. Note precision of thermocouple placement was ± 3 mm.

The outputs of all thermocouples were continuously monitored for the duration of the heating and cooling cycle, using the System 5000 digital data acquisition system mentioned previously in Chapter 3 (recording data at a frequency of 1 Hz). The aforementioned placement of thermocouples was chosen such that the longitudinal temperature profile could be determined along the full length of each strand during heating. It was noted during testing that strand temperature decreased gradually from the centre of the furnace toward each end of the enclosure, while a steep decrease in temperature was observed just inside the insulation plugs at each end of the furnace and another steep decrease in temperature was observed just outside the insulation plugs (see Appendix B for additional details).

Thermocouples were fastened to each specimen with stainless steel hose clamps, spring loading the thermocouple wires to each specimen to prevent loss of surface contact during heating and ensuring a surface temperature measurement rather than an ambient gas phase measurement was recorded, as described in Chapter 3.

To continuously monitor prestress force during transient thermal exposures, centre-hole load cells, manufactured in the Department of Civil Engineering, were used in relaxation tests at each end of the prestressing bed. Each load cell consisted of four commercial strain gauges, with an output precision of ± 1.00% (microstrain), which were affixed to a precision machined stainless-steel block and encased in a cylindrical protective lining. Since the load cells were calibrated against a certified load cell before and after testing, the precision of these instruments was affected only by the precision of

the strain gauges used. During initial calibration, readings over a range of 0 kN to 150 kN were made at seven discrete points and were compared against a professionally calibrated load cell documented to have a maximum output variation of ± 0.87% (of observed load in kN). These points were recorded in the digital data acquisition system, previously mentioned, and on-board software was used to fit a linear least squares calibration curve for each of the load cells. With calibration functions established, each of the three loads cells used was verified against the calibrated load cell through loading to 150 kN, and again during unloading. This was done prior to and upon completion of the relaxation test series to ensure instrumentation was not damaged and did not drift during testing. The precision of the loads cells used in testing and the calibration cell was determined to be ± 1.76% over the range of 0 kN to 150 kN (vector sum of precision for load cell used in testing and the calibration load cell).

Finally, a Novotechnik TRS 100 linear potentiometer (LP), having precision of ± 0.075% (in output displacement in mm), was affixed to the stressing bed floor on a magnetic base to monitor any movement of the bearing plates at the dead end of the prestressing bed. Note that during normal operation of the prestressing bed, prestress force can be released at the dead end abutment by altering the vertical position of large wedges attached to the bed's frame, which are received by similar inverted wedges on the back of the abutment. During the study presented herein, these wedges were bolted into place using a torque wrench to ensure no movement of the abutment during testing. Linear potentiometer readings were used to confirm that no significant deflection or shifting of the abutment relative to the rigid frame occurred during testing (i.e., measured displacement was within instrumental uncertainty).

4.1.5 Setup and Procedure

As previously mentioned, the same custom fabricated tube furnace as described in Chapter 3 was used in this portion of the experimental investigation. However, in the case of the relaxation testing only one continuous strand specimen was passed through the furnace during each thermal cycle, as opposed to six specimens during the residual testing described in Chapter 3. The reader will note that localized heating of a prestressing tendon, such as that used herein, is intended to be representative of a heating scenario that one might expect for either an unbonded tendon with very small concrete cover (i.e. a strand placement error during construction) or a slab which experiences localized spalling of the concrete cover during a fire. As well, draped unbonded tendon profiles common to post-tensioned floor slabs would experience considerably higher temperatures at midspan than near to supports due to varying depth of concrete cover to the prestressed reinforcement. This point is further discussed and elaborated in Chapter 5.

Once each strand specimen and its thermocouples were properly positioned within the tube furnace, each end of the specimen was passed through rigid abutments in the integrated loading frame (modified prestressing bed), as shown in Figures 4.1 and 4.2. Note that the end plates of the loading frame were adjusted vertically to ensure adequate clearance of the stressed strand from the furnace coils; their position was then kept constant for all tests in this series.

The dead end of the strand was passed through a centre-hole load cell and secured within standard prestressing chucks. The live end of the specimen was stressed using a centre-hole hydraulic jack (by Enerpac^{TM}) and standard chucks, also incorporating a centre-hole load cell. Once the appropriate load, approximately 100 kN in the current study, or 55% of the ultimate room temperature tensile strength of a single prestressing

strand, was achieved, the strand was locked off against the stressing frame using a different chuck and load cell assembly. This second assembly was equipped with a threaded expansion cylinder such that final prestress adjustments could be made manually (with wrenches) after all seating losses had occurred (see Figure 4.3). Prestress load levels were monitored for two hours before final adjustments were made to ensure that short term losses had occurred prior to heating and would not influence the testing results. Because the magnitude of prestress force induced for the tests was relatively low, seating losses were assumed to be the most significant component of short term relaxation. The average prestress prior to heat treatment for the eight specimens was 1008.0 MPa (54% ultimate), with a standard deviation of 16.2 MPa (see Table 4.2). Note that the typical range of effective prestress (after all losses) for unbonded post-tension slabs is 50-60% of ultimate (PTI 1990).

After the thermocouples were affixed and stressing procedure complete, the position of the furnace unit itself was adjusted about the strand's length in order to ensure thermocouples were centered within the unit.

As with the residual strength testing discussed in Chapter 3, all specimens were heated to a predetermined set point using a controlled temperature ramp of 10°C / min., and held for 5, 45, or 90 minutes. Specimens were then allowed to slowly cool within the furnace enclosure to room temperature, with temperature and load being recorded continuously for the full duration of the test. Each test was considered complete when the maximum temperature recorded at any location on the strand fell to 30°C. In order to facilitate reasonable data sets, cooling within the furnace chamber was accelerated by

removing ceramic fibre end plugs upon completion of heating cycle to allow ambient air, circulated by a small fan, to enter.

After the completion of high temperature relaxation tests with a hold time of 90 minutes for specimens at 200°C (designated RLX-90-200), 300°C (RLX-90-300), 400°C (RLX-90-400), 500°C (RLX-90-500), and 700°C (RLX-90-700), large irrecoverable prestress losses of between 23% and 85% were noted at exposures of 400°C and higher (to be discussed later). As such, additional specimens were tested at 400°C to study the effects of different exposure durations of 45 minutes (RLX-45-400) and 5 minutes (RLX-5-400). A final specimen was tested at 400°C for 90 minutes (RLX-90-400A) to demonstrate the repeatability of the testing procedures and results (see Table 4.2 for summary of relaxation testing program).

Finally, once all relaxation tests had been completed, the core wire from each of the specimens used in the relaxation tests was removed and tested in direct tension as outlined for the residual specimens in Chapter 3. This was done to investigate the possibility of an effect of stress during heating on the residual mechanical properties of cold-drawn prestressing strand.

4.2 Results and Discussion

4.2.1 Relaxation Testing

The results of the elevated temperature relaxation tests are shown in Figures 4.4 to 4.6. At low temperatures (i.e., below 300°C) the rate of prestress loss remains fairly constant and exhibits a somewhat linear profile up to approximately 300°C. Above this temperature, a drastic increase in the rate of prestress loss occurs signifying a critical temperature for the activation of thermal creep. Furthermore, it was found that

specimens held at 200°C and 300°C recovered at least 97% of their original prestress force (100 kN ±) upon cooling. By contrast, the results shown in Figure 4.4 indicate that a significant irrecoverable relaxation was exhibited by specimens heated to temperatures at or above 400°C (i.e., recovering 78% of original prestress at 400°C and 15% at 700°C).

These results are consistent with the findings of Abrams and Erlin (1961), who noted drastic prestress losses at temperatures above 315°C, as well as with assertions made in other works regarding high temperature creep in metals reviewed previously (Lie 1992; Malhotra 1982; Schneider 1988).

It can also be seen from these data that even short durations of exposure at 400°C can result in significant irrecoverable prestress loss (see Figure 4.5). The specimen held at 400°C for five minutes exhibited a 15% irrecoverable loss in initial prestress force, while the specimen held for 45 minutes exhibited a 20% loss in initial prestress (as compared against 23% after 90 minutes). This finding is highly significant for the residual performance of unbonded post-tensioned members after exposure to fire, given that a typical 150 mm slab with carbonate aggregate, 5% moisture content, and concrete cover of 20 mm exposed to the ASTM E119 Standard Fire (ASTM 2001d) reaches a strand temperature of 400°C in approximately 30 minutes; further discussion on this issue is provided in Chapter 5. Therefore, a common slab designed with sufficient specified concrete cover to achieve a one hour fire rating (see Table 2.8) could experience significant irrecoverable strand damage and prestress loss in about 30-35 minutes of exposure to a standard fire.

Finally, the repeatability of the results using the test setup, instrumentation, and data acquisition discussed previously were examined through an additional 90 minute test

at 400°C (see Figure 4.6). Both specimens began with approximately the same prestress force, 99.2 kN for RLX-90-400 and 100.4 for RLX-90-400A. During the heating regimen both specimens exhibited virtually identical prestress loss (differing by a maximum of 3% of the average initial prestress force). Upon completion of heating and cooling, both specimens experienced similar overall irrecoverable prestress losses; 22% for RLX-90-400 and 23% for RLX-90-400A. It should be noted that although similar heat treatments were utilized, the exact rate of heating and cooling experienced varied slightly. Heating and cooling curves for all specimens discussed in this chapter are provided in Appendix B.

4.2.2 Residual Properties

Upon completion of the elevated temperature relaxation tests, the core wires of each of the seven-wire strand specimens were removed, and tension tests were performed in accordance with the procedures outlined in Chapter 3, to examine the effect of stress at high temperature on residual properties; see Appendix C for experimental stress-strain curves and mechanical property calculations.

It was not possible to obtain a mean or standard deviation for these residual mechanical property data, because in all but one case, only one stressed-while-heated specimen was available. Consequently, in order to make a comparison between the residual mechanical properties of the unstressed-while-heated specimens (tested in Chapter 3) and the stressed-while-heated specimens used in elevated temperature relaxation tests, it was assumed that the application of stress had no effect on residual mechanical properties (and that residual mechanical properties have a normal distribution). The mechanical properties for stressed specimens were then compared

against the unstressed data using a *One Sided T-Test* as per ASTM E178-01 (ASTM 2001e). Where the results of such a test indicate the stressed-while-heated specimen is an outlier at the corresponding level of significance, the application of stress may have a significant affect on the residual mechanical property being investigated (see Tables 4.3 to 4.7).

The standard deviation of the residual ultimate tensile strength of specimens heated to 200°C and 300°C for 90 minutes (including both unstressed and stressed samples) was found be less than the calculated experimental uncertainty (± 20.2 MPa). The T-Test indicates that the stressed specimens (RLX-90-200 and RLX-90-300) did not constitute outliers at any level of significance (i.e., α = 10%, 5%, or 1%); thereby indicating that the application of stress (through constant elongation), up to 54% of ultimate strength, does not have a marked effect on residual ultimate tensile strength of prestressing steel (see Table 4.3).

The standard deviation of the ultimate tensile strength upon cooling of samples heated to 400°C was found to be outside the experimental uncertainty calculated. Statistical analysis again indicated that the stressed specimens (RLX-90-400 and RLX-90-400A) did not constitute outliers at any level of significance.

Finally, the standard deviations of samples heated in excess of 400°C were found to be well outside the experimental uncertainty computed. Statistical analysis showed that the stressed samples were outliers at the 0.1% and 0.5% significance levels for RLX-90-500 and RLX-90-700 respectively; thus indicating that the application of stress at temperatures in excess of 400°C may have a mild detrimental effect on the residual ultimate tensile strength of cold-drawn prestressing steel (see Table 4.3).

A similar trend was found when examining the 0.2% offset yield strength of specimens heated under stress for 90 minutes; with specimens heated up to 400°C not constituting outliers at any level of significance, while specimens heated to temperatures in excess of 400°C were found to be outliers at the 0.1% significance level (see Table 4.4).

When examining the residual elastic modulus of specimens stressed during heating, no alteration in the trend of residual data was evident given that the large experimental uncertainty for these specific data overshadows statistical analysis of the data (see Table 4.5). Also, when examining residual elongation at rupture, it was found that, for any given temperature exposure examined, the stressed specimens did not constitute outliers at any level of significance (see Table 4.6).

Finally and as expected, very short (i.e., 5 minute) elevated temperature exposures appear to have a lesser effect on both the ultimate tensile strength and the 0.2% offset yield than do exposures for 90 minutes or more (see Table 4.7).

4.3 Analytical Investigation

4.3.1 General

As previously mentioned, no analytical approach is apparently currently available to aid the engineer in estimating the amount of prestress remaining in an unbonded tendon after being subjected to the temperatures associated with standard fire exposures (nor, apparently, have the consequences of such irrecoverable prestress loss been considered or studied in any significant detail). The following section describes the preliminary development of such a model and its comparison to the experimental data presented in the preceding sections. The model described herein addresses both the recoverable and

irrecoverable strain variations experienced under transient heating and cooling, and consequently variable stress. Because the model facilitates the discretization of the strand into finite elements of constant length and temperature, it is capable of simulating scenarios where only a portion of a tendon's total length has been exposed to elevated temperatures; such is the case of a fire compartmentalized in a single bay of a multi-bay slab, for example. Finally, the ability to model finite strand elements of constant temperature allows the effect of variable cover, as would be present for unbonded members with draped tendons, to be investigated.

4.3.2 Model Formulation

Since unbonded tendons are free to expand and contract within the slab on heating and cooling, two significant effects of fire can cause changes in prestress force to occur. Recall from Chapter 2 that as the temperature of the reinforcement is raised during a fire, the tendon will experience thermal expansion, Δl, as described below:

$$\Delta l / l = -2.016 \times 10^{-4} + 1.0 \times 10^{-5} T + 0.4 \times 10^{-8} T^2 \quad 20°\text{C} < T < 1200°\text{C} \qquad (2.1)$$

where l represents the unheated specimen length and T represents temperature in Celsius (Rigberth 2000). Thermal expansion in the absence of stress is a reversible process, where any stress lost as a result of thermal elongation during heating is recovered upon cooling. Conversely, at thermal exposures above a temperature particular to the metal being examined (in the current case about 300°C), high temperature creep will be initiated under stress, and the resulting creep-related relaxation of the tendon is thus irrecoverable; resulting in permanent loss of prestress (Collins and Mitchell 1987; Malhotra 1982; Hill and Ashton 1957; Schneider 1990).

The effects of temperature on creep rate in metals are most often accounted for by the inclusion of a *temperature-time parameter*, such as the Sherby-Dorn or Larson-Miller parameters, in analytical creep formulations (Dowling 1998). Previous publications specific to the elevated temperature performance of various steels used in the construction industry have focused primarily on an approach proposed by Dorn (Anderberg 1983; Anderberg 1988; Dorn 1955; Harmathy 1967; Harmathy and Stanzak 1970). In this approach, the material is idealized as behaving like a Newtonian liquid with very high viscosity. At elevated temperatures, the average oscillations of atoms about their equilibrium points increase, resulting in more frequent stress-driven molecular rearrangements. These rearrangements contribute to the creep phenomena. As such, the entire creep process is said to be *thermally activated*, and therefore the rate of creep can be described using a variation of the Arrhenius Equation. The integration of this creep rate function results in creep strains (engineering strain), ε, for constant stress:

$$\varepsilon = A(\sigma)\int e^{\frac{-\Delta H}{RT}}\, dt \tag{2.6}$$

where ΔH is activation energy and is a measure of the amount of energy required to cause molecular motion, R is the universal gas constant, $A(\sigma)$ is a stress dependent constant, t is time, and T is the absolute temperature in degrees Kelvin. From this expression the temperature-compensated time parameter, θ, can be extracted and is described below:

$$\theta = \int_0^t e^{\frac{-\Delta H}{RT}}\, dt \tag{2.7}$$

or for constant temperature:

$$\theta = te^{\frac{-\Delta H}{RT}} \tag{2.8}$$

Note that $\Delta H/R$ is therefore a constant and was determined experimentally by Harmathy and Stanzak (1970) to be 30,556°K.

As the solution of Equation 2.6 is impractical without the formulation and validation of a computer algorithm, it is necessary to derive an equation of a modified form. A semi-empirical alternative is described by making use of the principle of temperature-compensated time.

In plotting experimental strain data versus temperature-compensated time, it is possible to quantify the *Zener-Hollomon* parameter, Z, and a dimensionless creep parameter, $\varepsilon_{cr,0}$, both of which have been used in the development of analytical expressions describing high temperature creep in metals (Anderberg 1983; Anderberg 1988; Harmathy 1967; Harmathy and Stanzak 1970). By determining these parameters for various steels at different stress levels and temperatures, Harmathy (1967) proposed the expression:

$$\varepsilon_{cr} = \frac{\varepsilon_{cr,0}}{\ln 2} \cosh^{-1}\left(2\exp\left(Z\theta / \varepsilon_{cr,0}\right)\right) \quad \text{for } \sigma \text{ constant} \tag{2.9}$$

to describe primary and secondary creep (under which no change in cross-sectional area due to necking occurs) as a function of temperature and time at a given stress level.

As previously mentioned, Harmathy and Stanzak (1970) performed elevated temperature creep tests on Grade 1725 prestressing steel, deriving the following expression for Z, and $\varepsilon_{cr,0}$:

$$Z = 195.27\text{x}10^{6}\,\sigma^{3} \quad \text{for } \sigma \le 172 \text{ MPa} \tag{4.1a}$$

$$Z = 8.21\text{x}10^{13}\,e^{0.0145\,\sigma} \quad \text{for } 172 < \sigma \le 690 \text{ MPa} \tag{4.1b}$$

$$\varepsilon_{cr,0} = 9.262\text{x}10^{-5}\,\sigma^{0.67} \tag{4.2}$$

where σ is stress in MPa.

To evaluate the performance of realistic structures during and after standard fires, the instantaneous stress-related strain calculated using Equation 2.9 must be related to the magnitude of stress present in the tendon during heating. Since the total elongation of the tendon is constant, the sum of all strains (thermal, creep, and stress-related) must also be a constant. Therefore, an increase in creep strain must be followed by a proportional decrease in strain resulting from applied loading (prestress force and gravity loads), which influences creep, and so on. Therefore the total strain in the tendon can be described as:

$$\varepsilon_{tot} = const = \varepsilon_{\sigma}(\sigma) + \varepsilon_{T}(T) + \varepsilon_{cr}(\sigma, T, t) \tag{2.10}$$

where ε_{σ} represents the strain due to prestress and applied loading (which is a function of modulus of elasticity), ε_{T} represents strain resulting from thermal expansion / contraction, and ε_{cr} represents creep strain. Note that this is only true if it is assumed that the total length of the tendon does not change during a fire as a result of secondary effects, such as global thermal elongation of the slab and thermally-induced bowing.

Finally, an expression describing the change in elastic modulus at various temperatures was obtained by performing regression analysis on data presented by Ruge and Winklemann in Anderberg (1983). It was found that the following second order polynomial represents these data:

$$\frac{E_T}{E_{20^\circ C}} = -2\times10^{-6}T^2 + 0.2\times10^{-6}T + 0.987 \tag{4.3}$$

where E_T is modulus at temperature, $E_{20°C}$ is modulus at room temperature, and T is temperature in Celsius ($R^2 = 0.9987$).

The aforementioned expressions were used in the formulation of a relaxation model capable of approximating the change in tendon stress as a result of transient heating and cooling, as follows:

1) The tendon is descritized into finite lengths over which the average (constant) temperature is recorded continuously, as in an experimental study, or determined using a finite element / finite difference heat transfer model in the absence of test data.
2) The continuous transient thermal exposure is discretized into individual time steps of a small finite duration such that they have approximately constant temperature.
3) Strain due to thermal expansion is computed for each finite length of strand at the current time step and temperature using Equation 2.1.
4) The current tendon stress level at the current time step is used to compute Z and ε_{cr} using Equation 4.1 and Equation 4.2.
5) Creep strain (engineering strain) is computed for each finite length of strand at the current time step using values computed in Step 4) and Equation 2.9.
6) Again using the values computed in Step 4) and Equation 2.9, creep strain (engineering strain) is predicted for the time step $t + 1$.
7) The change in creep strain is determined by subtracting the value of creep strain determined in Step 5) from the value of creep strain determined in Step 6)
8) Finally the change in strain due to prestress loss from Step 7) is converted into stress using varying values of elastic modulus computed for each constant temperature element using Equation 4.3.

9) The change in stress due to thermal expansion and creep for each length of strand (element) are then added giving the change in stress for the entire specimen length; this change in stress is then used to update the value of stress from the previous time step.

10) The process beginning at Step 3) is repeated.

The model can be used to predict tendon stress versus time during heating for a strand of a given length, stress level, and longitudinally varying transient thermal regime.

4.3.3 Comparison of Predictions and Experimental Results

The preliminary analytical model described in the previous section was used along with temperature-time profiles generated during the relaxation tests conducted to predict the change in prestress under transient heat exposure. Since the thermocouples in each test were placed in a fixed location, the tendon was discretized into elements of known length. The average of thermocouples bounding tendon segments was taken to be the constant temperature applied to each element. However, even given the relative coarseness of the resulting tendon discretization, the response of the model is seen below to give appropriate trends and conservative magnitude predictions of experimental results discussed in the previous sections.

Figures 4.7, 4.8, and 4.9 display both observed and predicted stress levels versus elapsed time. The profiles of the model follow the trends exhibited by the experiments reasonably closely as the temperature rises and falls. During the constant hold time (at the predetermined set point) however, creep predictions tend to be over conservative, suggesting that refinement of the creep parameters used may be warranted. It should also be noted that these data and their associated analytical model serve to confirm the

mechanisms (thermal elongation and creep-relaxation) assumed to be significant to the change in prestress level at various temperatures for these prestressing steels.

From Figure 4.10, it can be seen that at the high and low end of the temperature range tested herein the model accurately predicts the prestress force remaining upon test completion. For the 200°C, 300°C, and 700°C tests (90 min in duration) the model prediction differs by a maximum of 4% (from the actual experimental response). For the 400°C tests of 5, 45, and 90 minutes in duration, the model predictions were found to differ by 5%, 14%, and 18% (from the actual experimental response), respectively. Finally, the creep prediction for the 500°C temperature exposure differs by approximately 36% from the observed data. Since the lower range of temperature exposures (below 300°C) are governed by thermal expansion, and the higher range of temperature exposures (nearing 700°C) are governed by creep-related relaxation and metal softening, it is not surprising that the analytical model most accurately predicts experimental behaviour in these temperature ranges. Also not surprisingly, where the interplay of both thermal expansion and creep mechanisms occurs, the model has the most difficulty in predicting the true transient loss of prestress force. However, the performance of the analytical model developed herein is impressive (and not unreasonable given the scatter of experimental data cited during the determination of the creep parameter, Z, used in the current model (Harmathy and Stanzak 1970) and that the higher stress levels investigated in the current study necessitated the extrapolation of these available data). Furthermore, the number of channels of thermocouple input in the digital data acquisition system used in the current study limited the number and length of elements that could be used in the analytical model. It is demonstrated in Chapter 5 that the refinement in element length

can have a marked effect on relaxation predictions, and additional testing with better longitudinal thermal resolution may be warranted.

4.4 Summary

The data presented in this section clearly indicate that currently used North-American prestressing steel experiences a pronounced and irrecoverable loss of prestress force at temperature exposures between 300°C and 400°C when stressed to realistic service levels during heating. It should be noted that, in a real unbonded post-tensioned concrete structure exposed to fire, the prestress loss may also depend on the ratio of the heated portion of the strand to the overall length of the strand, overall thermal expansion of the concrete slab itself, and thermal bowing effects. Unbonded strands in a real concrete slab can be much longer (up to 100 m) than those tested in this study. The interaction of overall length, heated length, tendon stress level, and creep at high temperature is extremely complex and requires further investigation and parametric study. Parametric studies using a model such as that developed and presented herein are required in order to gain a more complete understanding of the process, and are indeed planned for future studies at Queen's University. In Chapter 5, the preliminary analytical model discussed in this chapter is applied to a typical realistic post-tensioned concrete slab having varying heated length ratios and amounts of concrete cover, in order to determine the effect of elevated temperatures on the residual moment capacity of several potential slab configurations.

Finally, Figures 4.8 and 4.9 demonstrate that the overall fit of the proposed analytical model follows the actual stress reduction profile recorded during testing, and also clearly illustrate the importance of strand temperature exposures for the residual

performance and post-fire assessment of unbonded post-tensioned slabs. However, given the variation in the model's prediction when compared to experimental behaviour at intermediate temperatures, further study is apparently necessary. Refinement of creep parameters for cold-drawn prestressing steel wires to represent stress levels realistic to those found in service conditions (rather than extrapolation of existing data from the literature where lower stress levels were used), as well as the determination of creep parameters for entire seven-wire prestressing strand assemblies, rather than simply the individual core wires would, in the Author's opinion, prove beneficial to this endeavor.

Table 4.1: Thermocouple Location for Relaxation Testing (see Figure 4.1)

Designation	TCC	TC1	TC2	TC3	TC4	TC5	TC6
Dist. Dead End (mm)	2920	2920	2770	2620	2570	3220	1770
Dist. TC1 (mm)	0	0	150	300	350	-300	1150

Experimental precision ± 3 mm

Table 4.2: Relaxation Test Summary (with Final Prestress Prior to Heating)

Designation	Soak (min)	Temp. (°C)	LC1 (kN)	LC2 (kN)	$\bar{x}$	f / f_{pu}
RLX-90-200	90	200	100.0	98.5	99.3	0.54
RLX-90-300	90	300	100.2	99.2	99.7	0.54
RLX-90-400	90	400	100.2	98.2	99.2	0.54
RLX-90-400A	90	400	101.4	99.4	100.4	0.55
RLX-90-500	90	500	100.8	98.0	99.4	0.54
RLX-90-700	90	700	99.1	95.0	97.1	0.53
RLX-45-400	45	400	102.6	99.9	101.3	0.55
RLX-5-400	5	400	103.1	101.5	102.3	0.56
		$\bar{x}$	100.9	98.7	99.8	0.54
		s	1.4	1.9	1.6	0.00

Experimental precision ± 1.0 kN; conversion to MPa multiply values by 10.1

Table 4.3: Residual Ultimate Tensile Strength (f_{pu}); Stressed Specimens, 90 min RLX-90-*T* (MPa)

Temp.	$\bar{x}_1$	s_1	RLX	$\bar{x}_2$	s_2	ε_{exp}	T_1	α	T_{crit}
200°C	2001.5	10.8	2010.1	2002.9	10.3	20.2	0.701	**10%**	1.729
300°C	2006.1	14.4	2020.3	2008.5	14.1	20.3	0.836	**10%**	1.729
400°C	1894.5	16.0	1830.4*	1879.4	29.7	19.2	1.648	**10%**	1.828
500°C	1554.5	15.9	1402.6	1529.2	63.6	15.7	1.990	**0.1%**	2.011
700°C	767.1	6.8	714.7	758.4	22.2	7.7	1.964	**0.5%**	1.973

$\bar{x}_1$ and s_1 from Chapter 3

$\bar{x}_2$ and s_2 revised to include RLX-90-*T* specimen(s)

*RLX-90-400A; RLX-90-400 = 1852.5 MPa included in calculation of revised $\bar{x}$ and s

Table 4.4: Residual 0.2% Offset Yield Strength (f_{py}); Stressed Specimens, 90 min RLX-90-*T* (MPa)

Temp.	$\bar{x}_1$	s_1	RLX	$\bar{x}_2$	s_2	ε_{exp}	T_1	α	T_{crit}
200°C	1813.0	11.5	1853.2	1819.7	19.4	18.5	1.728	**10%**	1.729
300°C	1863.6	18.3	1865.1	1863.8	16.4	18.9	0.078	**10%**	1.729
400°C	1676.8	17.0	1581.7*	1653.1	43.3	17.0	1.648	**10%**	1.828
500°C	1417.2	11.4	1274.2	1393.3	59.2	14.3	2.011	**0.1%**	2.011
700°C	697.1	7.6	633.7	686.6	26.8	7.1	1.974	**0.1%**	2.011

$\bar{x}_1$ and s_1 from Chapter 3

$\bar{x}_2$ and s_2 revised to include RLX-90-*T* specimen(s)

*RLX-90-400A; RLX-90-400 = 1606.2 MPa included in calculation of revised $\bar{x}$ and s

Table 4.5: Residual Elastic Modulus (E); Stressed Specimens, 90 min RLX-90-T (MPa)

Temp.	$\bar{x}_1$	s_1	RLX	$\bar{x}_2$	s_2	ε_{exp}	T_1	α	T_{crit}
200°C	219610	4106	215200	218875	4090	28303	0.898	10%	1.729
300°C	217734	414	215140	217301	1122	27272	1.927	1.0%	1.944
400°C	222184	5423	212250*	219534	6342	28851	1.148	10%	1.828
500°C	220238	289	206400	217931	5655	27587	2.039	0.1%	2.011
700°C	222876	3424	200990	219228	9445	28212	1.931	1.0%	1.944

$\bar{x}_1$ and s_1 from Chapter 3

$\bar{x}_2$ and s_2 revised to include RLX-90-T specimen(s)

*RLX-90-400A; RLX-90-400 = 213 570 MPa included in calculation of revised $\bar{x}$ and s

Table 4.6: Residual Strain at Rupture (ε_u); Stressed Specimens, 90 min RLX-90-T (% Strain)

Temp.	$\bar{x}_1$	s_1	RLX	$\bar{x}_2$	s_2	ε_{exp}	T_1	α	T_{crit}
200°C	5.0	0.4	4.8	5.0	0.4	0.25	0.542	10%	1.729
300°C	5.0	0.3	5.0	5.0	0.3	0.25	0.000	10%	1.729
400°C	4.9	0.1	5.1*	4.9	0.1	0.25	1.242	10%	1.729
500°C	4.9	0.3	5.1	4.9	0.3	0.25	0.564	10%	1.729
700°C	11.1	0.2	10.5	11.0	0.3	0.25	1.771	10%	1.729

$\bar{x}_1$ and s_1 from Chapter 3

$\bar{x}_2$ and s_2 revised to include RLX-90-T specimen(s)

*RLX-90-400A; RLX-90-400 = 4.9% strain included in calculation of revised $\bar{x}$ and s

Table 4.7: Residual Properties of Stressed Specimens Heated to 400°C Varying Soak

	Soak (min)	f_{pu} (MPa)	f_{py} (MPa)	f_{py} / f_{pu}	E (MPa)	ε_u (%)
RLX2	90	1852.5	1606.2	0.88	213570	4.9
RLX7	90	1830.4	1581.7	0.86	212250	5.1
RLX8	45	1885.4	1651.3	0.88	213340	4.7
RLX6	5	1956.8	1738.4	0.89	213720	5.3

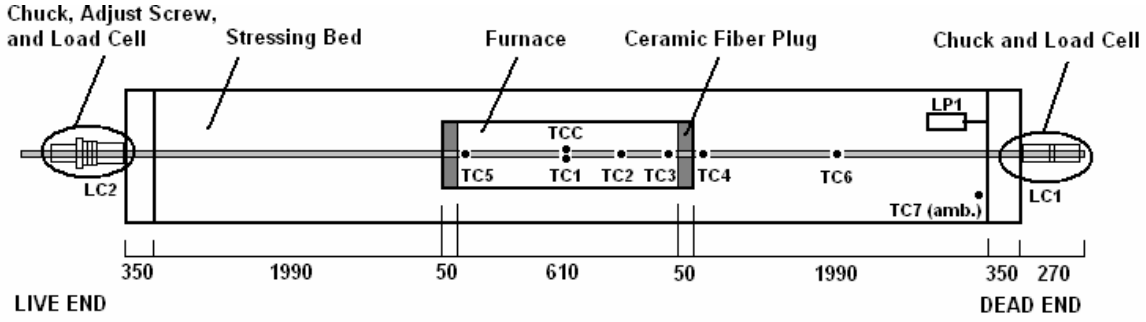

Figure 4.1: Relaxation Test Instrumentation Schematic (plan view, dimensions in mm)

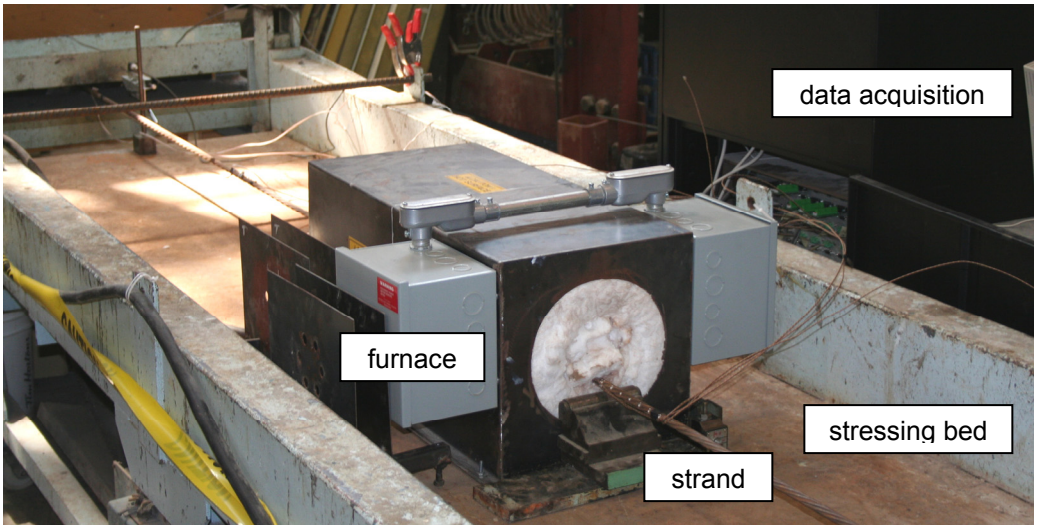

Figure 4.2: Relaxation Test Experimental Setup

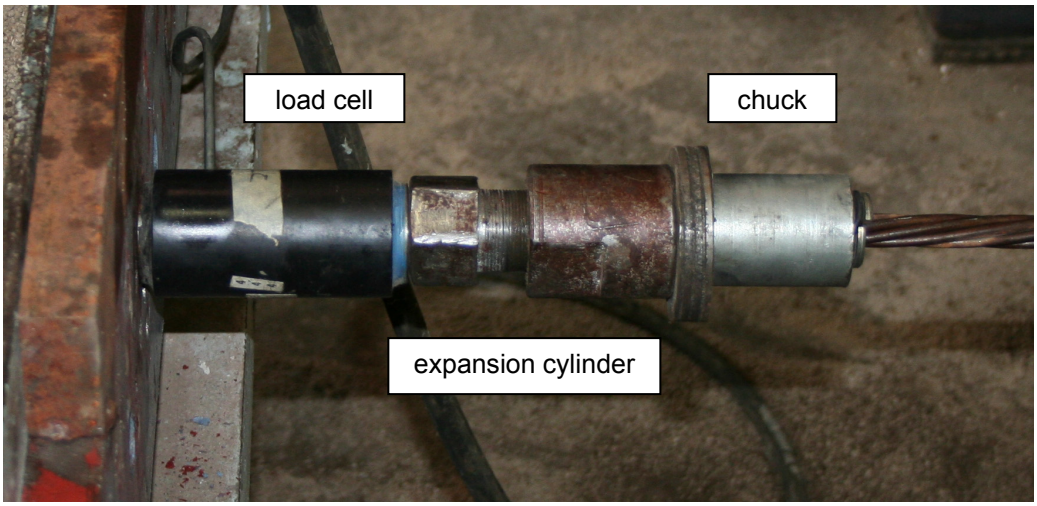

Figure 4.3: Centre-hole Load Cell, Adjustment Screw and Chuck Assembly

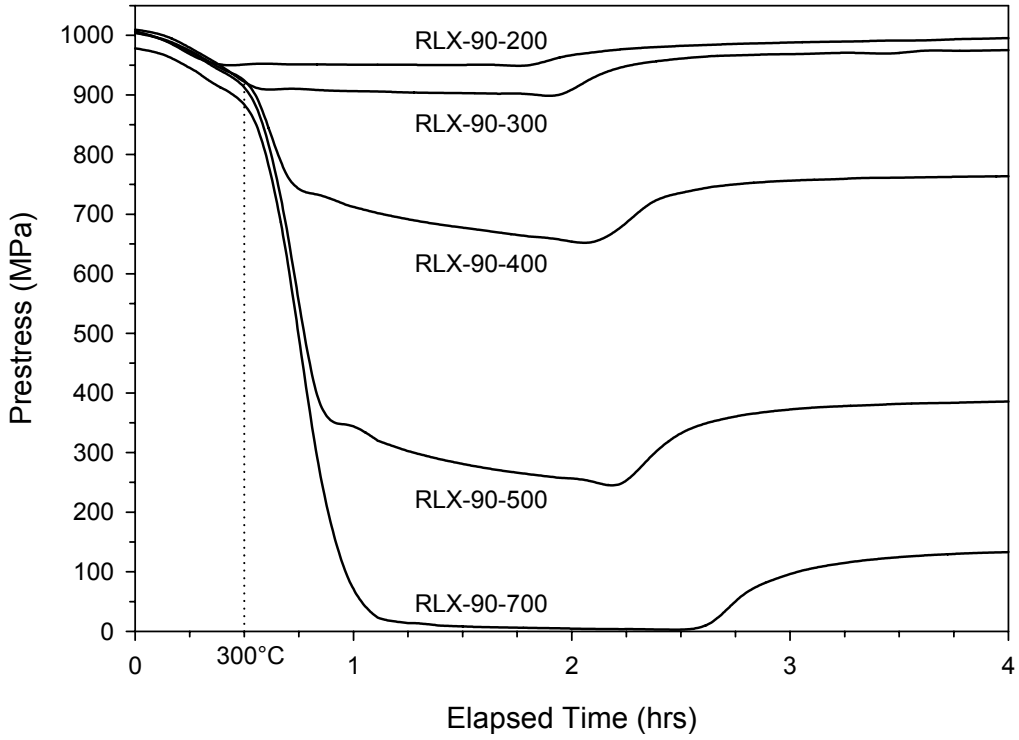

Figure 4.4: Stress Relaxation at Various Temperatures – 90 min. hold time

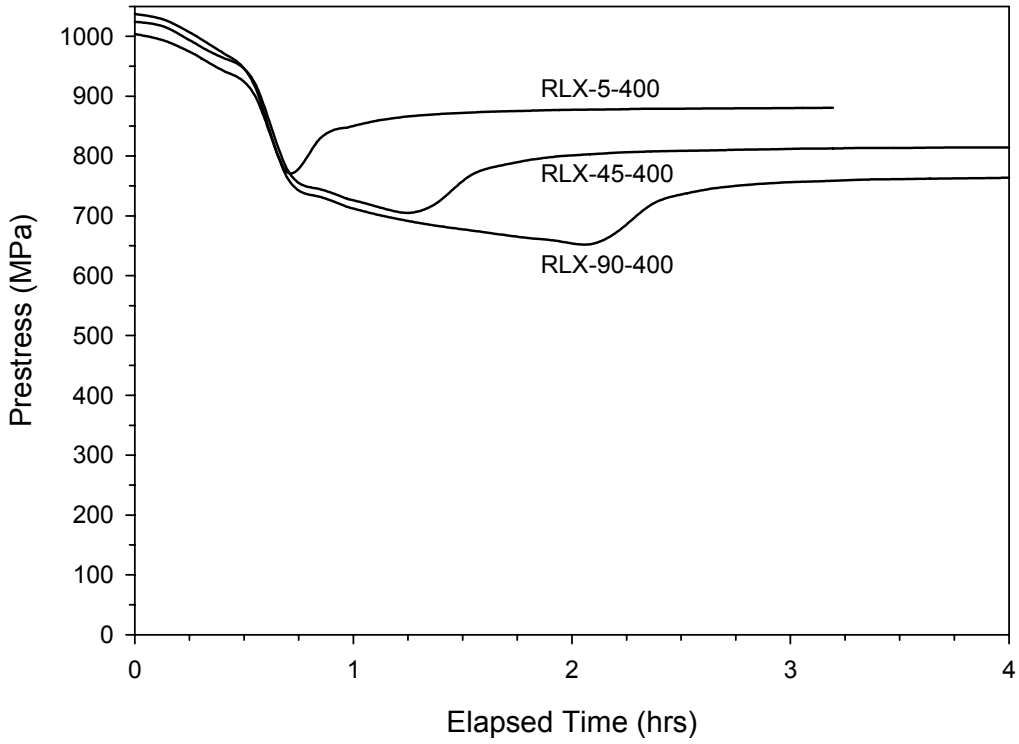

Figure 4.5: Stress Relaxation at 400°C – varying hold times

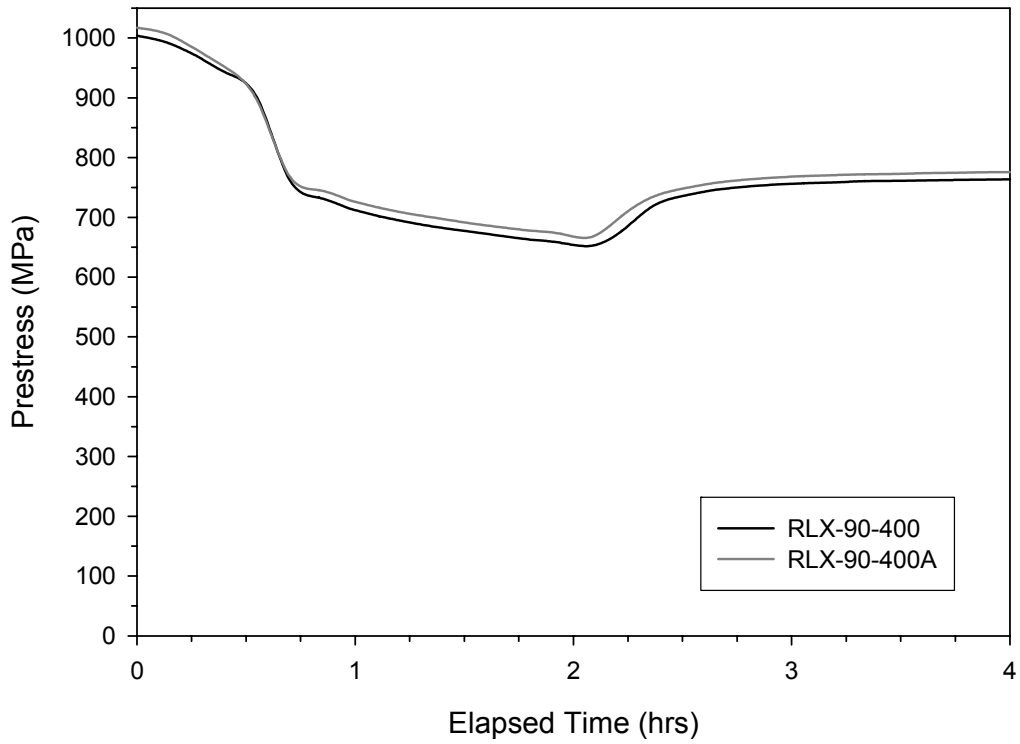

Figure 4.6: Stress Relaxation at 400°C – 90 min. hold time

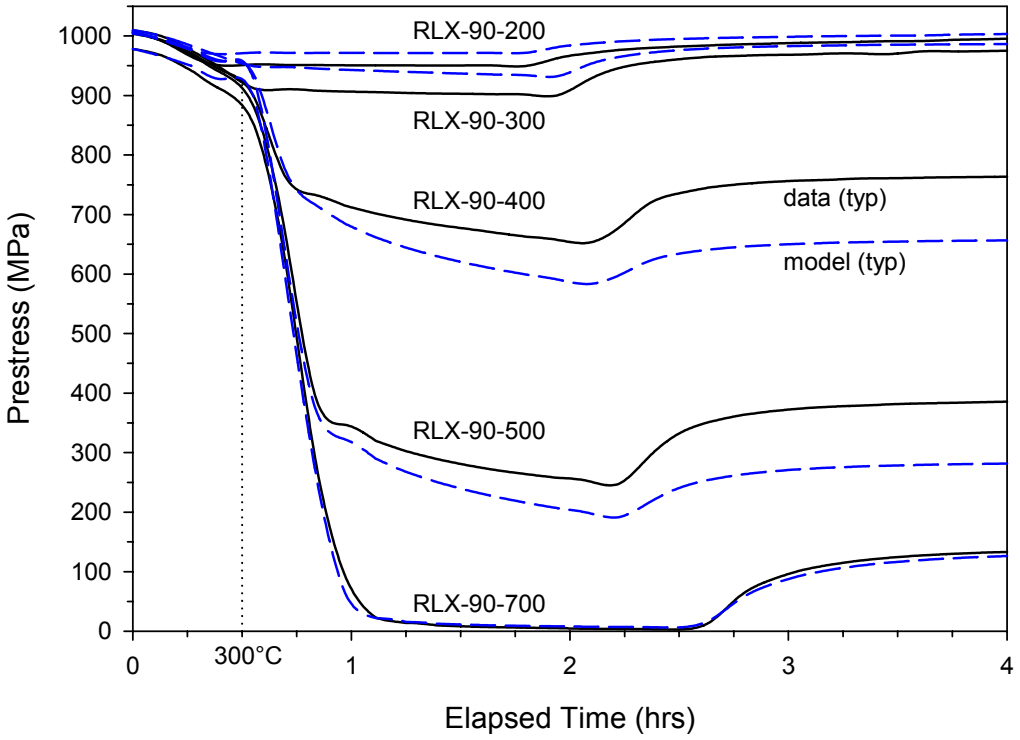

Figure 4.7: Stress Relaxation at Various Temperatures with Analytical Prediction – 90 min. hold time

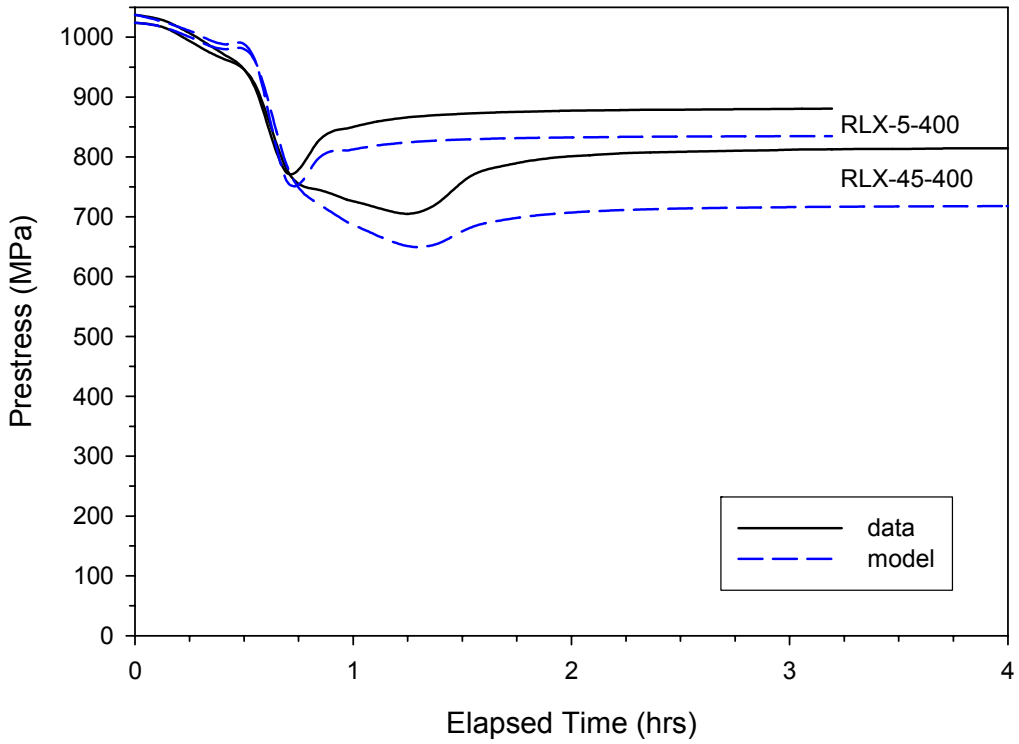

Figure 4.8: Stress Relaxation at 400°C with Analytical Prediction – varying hold time

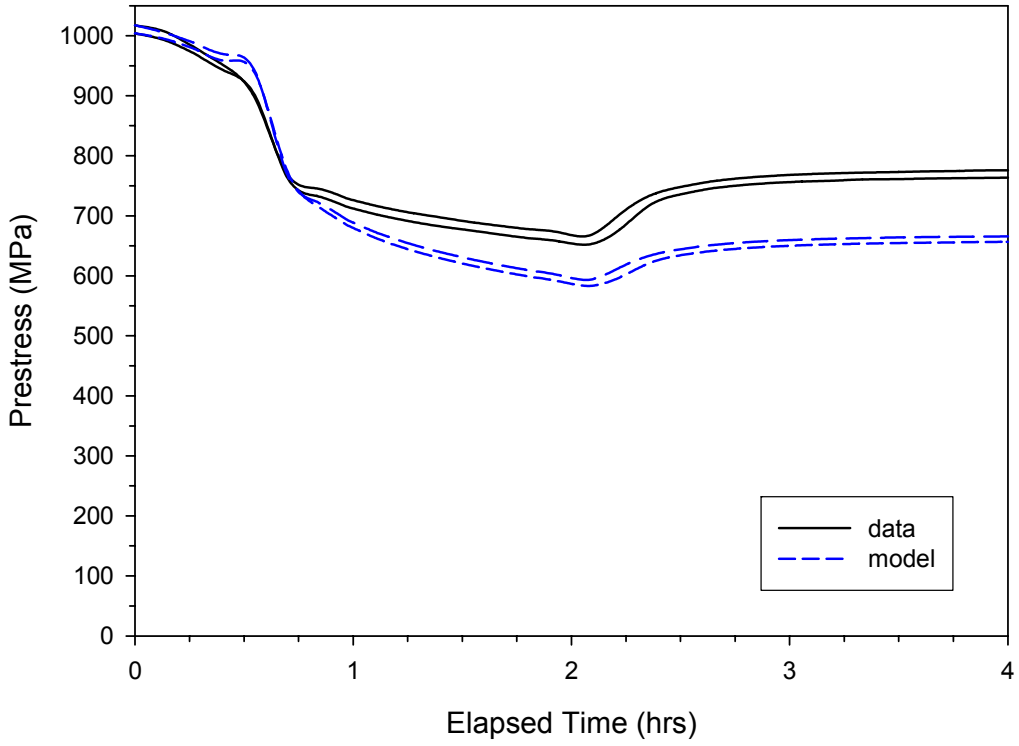

Figure 4.9: Stress Relaxation at 400°C with Analytical Prediction – 90 min. hold time (RLX-90-400; RLX-90-400A)

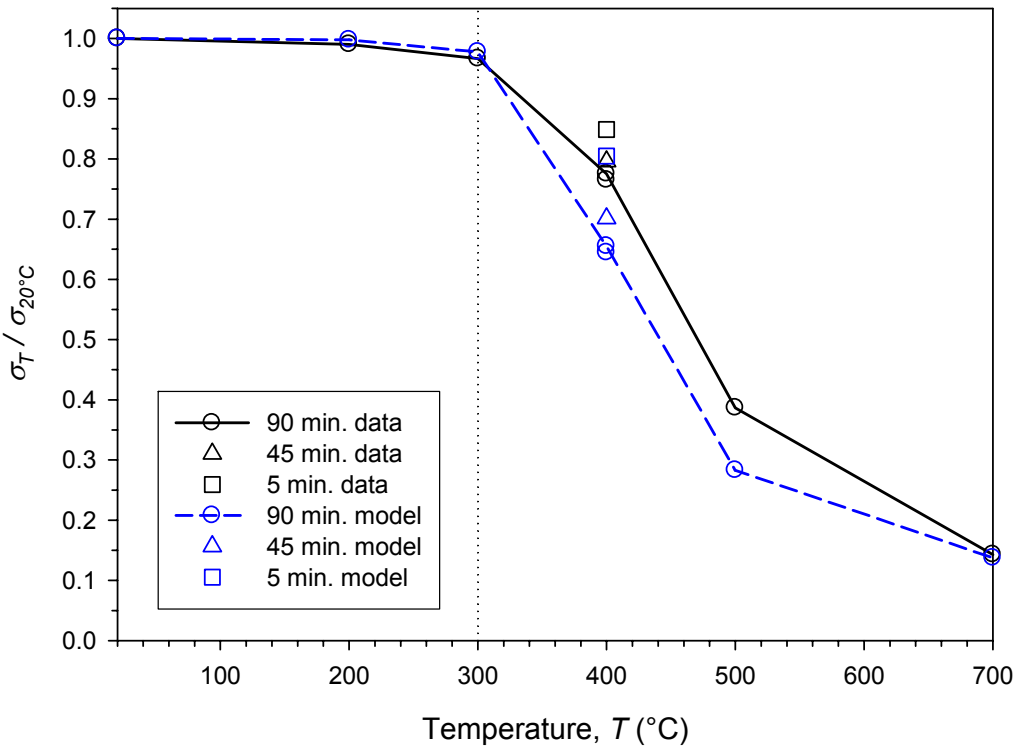

Figure 4.10: Comparison of Experimental Remaining Prestress Fraction with Analytical Prediction

CHAPTER 5 – Consequences for the Post-Fire Performance of Unbonded Post-Tensioned Members

5.0 General

From the previous discussions of the residual degradation of mechanical properties and stress relaxation it has been shown that significant losses of residual strength and prestress begin to occur at temperatures between 300°C and 400°C. To provide the reader with some useful perspective on the duration and intensity of fire necessary to significantly reduce the moment capacity and flexural stiffness of a typical unbonded post-tensioned slab, a finite-difference heat transfer model is applied herein to a common unbonded post-tensioned concrete slab configuration, and the effects of concrete cover and various standard fire durations on consequent structural performance are discussed. Additionally, recommendations for further experimental investigation and analytical model refinement are suggested.

5.1 Finite Difference Heat Transfer Model

A numerical heat transfer analysis was used herein to determine temperature distributions through a typical unbonded post-tensioned concrete slab subjected to a standard fire. This has been performed using the software *QSFIRE*, an explicit finite-difference formulation created and validated by Bisby (2003). The program was coded in DIGITAL™ Visual Fortran, and is capable of calculating the spatial and temporal variations in temperature throughout concrete members subjected to any standard fire (e.g., ASTM 2001d) using an elemental energy balance approach.

In *QSFIRE*, concrete slabs are assumed to be of infinite size horizontally (i.e., one-dimensional heat transfer with no edge effects) and the effect of thermal

conduction within reinforcing steel is ignored (an approach which has been proven by Bisby (2003) to be valid). The program is able to account for the specific thermodynamic properties of different aggregates commonly found in concrete in North America, as well as the evaporation of moisture from concrete occurring at temperatures near 100°C. Concrete slabs are discretized into horizontal elemental layers with ambient conditions modelled at the uppermost and lowermost elements using empirical approximations (determined by comparison with results from full scale fire endurance tests). The ambient temperature at the lowermost element is increased through predominantly radiative heat transfer in accordance with the ASTM E119 (ASTM 2001d) standard fire curve. The uppermost element is assumed to be exposed to normal ambient conditions and accounts for convective heat loss from the top of the slab using empirical free convection relationships. Further information on the specific equations and procedures used by *QSFIRE*, and its validation based on comparisons against numerous medium and full scale experiments, can be found in Bisby (2003).

5.2 Practical Example

5.2.1 General

QSFIRE was used to generate temperature versus time profiles at 1 mm increments over the entire depth of a typical unbonded post-tensioned reinforced concrete slab. The chosen exemplary slab is a 150 mm carbonate aggregate concrete slab having an initial volumetric moisture content of 5% (which is at the conservative end of the likely volumetric moisture content range for an in-service concrete slab with an interior exposure condition), exposed to the ASTM E119 Standard Fire (ASTM 2001d). Outputs from *QSFIRE* at 5 mm depth increments from 10 mm to 60 mm clear cover are presented

in Figure 5.1 to provide the reader with a sense of the elapsed time required to reach the important irrecoverable prestress loss temperature exposure range of 300°C to 400°C established in the previous chapters. It can be seen with reference to Figure 5.1 that, for standard fire exposure and a concrete cover to the prestressed reinforcement of approximately 20 mm, damage to the prestressing tendons and irrecoverable prestress loss can be expected to occur between 20 and 40 minutes of exposure to the standard fire.

Given that both the ultimate tensile strength of prestressing strand and the amount of applied prestress clearly affect the ultimate moment capacity of unbonded slabs, this typical slab configuration and heat transfer behaviour (under standard fire exposure) is used to highlight the potential post-fire residual behaviour of these types of members, and to illustrate the need for additional research in this area. Several variations of the following configuration are used in a parametric study of the effect of heated length, l_h, to total length, l, (referred to in the following sections as the heated length ratio, $n_{hl} = l_h / l$) and amount of concrete clear cover provided. In the definition of heated length ratio, the entire bay length was deemed heated so as not to exclude the effect of small increases in strand temperature seen where large depths of concrete cover are present (at supports).

5.2.2 Example Slab Definition

The typical example structure used for discussion herein has been adapted from *Example 5.5.4 – Flat Plate Apartments* in the Post-Tensioning Institute Manual (PTI 1990), and has been slightly modified, as follows. The 163 mm flat plate slab with end spans of 5200 mm and interior spans of 7700 mm was reduced to a thickness of 150 mm for the example, since minimal amounts of prestressed and mild reinforcement were calculated in the PTI example (see Figures 5.2 and 5.3). A parabolic tendon profile

was assumed, with 20 mm clear cover to the tendon at column centerlines and at midspan. From this, a second order polynomial was used to define tendon depths at any location within a typical 7700 mm interior span. This function was subsequently used to aid in the rational discretization of the tendon into different longitudinal segments of constant temperature, as described later.

Lines of 350 mm × 800 mm columns were assumed to be transversely spaced at 6100 mm on centre. A similar but slightly higher amount of bonded and unbonded longitudinal reinforcement was assumed, with twelve 13 mm diameter Grade 1860 seven-wire tendons and ten 10M Grade 400 bars placed within the 6100 mm wide design strip. Tendons were assumed to have an applied prestress of 60% of ultimate (i.e., 1118 MPa) under service conditions. The concrete strength was taken to be 30 MPa, and the aggregate was assumed to be carbonate (i.e., limestone). Finally, the volumetric moisture content was assumed to be 5%. The aforementioned slab and reinforcement configuration would be appropriate and economical for typical apartment or condominium designs, where the total service dead load (including finishes, partitions and slab self-weight) is approximately 4.5 kPa, and the associated service live load is 1.9 kPa. Since residential units constructed in unbonded post-tensioned concrete structures are typically compartmentalized for fire safety, as opposed to the open floor layouts common in modern unbonded post-tensioned concrete office buildings, the current example is appropriate for use in providing insights into the performance of these types of structures with different heated length ratios (i.e., because there are fire stops between adjacent bays). Note that the design bending moment capacity of the slab has been calculated in accordance with the requirements of CAN/CSA A23.3-94 (CSA 1994).

5.2.3 Determination of Irrecoverable Prestress Loss

As previously mentioned, a parabolic tendon profile has been assumed, with 20 mm clear cover at midspan and at the column centerlines. As a result, the depth of the tendon at both its ends and its mid-length are known and the total length of the tendon's parabola is also known (approximately equal to the length of the bay, 7700 mm). Thus, the equation of the parabola defining the tendon profile is:

$$b_c = 7.61^{-6} x^2 - 0.0586x + 130 \tag{5.1}$$

where b_c represents the distance of the tendon from the bottom of the slab in mm, and x represents the longitudinal distance from a supporting column to the tendon location being considered, in mm.

It was decided that the effects of one hour of exposure to the ASTM Standard Fire would be examined, since, according to ACI 318 (ACI 2002), 20 mm of cover to the prestressed reinforcement provides a one hour fire rating for a carbonate aggregate slab (see Table 2.8). Note also that the fire was assumed to be contained within interior bays of the multi-bay continuous slab. Different heated length ratios were examined by varying the number of interior bays and the number of those bays exposed to fire. With a reasonable duration of fire exposure selected, Equation 5.1 was subsequently used to discretize the tendon into different series of elements having constant length, l_{elem}, and temperature by computing the depth of cover, b_c, at the beginning and end of each element and taking the average of these two values as the element depth. The reader will note that this procedure necessitates an assumption that no heat is transferred longitudinally along the steel tendon; an assumption which has been shown to be valid (see Appendix B).

Initially, five elements 1540 mm in length and ten elements 770 mm in length, or 20% and 10% of the total heated length of 7700 mm, were considered. Average element depths were computed (see Tables 5.1 and 5.2), and the corresponding *QSFIRE* fire outputs, along with appropriate element lengths were input into the transient relaxation model developed herein and presented in Chapter 4. The model was then applied to the example slab described previously having one interior span of 7700 mm and two end spans of 5200 mm. The results of total relaxation versus time for each of the two element lengths were compared and found to have a difference of 22% after one hour of exposure. As a result of the large difference between the previous element lengths, the tendon approximation was further refined to utilize ten elements 385 mm in length (assuming symmetry at midspan), which constitutes 5% of the total heated length. With this refinement and considerably more computational effort, a small change in total relaxation of less than 3% difference was found to occur after one hour of exposure (see Figure 5.4). The longitudinal position and corresponding average depth of cover used for the final tendon discretization is summarized in Table 5.3. It should be noted that ten elements of 385 mm in length were adopted for the remainder of this parametric study and that tendon symmetry at midspan was assumed in this formulation.

Although temperatures critical to initiate significant transient relaxation or to cause substantial reductions in material strength are not likely achieved through the full thickness of the slab within the first hour of exposure, the entire length of tendon was discretized in order to accurately incorporate the correct amount of thermal expansion experienced, which occurs in appreciable amounts at much lower temperatures. As such, the total heated length, $l_{h,}$ was taken to be the total length of fire exposed bays (as noted previously).

With the tendon appropriately discretized, a series of specific configurations were modelled to determine the significance of heated length ratio on the amount of irrecoverable relaxation experienced. The effect of relatively low heated length ratios was examined by assuming the standard fire to be compartmentalized in one bay while varying the number of interior spans from one to three, with the depth of concrete cover held constant at 20 mm. This provided relaxation data for heated length ratios of 0.43, 0.30, and 0.23 respectively. Similarly, the effect of relatively high heated length ratios, 0.60 and 0.69, was examined by assuming all interior bays were exposed to the standard fire.

The results of the application of the transient relaxation model (defined in Chapter 4) to each of the five aforementioned scenarios are summarized in Figures 5.5 and 5.6, with recoverable relaxation (thermal expansion) and total relaxation (i.e. thermal expansion plus creep related thermal relaxation) shown separately. Note that the instantaneous irrecoverable relaxation (which is a function of elevated temperature creep) is represented by the difference between the two curves mentioned previously. For the configurations investigated, the model indicates that the heated length ratio has little effect on the amount of total relaxation experienced, as can be seen in the difference between solid lines in Figures 5.5 and 5.6. However, variation in heated length ratio was seen to have a more appreciable effect on the amount of irrecoverable relaxation exhibited; with smaller heated length ratios actually exhibiting more irrecoverable relaxation (see Figure 5.7). This result suggests that localized exposure of unbonded prestressing tendons to elevated temperature is potentially more severe in terms of irrecoverable prestress loss than full tendon exposures; an important yet counterintuitive result. This is because full tendon exposure causes greater (temporary and recoverable)

reduction in tendon force due to thermal expansion, leading in turn to less (permanent and irrecoverable) relaxation losses.

Next, the effect of variation in concrete cover to the prestressed reinforcement on relaxation levels was investigated. The example configuration with a heated length ratio of 0.30, representing the case with two end bays and two interior bays, was used with the same length of constant temperature elements (l_{elem} = 385 mm) previously described. Temperature-time curves for each element were varied by either increasing or decreasing the concrete cover used in the heat transfer analysis by 10 mm, such that transient relaxation profiles for slabs having clear covers of 10 mm and 30 mm to the prestressed reinforcement were approximated, with the results of this analysis shown in Figure 5.8. As in Figures 5.5 and 5.6, both the total and recoverable relaxation profiles were determined for each level of concrete cover. The amount of irrecoverable prestress loss due to thermal creep related relaxation was subsequently determined assuming the tendon was cooled instantaneously to room temperature (i.e., recoverable thermal expansion subtracted from total transient relaxation) and is shown in Figures 5.9 to 5.11. Not surprisingly, the depth of concrete clear cover to the prestressed reinforcement has a marked effect on the amount of prestress force lost as a result of fire exposure; thus illustrating the importance of construction tolerances in these types of structures to provide adequate fire safety against collapse.

5.2.4 Determination of Moment Capacity

Using the aforementioned analytical procedure, the amount of irrecoverable loss in prestress for a typical 150 mm thick post-tensioned residential concrete floor slab after one hour of exposure to the ASTM Standard Fire (ASTM 2001d) was determined to be

849 MPa, 478 MPa, and 76 MPa for 10 mm, 20 mm, and 30 mm of concrete clear cover to the reinforcement, respectively. These changes in effective prestress force, f_{pe}, under service conditions were used with provisions of CAN/CSA A23.3-94 (CSA 1994) to determine the effect of fire on the residual moment capacity of each slab, as described in the following section.

The moment capacity of the previously described example slab was determined using code provisions outlined in Section 2.6 of this thesis as follows (CSA 1994):

1) the depth of the neutral axis at a plastic hinge, c_y, assuming $f_{pr} = f_{py} = 0.9f_{pu,T}$ was determined using Equation 2.17 given known slab properties for the current example;

$$c_y = \frac{\phi_p A_{ps} f_{py} + \phi_s A_s f_s - \phi_s A'_s f'_s - 0.85\phi_c f'_c h_f (b - b_w)}{0.85\phi_c \beta_1 f'_c b_w} = \frac{\phi_p A_{ps} f_{py} + \phi_s A_s f_s}{0.85\phi_c \beta_1 f'_c b_w}$$

$$c_y = \frac{0.90 \cdot 12 \cdot 99 \cdot 0.9 \cdot f_{pu,T} + 0.85 \cdot 10 \cdot 100 \cdot 400}{0.85 \cdot 0.60 \cdot 0.90 \cdot 30 \cdot 6100} = \frac{f_{pu,T} + 353.3}{87.3}$$

2) the effective tendon length, l_e, was determined for a typical interior span assuming total tendon length equal to the summation of bay lengths (although this approximation results in a slightly shorter tendon than would actually be used, it was deemed appropriate given the relative insensitivity of irrecoverable thermal relaxation to heated length ratio);

$$l_e = \frac{5200 + 7700 + 7700 + 5200}{3} = 8600$$

3) the stress in the unbonded prestressed reinforcement at nominal strength, f_{pr}, was determined as a function of effective stress, f_{pe}, depth of concrete clear cover, b_c, and ultimate tensile strength of the prestressed reinforcement, f_{pu};

$$f_{pr} = f_{pe,T} + \frac{8000}{l_e}(d_p - c_y) = f_{pe,T} + \frac{8000}{8600}\left(150 - \frac{12.7}{2} - b_c - \frac{f_{pu,T} + 353.3}{87.3}\right)$$

$$f_{pr} = f_{pe,T} - 0.011 f_{pu,T} - 0.93 b_c + 129.86 \le 0.9 f_{pu,T}$$

4) for residual moment capacity, effective stress in prestressed reinforcement, $f_{pe,T}$, was determined by subtracting the irrecoverable relaxation in prestress determined previously from the original value of f_{pe} (1118 MPa), while residual ultimate tensile strength, $f_{pu,T}$, was calculated using Equation 3.1 and the instantaneous peak temperature of the reinforcement at one hour of fire exposure using Figure 5.1;

5) the depth of the neutral axis, c, at nominal strength was defined in terms of f_{pr}; and

$$c = \frac{\phi_p A_{ps} f_{pr} + \phi_s A_s f_s}{0.85 \phi_c \beta_1 f'_c b_w} = \frac{0.90 \cdot 12 \cdot 99 \cdot f_{pr} + 0.85 \cdot 10 \cdot 100 \cdot 400}{0.85 \cdot 0.60 \cdot 0.90 \cdot 30 \cdot 6100} = \frac{f_{pr} + 318.0}{78.6}$$

6) finally, moment resistance, M_r, was defined in terms of f_{pr} and b_c;

$$M_r = \phi_p A_{ps} f_{pr}\left(d_p - \frac{\beta_1 c}{2}\right) + \phi_s A_s f_s\left(d_s - \frac{\beta_1 c}{2}\right)$$

$$M_r = (0.90 \cdot 12 \cdot 99 \cdot f_{pr} + 0.85 \cdot 10 \cdot 100 \cdot 400) \cdot (141.8 - 0.006 f_{pr} - b_c)$$

$$M_r = (1069.2 f_{pr} + 340000) \cdot (141.8 - 0.006 f_{pr} - b_c)$$

thereby enabling the parametric investigation of the effect of concrete clear cover on the loss of flexural strength after a one hour standard fire. A summary of the aforementioned formulation is provided in Table 5.4, which reveals that a slab with 30 mm clear cover is predicted to experience a 5% reduction of factored moment resistance after one hour of standard fire exposure, while slabs with 20 mm and 10 mm clear cover are expected to experience reductions of 29% and 53%, respectively (see Figure 5.12).

It should be noted that the preliminary analytical investigation performed herein is actually unconservative, due to its failure to account for irrecoverable relaxation experienced during potentially prolonged cooling phases. The analysis also ignores the probable reductions in concrete strength which would be experienced due to heating, particularly in negative moment regions at the column lines where the compression concrete is directly exposed to the elevated temperatures of the fire. Localized strand weakening and reduction in prestress force affect the entire length of unbonded tendons, including negative moment regions where the strength of the concrete in compression could be expected to be seriously compromised by fire exposure from below. As such, both the tendon and the compression face of concrete are therefore damaged, a critical scenario also not considered in this analysis for which further investigation is clearly required.

5.3 Discussion and Summary

The analytical model developed by the Author and described in Chapter 4 was used in conjunction with a previously developed and validated finite difference heat-transfer model to investigate the effects of fire on the prestress loss and residual moment capacity of a typical unbonded post-tensioned slab.

The model was shown to have reasonable convergence when using elements constituting approximately 5% of the total tendon length, and demonstrated the relative insensitivity of transient prestress loss to heated length ratio.

More significantly, the example used in this Chapter suggested that there is a significant loss in moment capacity after one hour of standard fire exposure for slabs having various amounts of clear cover to the prestressed reinforcement. As well, since

post-tensioned slabs are relatively slender members (i.e., they generally have large span-to-depth ratios) high temperature residual punching shear capacity around columns is presumably a significant issue which is not discussed herein but which may require investigation to ensure fire safety in these types of structures. Large span-to-depth ratios result in relatively high shear forces at the column-slab junctions being resisted by a relatively thin concrete section. However, under ambient conditions component forces induced by post-tensioning serve to increase the punching shear capacity of these slabs. As seen herein, even relatively mild (1-hour) and localized fire exposure may greatly reduce the magnitude of the applied prestress force, which would in turn reduce the punching shear resistance of the slab around columns. As such, this topic may prove critical to the post-fire evaluation of post-tensioned slabs.

Finally, it should be noted that the preliminary analysis presented in this chapter suggests that a compartmentalized fire in a single bay of a multi-bay structure may drastically affect the structural performance of adjacent bays, since prestress force along the tendon length is relatively constant (i.e., ignoring frictional effects due to the tendon profile). Additional research studying the influence of frictional effects on tendon stress over multiple bays is also warranted due to changes in grease consistency and sheathing condition.

Table 5.1: Coarse Tendon Discretization (all dimensions in mm)

Element	l_{elem}	x	b_c	d_{elem}
		0	132	
1	1540			96
		1540	60	
2	1540			42
		3080	24	
3	1540			24
		4620	24	
4	1540			42
		6160	60	
5	1540			96
		7700	132	

Table 5.2: Intermediate Tendon Discretization (all dimensions in mm)

Element	l_{elem}	x	b_c	d_{elem}
		0	132	
1	770			112
		770	91	
2	770			76
		1540	60	
3	770			49
		2310	37	
4	770			30
		3080	24	
5	770			21
		3850	19	
6	770			21
		4620	24	
7	770			30
		5390	37	
8	770			49
		6160	60	
9	770			76
		6930	91	
10	770			112
		7700	132	

Table 5.3: Symmetric Ten Element Fine Discretization (all dimensions in mm)

Element	l_{elem}	x	b_c	d_{elem}
		0	132	
1	385			121
		385	111	
2	385			101
		770	91	
3	385			83
		1155	74	
4	385			67
		1540	60	
5	385			54
		1925	47	
6	385			42
		2310	37	
7	385			33
		2695	29	
8	385			27
		3080	24	
9	385			22
		3465	20	
10	385			20
		3850	19	

Table 5.4: Moment Resistance of Example Slab (unheated and residual)

b_c (mm)	$f_{pu,20℃}$ (MPa)	$f_{pe,20℃}$ (MPa)	$f_{pr,20℃}$ (MPa)	$M_{r,20℃}$ (kNm)	$f_{pu,T}$ (MPa)	$f_{pe,T}$ (MPa)	$f_{pr,T}$ (MPa)	$M_{r,T}$ (kNm)
30	1860.0	1118.0	1199.5	169.7	1748.5	1042.0	1124.7	162.0
20	1860.0	1118.0	1208.8	187.0	1428.7	640.1	735.6	132.2
10	1860.0	1118.0	1218.1	204.5	882.2	268.9	379.8	96.6

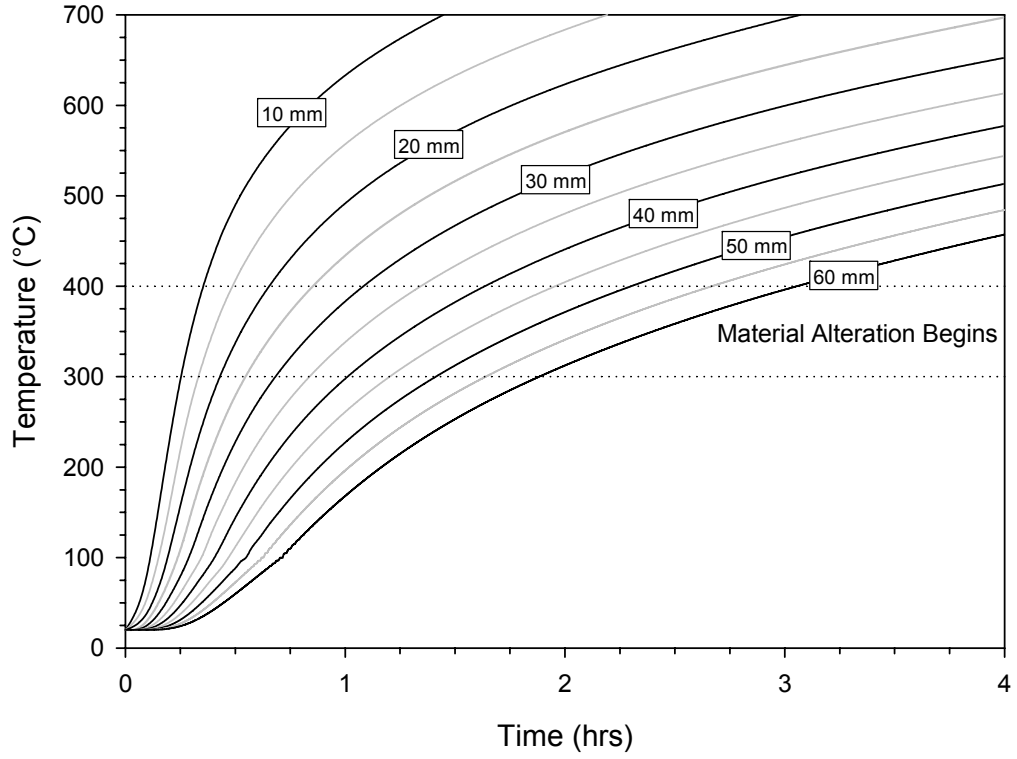

Figure 5.1: Thermal Profile of 150 mm Carbonate Slab 5% MC under ASTM E119 Fire

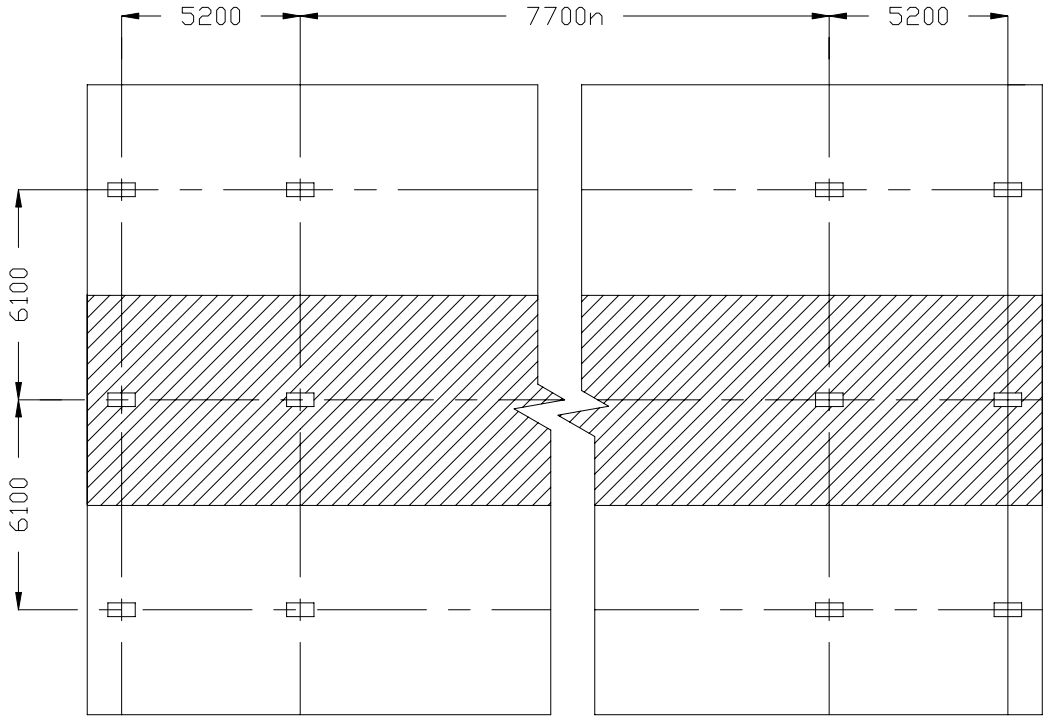

Figure 5.2: Example Slab with '*n*' Interior Spans, Plan View

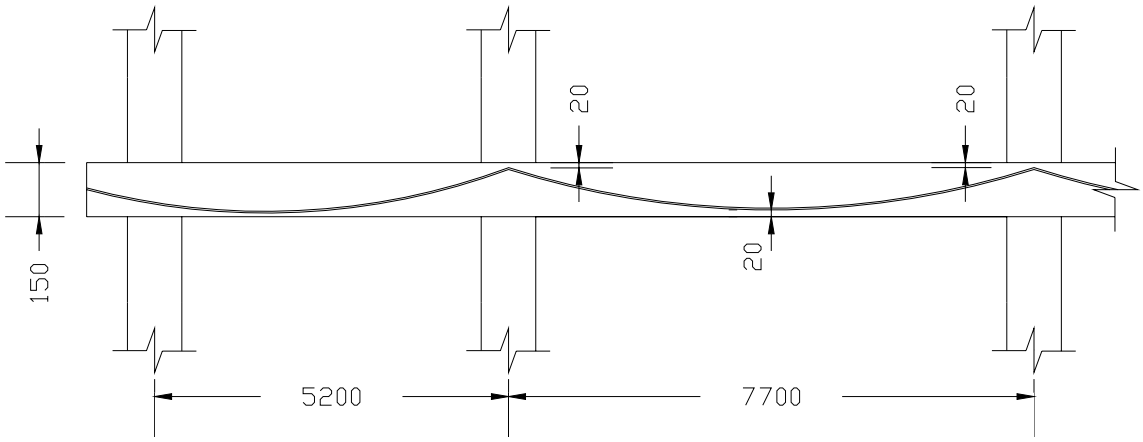

Figure 5.3: Example Slab Partial Elevation End Span and Interior Span

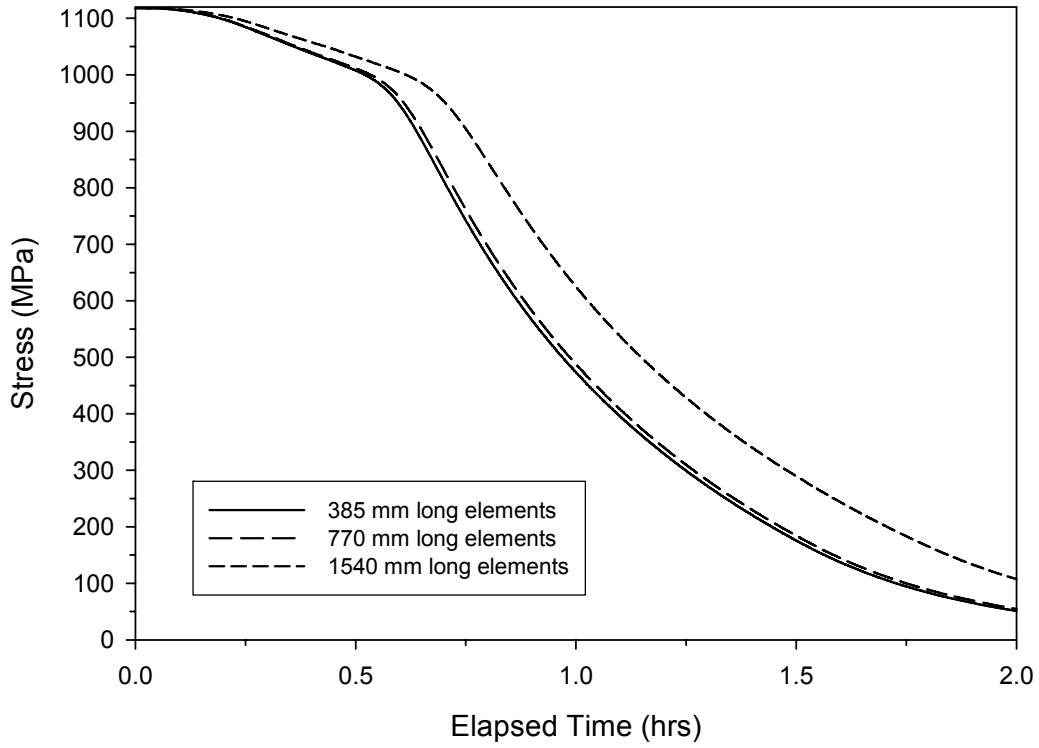

Figure 5.4: Element Length Convergence Analysis for Example Slab with One Interior Span

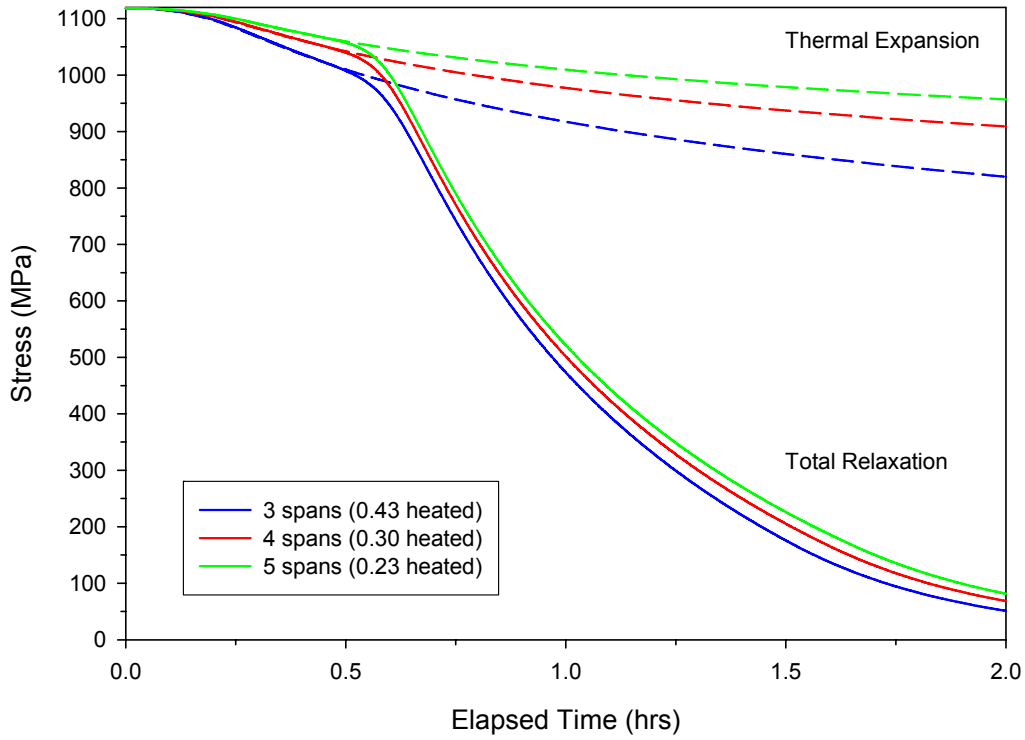

Figure 5.5: Predicted Relaxation 150 mm Slab 20 mm Cover; Low Heated Length Ratios

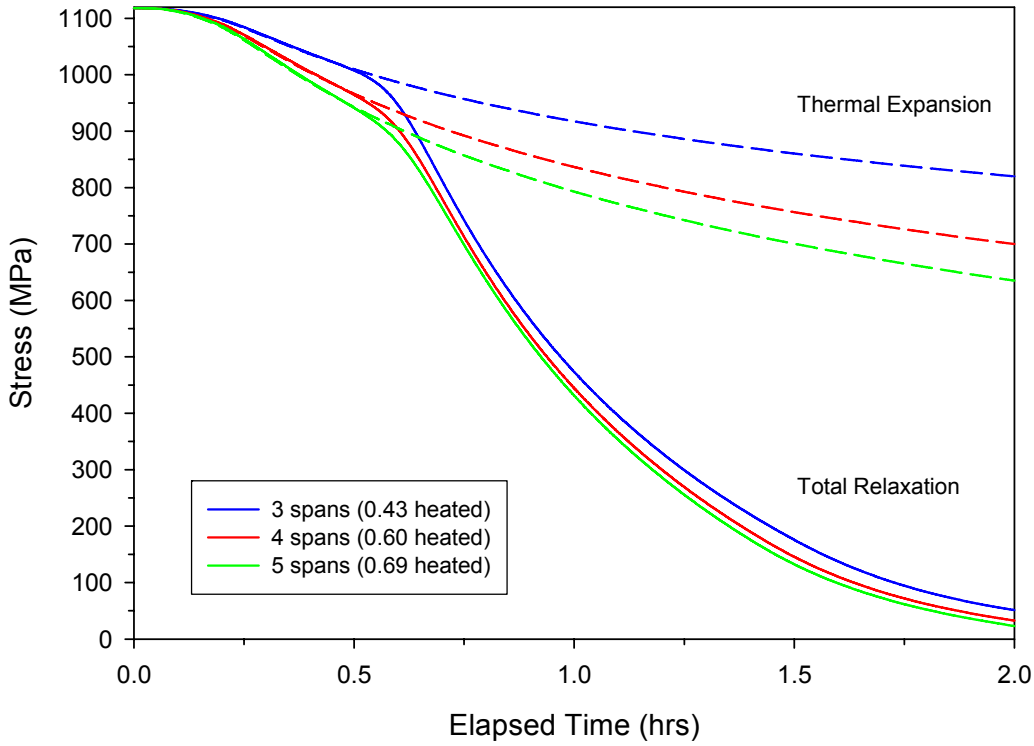

Figure 5.6: Predicted Relaxation 150 mm Slab 20 mm Cover; High Heated Length Ratios

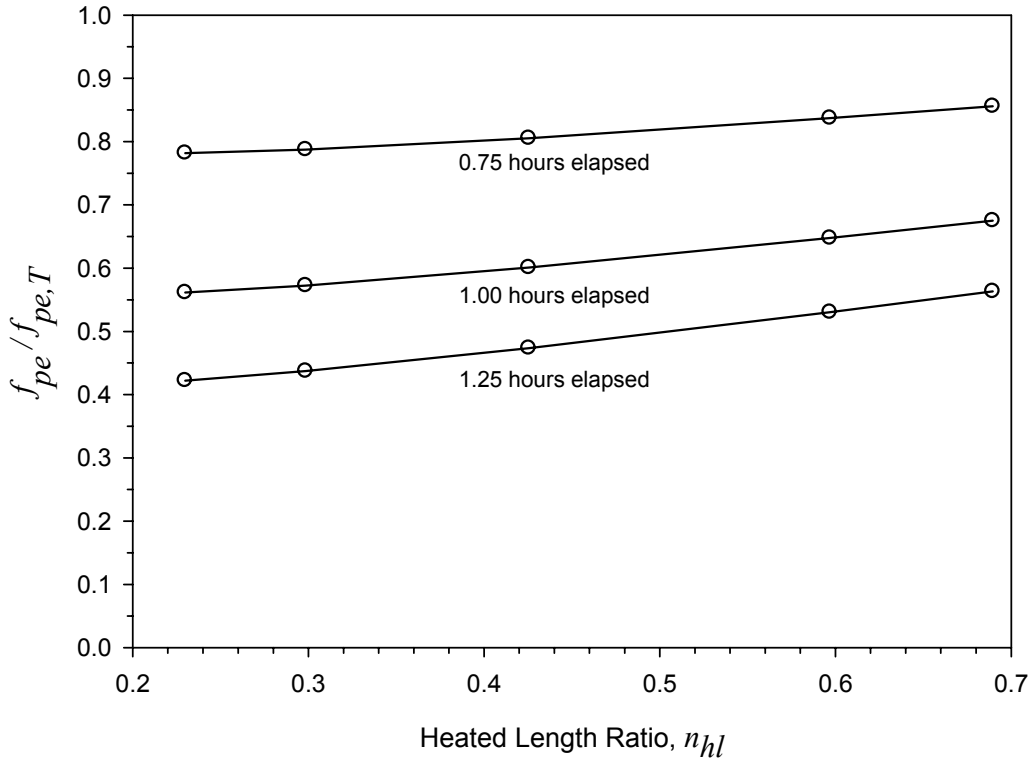

Figure 5.7: Effect of Heated Length Ratio on Remaining Effective Prestress (f_{pe})

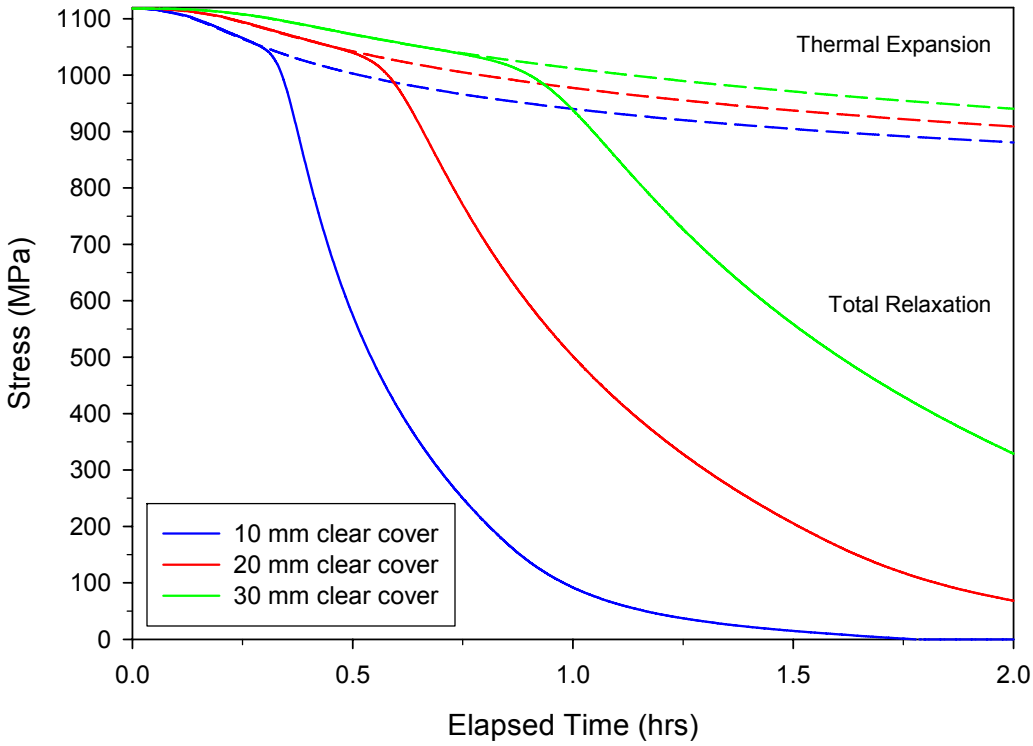

Figure 5.8: Predicted Relaxation 150 mm Slab with Varying Concrete Cover (n_{hl} = 0.30)

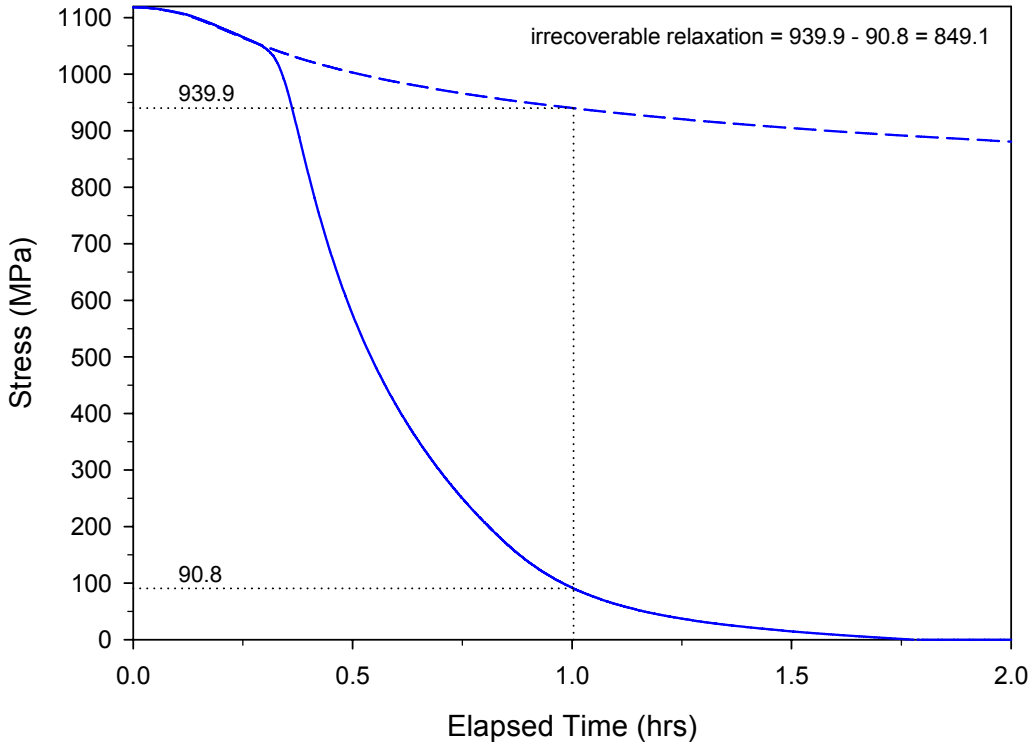

Figure 5.9: Predicted Irrecoverable Relaxation for Typical Slab with 10 mm Clear Cover

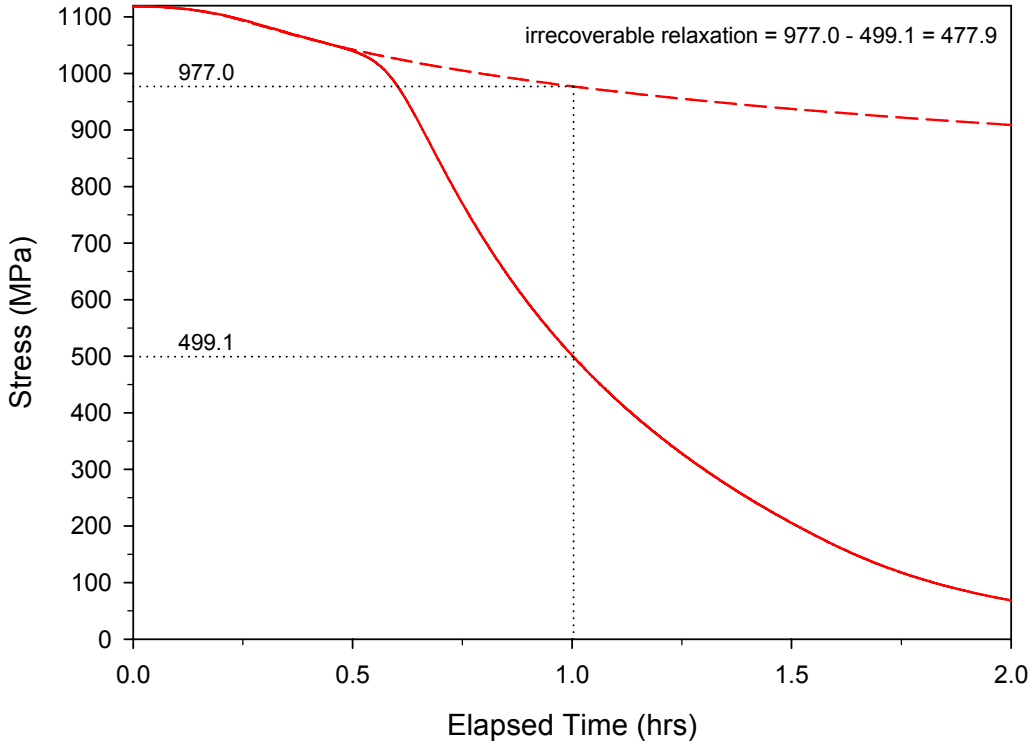

Figure 5.10: Predicted Irrecoverable Relaxation for Typical Slab with 20 mm Clear Cover

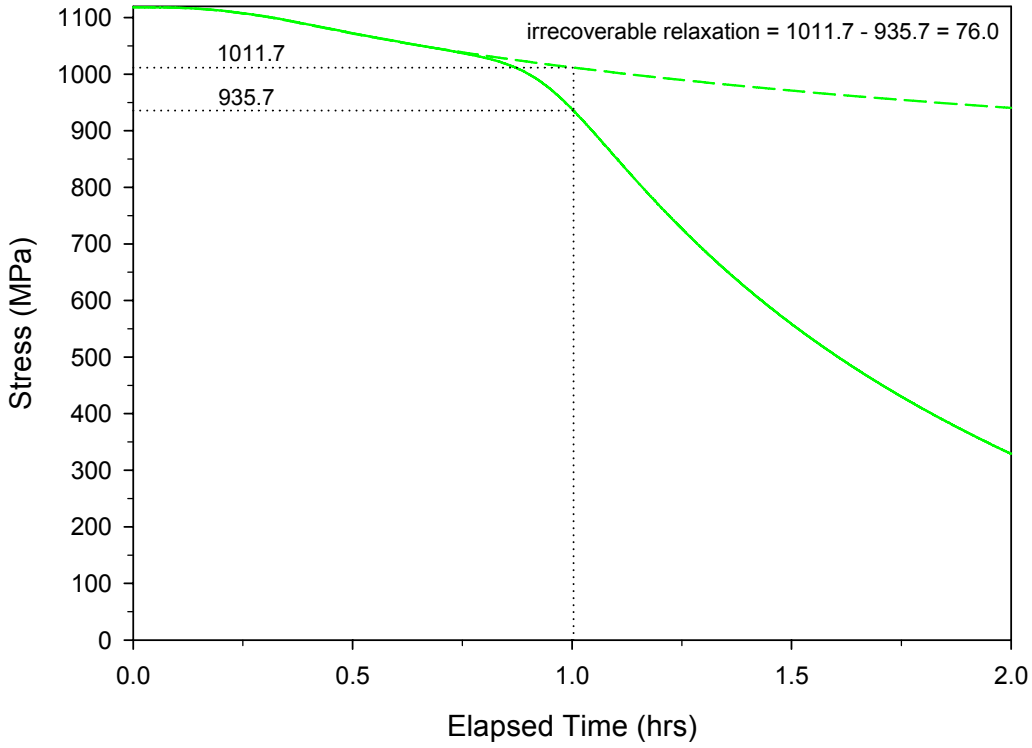

Figure 5.11: Predicted Irrecoverable Relaxation for Typical Slab with 30 mm Clear Cover

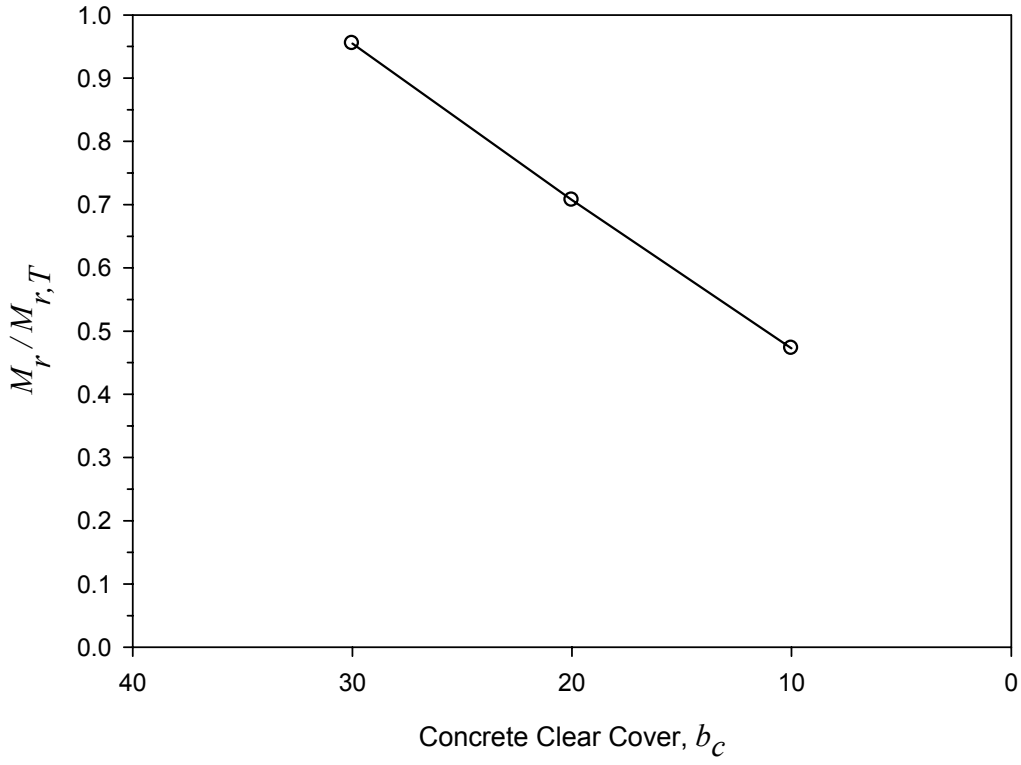

Figure 5.12: Predicted Residual Moment Capacity with Varying Clear Cover (n_{hl} = 0.30)

CHAPTER 6 – Conclusions and Recommendations

6.0 Conclusions

Based on the experimental data and preliminary numerical modelling presented in this thesis, the following conclusions can be drawn:

- A series of high temperature relaxation tests on locally heated seven wire prestressing strand have demonstrated that significant irrecoverable creep-induced prestress loss can occur for unbonded tendons during exposure to temperatures above about 300°C.
- A numerical model has been developed that can satisfactorily predict the variation in prestress level with time for unbonded post-tensioned steel reinforcement subjected to transient thermal regimes.
- The aforementioned model was used in conjunction with a well documented finite difference heat-transfer model to demonstrate the relative insensitively of transient prestress loss to heated length ratio, and more significantly, was used to demonstrate the appreciable loss in moment capacity after one hour of standard fire exposure (for slabs having with various amounts of clear cover to the prestressed reinforcement). It is important to note that adequate concrete cover is crucial to protect the strand from damage.
- The model was also used to confirm the mechanisms (thermal elongation and creep-relaxation) assumed to be significant to the change in prestress level at various temperatures for prestressing steel.
- Loss of prestress governs residual moment capacity and the transient decrease in tendon stress with temperature appears to preclude tendon rupture.

- Due to the lack of published experimentation, the interactions between thermal expansion, stress level and creep at elevated temperatures, and the resulting consequences for unbonded post-tensioned members are not well known.
- A series of residual strength tests performed on core wires from current North American seven-wire prestressing strand after exposure to elevated temperatures agrees well with available literature and indicates that residual strength is significantly affected by temperatures in excess of 300°C. The reader will note that this temperature is considerably less than the assumed ASTM E119 (2001d) critical temperature of 426°C for prestressing steel during fire; suggesting that particular care must be taken in the post-fire assessment of unbonded post-tensioned structures.
- As expected, heating specimens near to the eutectoid transformation temperature in the current study caused significant recrystallization effects resulting in tensile strengths comparable to non-cold-worked pearlite.
- The comprehensive review of literature presented in Chapter 2 of this thesis indicates that little recent data exist which describe the residual strength and relaxation behaviour of cold-drawn prestressing steel exposed to elevated temperatures.
- Finally since post-tensioned slabs are relatively slender members, the punching shear capacity around columns was identified as a significant issue not discussed herein but which requires further investigation, since under ambient conditions component forces induced by post-tensioning serve to increase punching shear capacity.

6.1 Recommendations

The data and analysis presented herein point to a number of areas where additional experimental research is warranted, particularly with respect to the consequences of prestress loss in realistic unbonded post-tensioned structures both during and after a fire.

The profiles of the analytical elevated temperature relaxation model developed in Chapter 4 follow the trends exhibited in experimental data reasonably well. However, creep predictions tend to be over conservative, suggesting that refinement of the creep parameters used in the model may be warranted. This is not unreasonable given the scatter of experimental data cited during the determination of the creep parameter, Z, used in the current model and that the higher stress levels investigated in the current study necessitated the extrapolation of these available data.

Furthermore, the number of channels of thermocouple input in the digital data acquisition system used in the current study limited the number and length of elements that could be used in the analytical model, which has been seen to have a marked affect on relaxation predictions. Therefore, additional testing with better longitudinal thermal resolution should be performed to further validate the model.

Also, as unbonded strands in a real concrete slab can be much longer than those tested in this study (up to 100 m in length), further full-scale fire endurance tests with appropriate strand instrumentation should be performed to better understand the complex interaction of overall length, heated length, tendon stress level, and creep at high temperature; as well as, the interplay existing between thermally induced bowing (occurring due to thermal gradients in the slab), overall thermal expansion of the slab as they may serve to increase tendon stress and therefore transient creep (secondary effect).

Finally, the effect of restraint and continuity over multiple bays must also be considered as it may allow slabs to carry higher loads during elevated temperature exposure than upon cooling.

Additionally, localized strand weakening and reduction in prestress force affect the entire length of unbonded tendons, including negative moment regions where the strength of the concrete in compression could be expected to be seriously compromised by fire exposure from below. Further refinements to the current model are necessary to incorporate this effect.

Finally, as noted above, the residual punching shear capacity around columns is presumably a significant issue which is not discussed herein but should be investigated further.

REFERENCES

Abrams, M. S., and Cruz, C. R. (1961). "Behavior at High Temperature of Steel Strand for Prestressed Concrete." *Portland Cement Association - Research and Development Laboratories - Journal,* 3(3), 8-19.

Abrams, M. S., and Erlin, B. (1967). "Estimating Post-Fire Strength and Exposure Temperature of Prestressing Steel by Metallographic Method." *Portland Cement Association - Research and Development Laboratories - Journal,* 9(3), 23-33.

ACI (2002). "Building Code Requirements for Structural Concrete." *Rep. No. ACI 318-02,* American Concrete Institute, Farmington Hills, MI.

ACI-ASCE Committee 423. (2005). *Recommendations for Concrete Members Prestressed with Unbonded Tendons.* American Concrete Institute, Farmington Hills, MI.

ACI Committee 423. (1998). "Corrosion and Repair of Unbonded Single Strand Tendons." *Rep. No. ACI 423.4R-98,* American Concrete Institute, Farmington Hills, MI.

Allouche, E. N., Campbell, T. I., Green, M. F., and Soudki, K. A. (1998). "Tendon Stress in Continuous Unbonded Prestressed Concrete Members - Part 1: Review of Literature." *PCI Journal,* 43(6), 86-93.

Allouche, E. N., Campbell, T. I., Green, M. F., and Soudki, K. A. (1999). "Tendon Stress in Continuous Unbonded Prestressed Concrete Members - Part 2: Parametric Study." *PCI Journal,* 44(1), 60-73.

Allouche, E. N. (1996). “Tendon Stress in Continuous Unbonded Prestressed Concrete Beams.“ M.Sc. Thesis, Queen's University, Kingston, ON

Anderberg, Y. (1983). "Properties of Materials at High Temperatures: Steel." *Rep. No. TVBB-3008,* Division of Building Fire Safety and Technology, Lund Institute of Technology, Lund University, Sweden.

Anderberg, Y. (1988). "Modelling Steel Behaviour." *Fire Safety Journal Vol.13,* no. 1.

Anderson, W. R. (1964). "Steel for prestressed concrete." *PCI Journal,* vol. 9(no. 2), 109-117.

ARUP. (2005). "Madrid Windsor Fire: The Arup View." http://www.arup.com/fire/feature.cfm?pageid=6150 (07/12, 2006).

ASTM. (2001a). "A370 / A370M-01 Standard Test Methods and Definitions for Mechanical Testing of Steel Products." *Rep. No. A370/ A370M-01,* American Society for Testing and Materials, West Conshohocken, PA.

ASTM. (2001b). "A416 / A416M-01 Standard Specification for Steel Strand, Uncoated Seven-Wire for Prestressed Concrete." *Rep. No. A416 / A416M-01,* American Society for Testing and Materials, West Conshohocken, PA.

ASTM. (2001c). "A421 / A421M-01 Standard Specification for Uncoated Stress-Relieved Steel Wire for Prestressed Concrete." *Rep. No. A421 / A421M-01,* American Society for Testing and Materials, West Conshohocken, PA.

ASTM. (2001d). "Test Method E119-01: Standard Methods of Fire Test of Building Construction and Materials." *Rep. No. E119-01,* American Society for Testing and Materials, West Conshohocken, PA.

ASTM. (2001e). "Test Method E178-01: Standard Practice for Dealing with Outlying Observations." *Rep. No. E178-01,* American Society for Testing and Materials, West Conshohocken, PA.

Avner, S. H. (1974). *Introduction to Physical Metallurgy.* McGraw-Hill, New York, NY.

Bisby, L. A. (2003). "Fire Behaviour of Fibre-Reinforced Polymer (FRP) Reinforced or Confined Concrete." Ph.D. Thesis, Queen's University, Kingston, ON

Buchanan, A. H. (2001). *Structural Design for Fire Safety.* Wiley, New York, NY.

Chacos, G. P. (1988). "Resolution of Field Problems with Unbonded Single-Strand Tendons." *Concrete International,* 10(2), 40-44.

CMHC. (2002). "Investigation Protocol for Evaluation of Post-tensioned Buildings." *Rep. No. 63044,* Canada Mortgage and Housing Corporation, Ottawa, ON.

Collins, M. P., and Mitchell, D. (1987). *Prestressed Concrete Basics.* Canadian Prestressed Concrete Institute, Ottawa, ON.

CPCI. (1996). *Design Manual: Precast and Prestressed Concrete.* Canadian Prestressed Concrete Institute, Ottawa.

CSA (1994). *CAN/CSA A23.3-94: Design of Concrete Structures.* Canadian Standards Association, Ottawa, ON.

Dorn, J. E. (1955). "Some Fundamental Experiments on High Temperature Creep." *J.Mech.Phys.Solids,* 3(2), 105-116.

Dowling, N. E. (1998). *Mechanical Behavior of Materials: Engineering Methods for Deformation, Fracture, and Fatigue.* Prentice-Hall, New Jersey.

Fan, J. (2004). "Experimental study on material properties of prestressed steel strand post high temperatures." *Nanjing Li Gong Daxue Xuebao/Journal of Nanjing University of Science and Technology,* 28(2), 186-189.

Freyermuth, C. L. (1991). "Durability of Post-Tensioned Prestressed Concrete Structures." *Concrete International,* 13(10), 58-65.

Gilvary, K. R., and Dexter, R. J. (1997). "Evaluation of Alternative Methods for Fire Rating Structural Elements." *Rep. No. NIST GCR 97-718; ATLSS Report No. 97-05,* National Institute of Standards and Technology, Gaithersburg, MD.

Glodowski, R. J. (1990). "Steel Wire Rod." *Metals Handbook- Properties and Selection: Irons, Steels, and High-Performance Alloys,* E. L. Langer, ed., ASM International, Materials Park, OH, 272-277.

Gustaferro, A. H. (1973a). "Design of Prestressed Concrete for Fire Resistance." *Journal of the Prestressed Concrete Institute,* 18(6), 102-116.

Gustaferro, A. H. (1973b). "Fire Resistance of Post-tensioned Structures." *Journal of the Prestressed Concrete Institute,* 18(2), 38-63.

Gustaferro, A. H., and Lin, T. D. (1986). "Rational Design of Reinforced Concrete Members for Fire Resistance." *Fire Safety Journal,* 11(1-2), 85-98.

Guyon, Y. (1953). *Prestressed Concrete.* Contractors Record and Municipal Engineering, London.

Hampton, T. (2004). "Another Chicago Fire Motivates Code Changes." http://www.enr.com/news/buildings/archives/041207.asp (12/7, 2004).

Harmathy, T. Z. (1967). "Deflection and Failure of Steel-Supported Floors and Beams in Fire." *Fire Test Methods- Restraint and Smoke 1966 ASTM Special Technical Publication 422,* C. C. Carlson, ed., American Society for Testing and Materials, Philadelphia, 40-62.

Harmathy, T. Z., and Stanzak, W. W. (1970). *Elevated-Temperature Tensile and Creep Properties of Some Structural and Prestressing Steels.* National Research Council of Canada. Division of Building Research, Ottawa, ON.

Hertz, K. D. (2004). "Reinforcement Data for Fire Safety Design." *Magazine of Concrete Research,* 56(8), 453-459.

Hill, A. W., and Ashton, L. A. (1957). "Fire Resistance of Prestressed Concrete." *Civil Engineering (London),* 52(617), 1249-1253.

Holmes, M., Anchor, R. D., Cook, G. M. E., and Crook, R. N. (1982). "Effects of Elevated Temperatures on the Strength Properties of Reinforcing and Prestressing Steels." *Structural Engineer, Part B: R&D Quarterly*, 60B(1), 7-13.

Hu, H. (1985). "Recovery, Recrystallization, and Grain-Growth Structures." *Metals Handbook- Metallography and Microstructures,* E. L. Langer, ed., ASM International, Materials Park, OH, 693-699.

Khoury, G. A. (2000). "Effect of Fire on Concrete and Concrete Structures." *Progress in Structural Engineering and Materials,* 2(4), 429.

Krauss, G. (1989). *Steels: Heat Treatment and Processing Principles.* ASM International, Materials Park, OH.

Lankford, W. T., United States Steel Corporation, and Association of Iron and Steel Engineers. (1985). *The Making, Shaping, and Treating of Steel.* Association of Iron and Steel Engineers, Pittsburgh, PA.

Lie, T. T. (1992). *Structural Fire Protection.* American Society of Civil Engineers, New York, NY.

Lie, T. T. (1972). *Fire and Buildings.* Applied Science Publishers Ltd., London.

Lim, L., Buchanan, A. H., and Moss, P. J. (2004). "Restraint of Fire-Exposed Concrete Floor Systems." *Fire and Materials,* 28(2-4), 95-125.

Lin, T. Y., and Burns, N. H. (1981). *Design of Prestressed Concrete Structures.* Wiley, New York, NY.

Malhotra, H. L. (1982). "Report on the Work of Technical Committee 44-PHT: Properties of Materials at High Temperatures." *Materials and Structures,* 15(86), 161-170.

Neves, I. C., Rodrigues, J. P. C., and de Padua Loureiro, A. (1996). "Mechanical Properties of Reinforcing and Prestressing Steels after Heating." *Journal of Materials in Civil Engineering,* 8(4), 189-194.

NRC. (1995). *National Building Code of Canada 1995.* National Research Council of Canada, Ottawa, ON.

Phan, L. T., and Carino, N. J. (2000). "Fire Performance of High Strength Concrete: Research Needs." *Advanced Technology in Structural Engineering: Proceedings of Structures Congress 2000,* American Society of Civil Engineers, Reston, VA.

Phan, L. T., and Carino, N. J. (1998). "Review of Mechanical Properties of HSC at Elevated Temperature." *Journal of Materials in Civil Engineering,* 10(1), 58-65.

PTI. (1990). *Post-Tensioning Manual - Fifth Edition.* Post-Tensioning Institute, Phoenix, AZ.

Rigberth, J. (2000). "Simplified Design of Fire Exposed Concrete Beams and Columns: An Evaluation of Eurocode and Swedish Building Code Against Advanced Computer Models." *Rep. No. TVBB-5063,* Department of Fire Safety Engineering, Lund Institute of Science and Technology, Lund University, Sweden.

Schneider, U. (1990). "Repairability of Fire Damaged Structures." *Fire Safety Journal,* 16(4), 251-329.

Schneider, U. (1988). "Concrete at High Temperatures - A General Review." *Fire Safety Journal,* 13(1), 55-68.

Schupack, M. (2001). "Prestressing Reinforcement in the New Millennium." *Concrete International,* 23(12), 38-45.

Schupack, M. (1994). "Unbonded Tendons- Evolution and Performance." *Concrete International,* 16(12), 32-35.

Soules, G. (2004). "Venezuela's Tallest Building Can Be Salvaged After Blaze." http://www.enr.com/news/buildings/archives/041025.asp (10/21, 2004).

ULC (1989). "Standard Methods of Fire Endurance Tests of Building Construction and Materials." *Rep. No. CAN/ULC-S101-M89,* Underwriters' Laboratories of Canada, Scarborough, ON.

Xiao, J., and König, G. (2004). "Study on Concrete at High Temperature in China - an Overview." *Fire Safety Journal,* 39(1), 89-103.

APPENDIX A – Furnace Control and Longitudinal Temperature Distribution

A.1 General

The CNi3243-C24 digital programmable controller driving the solid state relay was tuned manually through trial and error. In all cases the process variable, temperature, was monitored using a standard NIST Type-K thermocouple with a precision ± 1.7°C at 427°C (as provided by the manufacturer). Controller settings such as: proportional band (PB); rate (RA); reset (RS); cycle time; and damping ratio were configured using manufacturer's literature and technical support.

The aim in configuring the controller was to minimize overshoot and droop at the transition from ramp to soak modes for a set-point of 400°C. This temperature was selected as it constitutes the approximate midpoint of the temperature range being examined (200°C to 700°C). As well, since the furnace has a high wattage output relative to the thermal mass being heated, as per manufacturer's literature, control was assumed to be more easily maintained at higher temperature levels.

A.2 Controller Configuration

Two standard NIST Type-K thermocouples, with precision as mentioned previously, were surface-mounted on a length of seven-wire prestressing steel. The strand was placed on temporary supports such that the thermocouples were positioned approximately in the centre of the cylindrical heating chamber. One of the two thermocouples was used to control the process variable, and the other was attached to a

16 bit digital data acquisition system (Vishay Measurements Group System 5000) recording data at a frequency of 1 Hz.

Initial controller settings were calculated based on manufacturer's literature and advice from their technical support group. As such, the proportional band was set to 20, the cycle time to 4, and the damping ratio to 2 for the first iteration. Rate and reset were left at the default value of zero, and the anti-integral feature was disabled. In this state the controller was functioning as a *single mode* or *proportional* controller. With aforementioned settings input, the controller was ramped at a rate of 10°C / min. to a set-point of 400°C. The temperature-time profile was recorded simultaneously using the digital data acquisition system and independent thermocouple.

The calibration process was repeated with various proportional band settings used for each iteration, until overshoot was less than 10°C (2.5%) above the set-point of 400°C. Ultimately, a range of values from 20 to 207.5 was investigated before PB of 60 was found to be optimal. Approximately ten iterations were performed before this setting was chosen.

With adequate control achieved (while the controller operated as a single mode unit) fine tuning was attempted by adjusting rate and reset values. Both values were varied in the range of 0 to 150. However, these attempts were not successful in improving initial overshoot and droop as fine adjustment to either parameter necessitate changes to other control parameters. As such, it was decided that the performance of the furnace with single mode control was adequate given the difficulty in configuring an overpowered unit for fine temperature adjustment. Note that as the preceding method for manually tuning the controller resulted in many iterations being performed, only select

temperature-time profiles generated during the configuration phase of furnace construction are contained herein.

Finally, the CNi3243-C24's built-in autotune feature was used in an attempt to further optimize control. However, it was found that the settings determined during the autotune cycle caused increased droop at a set-point of 400°C.

A.3 Longitudinal Thermal Profile of Middle Half of Furnace Chamber

Once appropriate control parameters were selected, a series of preliminary tests were conducted in order to quantify the longitudinal thermal profile of the heating chamber. In such tests, a single instrumented strand was placed along the centerline of the furnace, with the surface-mounted controller thermocouple at its midpoint. Seven additional, thermocouples were positioned along its length at approximately 25 mm intervals (see Tables A.1, A.2, and A.3). All thermocouples were positioned within ± 5 mm using a standard metric ruler. A total length of 160 mm ± 5mm from the furnace's centerline was instrumented. With symmetry at the centerline assumed, these readings characterize the longitudinal thermal profile of the middle half of the 610 mm long heating chamber.

Set-points of 200°C, 300°C, and 400°C were investigated using the same instrumented strand to ensure the location of the thermocouples was consistent for each test. Thermocouple positioning and condition were assessed visually between each test. Tables A.1, A.2, and A.3 summarize the maximum, time-averaged, and minimum temperatures observed by each thermocouple, normalized to set-point temperature. It should be noted, that all time-averaged values were determined using an 80 minute soak

time. During actual residual mechanical testing, a slightly longer soak time of 90 minutes was used to reduce the affects of overshoot and droop on this average.

The complete temperature-time profiles for each of the three aforementioned tests are shown in Figures A.1, A.2, and A.3 for the central and outermost thermocouples. In these figures the shaded areas represent the complete range of temperatures experienced in the middle half of the furnace unit (assuming symmetry at the furnace centerline). It should be noted that a gauge length of 200 mm was used for all residual tension tests (corresponding to the maximum gauge length of the extensometer used). As a result, temperature variation between thermocouples THC1 and THC5 is of practical importance (see Tables A.1, A.2, and A.3).

A.4 Summary

It can be seen from Tables A.1, A.2, and A.3 that the longitudinal variation in temperature for the middle half of the furnace decreases as the set-point is increased; as expected. As well, the amount of overshoot and droop also appears to decrease with increased set-point. As such, no further longitudinal profiles were deemed necessary for temperature exposures above 400°C and the control parameters used: PB = 60, RA = 0, RS = 0, cycle time = 4 and damping ratio = 2 were deemed adequate for the precision of temperature control required.

Note that, the cooling rate recorded is much less than the ramp of 10°C / min. used, as expected (see Figures A.1, A.2, and A.3).

Table A.1: Longitudinal Temperature Distribution for 200°C Set-Point

Thermocouple	THC1	THC2	THC3	THC4	THC5	THC6	THC7
x[1] (mm) =	0	30	55	83	105	130	160
Max. Temp. / Set-Point[2]	1.035	1.045	1.030	1.030	1.015	1.000	0.985
Ave. Temp. / Set-Point[3]	0.985	0.980	0.984	0.982	0.975	0.962	0.949
Min. Temp. / Set-Point[4]	0.975	0.960	0.970	0.965	0.935	0.925	0.915

[1] nominal distance from furnace centerline; ± 5 mm

[2] a measure of the amount of overshoot observed; ± 0.009

[3] a measure of the amount of control observed over soak duration; ± 0.009

[4] a measure of the amount of droop observed; ± 0.009

Table A.2: Longitudinal Temperature Distribution for 300°C Set-Point

Thermocouple	THC1	THC2	THC3	THC4	THC5	THC6	THC7
x[1] (mm) =	0	30	55	83	105	130	160
Max. Temp. / Set-Point[2]	1.003	1.013	1.000	1.000	0.983	0.970	0.957
Ave. Temp. / Set-Point[3]	0.984	0.982	0.981	0.978	0.973	0.962	0.950
Min. Temp. / Set-Point[4]	0.977	0.973	0.973	0.970	0.963	0.950	0.940

[1] nominal distance from furnace centerline; ± 5 mm

[2] a measure of the amount of overshoot observed; ± 0.006

[3] a measure of the amount of control observed over soak duration; ± 0.006

[4] a measure of the amount of droop observed; ± 0.006

Table A.3: Longitudinal Temperature Distribution for 400°C Set-Point

Thermocouple	THC1	THC2	THC3	THC4	THC5	THC6	THC7
x[1] (mm) =	0	30	55	83	105	130	160
Max. Temp. / Set-Point[2]	0.998	1.000	0.993	0.993	0.980	0.970	0.960
Ave. Temp. / Set-Point[3]	0.985	0.982	0.981	0.979	0.976	0.967	0.958
Min. Temp. / Set-Point[4]	0.978	0.975	0.975	0.973	0.968	0.960	0.948

[1] nominal distance from furnace centerline; ± 5 mm

[2] a measure of the amount of overshoot observed; ± 0.004

[3] a measure of the amount of control observed over soak duration; ± 0.004

[4] a measure of the amount of droop observed; ± 0.004

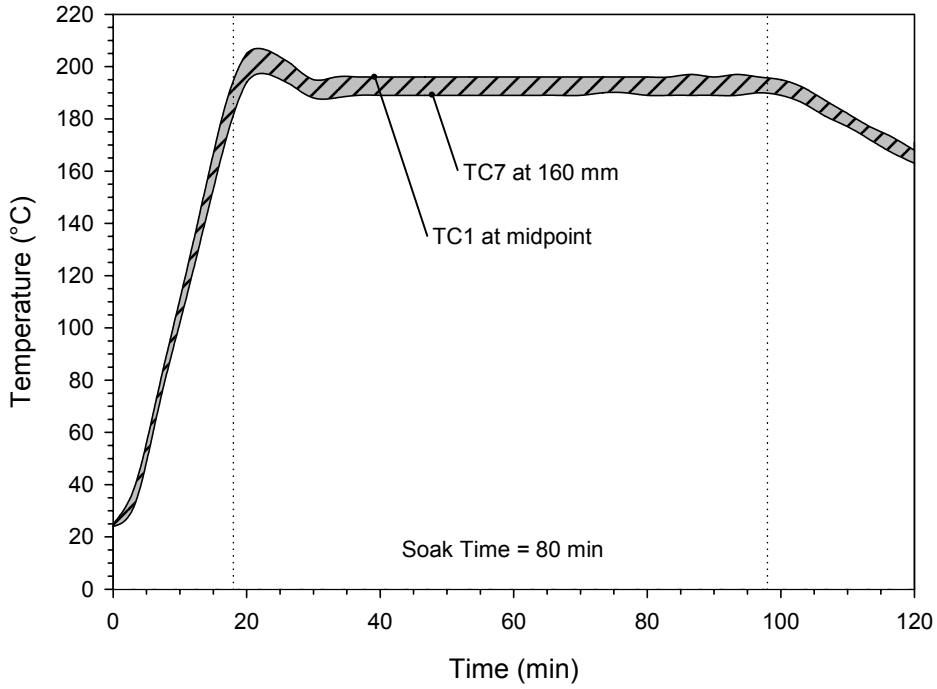

Figure A.1: Variation in Temperature for 200°C Set-Point, Over Middle 320 mm of Furnace Length

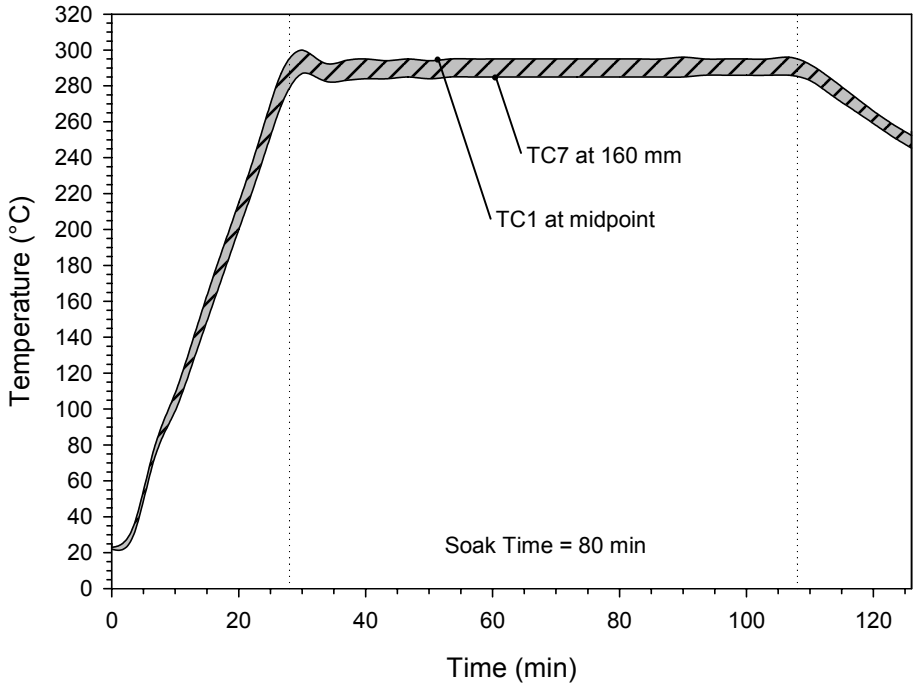

Figure A.2: Variation in Temperature for 300°C Set-Point, Over Middle 320 mm of Furnace Length

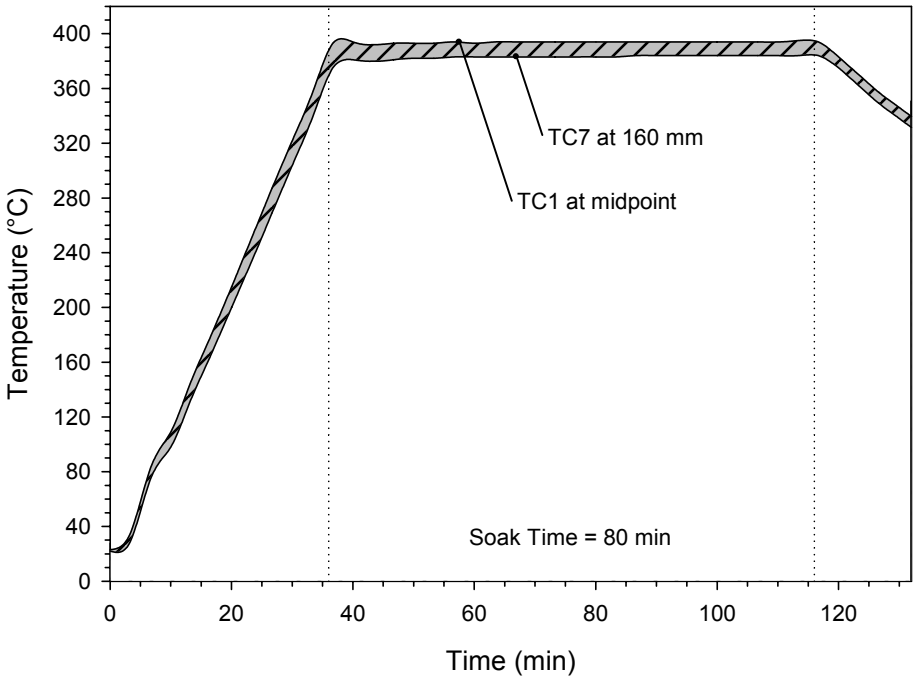

Figure A.3: Variation in Temperature for 400°C Set-Point, Over Middle 320 mm of Furnace Length

APPENDIX B – Experimental Thermal Profiles

B.1 General

For all specimens exposed to elevated temperatures in the current study, temperature-time profiles were monitored with standard NIST Type-K thermocouples and their output continuously recorded using a 16 bit digital data acquisition system (Vishay Measurements Group System 5000) recording data at a frequency of 1 Hz. The thermocouples used had a precision of measurement of ± 1.7°C at 427°C (as provided by the manufacturer). Temperature-time profiles are presented in this appendix to demonstrate the level of temperature control achieved for each set of specimens tested.

B.2 Residual Mechanical Properties

For this test series, described in Chapter 3, six specimens were heated simultaneously for each of the (six) elevated soak temperatures investigated. During each elevated temperature exposure two thermocouples, one at the midpoint and the other at a distance of 100 mm ± 5 mm from the specimen midpoint were surface mounted on five of the six specimens. These thermocouples measured the temperature at the midpoint and at one end of each specimen's 200 mm gauge length. The remaining (sixth) specimen had one thermocouple placed at its midpoint, which was used to control the process variable by providing feedback to the furnace controller.

With specimens instrumented and properly positioned (outline in Chapter 3), the furnace temperature was increased at a rate of 10°C / min. to one of the predetermined set points of 200°C, 300°C, 400°C, 500°C, 600°C, or 700°C, and the temperature was held constant for 90 minutes. The furnace was then turned off to allow slow cooling to room temperature. Temperature-time profiles of five of the six specimens were recorded

simultaneously with the uppermost and lowermost curves shown in Figures B.1 to B.6, thereby defining the effective range of temperature observed (within tension test gauge length) by all specimens for a given treatment.

For specimens heated to 200°C, the maximum temperature observed (at midspan) by any given specimen within this group, was approximately 13.0% higher than the set-point. While the maximum average temperature observed at midspan was approximately 2.5% higher than the set-point; indicating good control of temperature for the heat treatment's duration (see Table B.1). The minimum average temperature observed 100 mm from the specimen centerline was approximately 7.6% lower than the set-point; indicating relatively uniform heating across each specimen's tension test gauge length (see Table B.2).

For specimens heated to 300°C, the maximum temperature observed (at midspan) by any given specimen within this group, was approximately 6.3% higher than the set-point. While the maximum average temperature observed at midspan was found to be less than the precision of measurement for the thermocouple; indicating good control of temperature for the heat treatment's duration (see Table B.3). The minimum average temperature observed 100 mm from the specimen centerline was approximately 4.6% lower than the set-point; indicating relatively uniform heating across each specimen's tension test gauge length (see Table B.4).

For specimens heated to 400°C, the maximum temperature observed (at midspan) by any given specimen within this group, was approximately 3.4% higher than the set-point. While the maximum average temperature observed at midspan was found to be less than the precision of measurement for the thermocouple; indicating good control of

temperature for the heat treatment's duration (see Table B.5). The minimum average temperature observed 100 mm from the specimen centerline was approximately 3.0% lower than the set-point; indicating relatively uniform heating across each specimen's tension test gauge length (see Table B.6).

For specimens heated to 500°C, the maximum temperature observed (at midspan) by any given specimen within this group, was approximately 2.3% higher than the set-point. While the maximum average temperature observed at midspan was found to be less than the precision of measurement for the thermocouple; indicating good control of temperature for the heat treatment's duration (see Table B.7). The minimum average temperature observed 100 mm from the specimen centerline was approximately 2.6% lower than the set-point; indicating relatively uniform heating across each specimen's tension test gauge length (see Table B.8).

For specimens heated to 600°C, the maximum temperature observed (at midspan) by any given specimen within this group, was approximately 0.4% higher than the set-point. While the maximum average temperature observed at midspan was found to be less than the precision of measurement for thermocouple; indicating good control of temperature for the heat treatment's duration (see Tables B.9). The minimum average temperature observed 100 mm from the specimen centerline was approximately 1.0% lower than the set-point; indicating relatively uniform heating across each specimen's tension test gauge length (see Table B.10).

For specimens heated to 700°C, the maximum temperature observed (at midspan) by any given specimen within this group, was approximately 0.3% higher than the set-point. While the maximum average temperature observed at midspan was found to be

less than the precision of measurement for the thermocouple; indicating good control of temperature for the heat treatment's duration (see Table B.11). The minimum average temperature observed 100 mm from the specimen centerline was approximately 1.8% lower than the set-point; indicating relatively uniform heating across each specimen's tension test gauge length (see Table B.12).

As well, for all specimens the temperatures recorded toward the top of the furnace were observed to be slightly higher than the temperatures recorded in the lower portion of the furnace, as expected.

Since overshoot occurs for a relatively short duration, and the maximum and minimum average temperatures, both at the specimen centerline and 100 mm from it, were deemed important when investigating temperature control. In all cases, the maximum and minimum average temperatures were found to be within 5% of the set-point (with the exception S3 and S4 for the 200°C exposure). Therefore, the degree of temperature control exhibited for this test series was concluded adequate.

B.3 Relaxation Testing

For this test series, described in Chapter 4, a single seven-wire strand specimen was instrumented with seven Type-K thermocouples to monitor surface temperatures along the specimen's length (and to provide control feedback for the tube furnace). The strand was then stressed (to a typical service level) in a rigid frame and heated. Details of the furnace and thermocouple placement are shown schematically in Figure 4.1. Two thermocouples were positioned in the centre of the furnace unit; one to regulate temperature, and the other to continuously record peak temperature on the surface of the specimen (TC1). Another thermocouple was placed halfway between the centre of the

610 mm long heating coils and a ceramic fibre end plug (TC2), approximately 150 mm from the furnace centre. The final two thermocouples located within the heating chamber were placed just inside the ceramic fibre plugs at each end, approximately 300 mm from the furnace centre (TC3 and TC5). An additional thermocouple was placed immediately outside the ceramic fibre plug at one end of the heating chamber, approximately 350 mm from the furnace centre (TC4). The remaining two thermocouples were positioned well outside the furnace unit. All thermocouples were placed with a precision of approximately ± 5 mm.

During testing strand temperature was seen to decrease gradually from the center of the furnace toward each end of the enclosure, with a steep decrease in temperature occurring just inside the insulation plugs at each end of the furnace, and another steep decrease occurring just outside the insulation plugs (see Figures B.7 to B.12).

For all tests conducted the middle 300 mm of the furnace (assuming symmetry) was seen to maintain a relatively uniform temperature distribution having a difference in temperature ranging from approximately 8°C at 200°C to approximately 4°C at 700°C (4% of set-point to 0.6% of set-point). The ends of the enclosure were seen to have a marked difference in temperature (when compared to the centre of the furnace) ranging from approximately 70°C at 200°C to approximately 180°C at 700°C; interestingly the temperatures observed just inside the insulation plugs were seen to between approximately 32% and 36% of the set-point temperature for all tests except the 700°C (where the temperature just inside the furnace was approximately 25% of the set-point). This is not unexpected given the lack of a separate heating zone and temperature control

at the ends of the furnace, as well as the inevitable heat transmission through voids between insulating material and the strand specimen.

Similarly, a large temperature gradient was observed across the furnace end plugs, as the heated strand outside the furnace was able to transfer heated convectively to the surrounding air at ambient temperature (see Figures B.7 to B.12).

Finally, when comparing the temperatures observed by thermocouples TC3 and TC5, the temperatures recorded differed by a maximum of approximately 7.5% of any given set-point, with variations as low as 0.1% for RLX-90-700; thus indicating the assumption of symmetry of heating about the furnace centerline to reasonably representative of actual conditions.

B.4 Summary

For elevated temperature exposures applied to unstressed-while-heated specimens, it was observed that a small temperature gradient occurred along the 200 mm tension test gauge length. As well, it was seen that very little variation in average temperature was observed between specimens exposed to the same soak temperature. Since no significant trend in temperature variation is apparent, any scatter in residual mechanical properties is not likely to be a result of differential heating. Therefore, the custom built furnace enclosure appeared to perform adequately given the amount of precision required for these tests.

Stressed-while-heated specimens experienced a slight variation in temperature between TC3 and TC5, indicating the assumption of temperature gradient symmetry about the furnace centerline to be valid. The likely cause of this difference is the misalignment of the furnace chamber with respect to the longitudinal axis of the stressed

strand specimen, which was unavoidable given that the furnace could not be permanently fixed to the rigid stressing frame due to instrumentation procedures. As expected, a significant temperature gradient was observed in proximity to the insulation plugs sealing the furnace openings at each end. The relative magnitude of the decrease in temperature over the outermost 300 mm of the furnace chamber may be one additional cause of variation observed between experimental relaxation data and analytical model predictions, as noted in Chapter 4. However, the lack of precision in quantifying the temperature gradient at the ends of the furnace was unavoidable given the number of channels of temperature input available on the System 5000 digital data acquisition system used.

Table B.1: Specimen Temperature at Centerline ± 5 mm for 200°C Set-Point

Thermocouple	S1	S2	S3	S4	S6
Furnace Zone[1]	Top	Middle	Bottom	Bottom	Top
Max. Temp. / Set-Point[2]	1.110	1.070	1.030	1.035	1.130
Ave. Temp. / Set-Point[3]	1.017	0.998	0.966	0.958	1.025
Min. Temp. / Set-Point[4]	0.995	0.945	0.910	0.930	1.000

[1] heating chamber diameter divided into thirds
[2] a measure of the amount of overshoot observed; ± 0.009
[3] a measure of the amount of control observed over soak duration; ± 0.009
[4] a measure of the amount of droop observed; ± 0.009

Table B.2: Specimen Temperature 100 mm from Centerline ± 5 mm for 200°C Set-Point

Thermocouple	S1	S2	S3	S4	S6
Furnace Zone[1]	Top	Middle	Bottom	Bottom	Top
Max. Temp. / Set-Point[2]	1.090	1.055	0.995	0.990	1.115
Ave. Temp. / Set-Point[3]	1.001	0.983	0.928	0.924	1.012
Min. Temp. / Set-Point[4]	0.980	0.925	0.870	0.850	0.990

[1] heating chamber diameter divided into thirds
[2] a measure of the amount of overshoot observed; ± 0.009
[3] a measure of the amount of control observed over soak duration; ± 0.009
[4] a measure of the amount of droop observed; ± 0.009

Table B.3: Specimen Temperature at Centerline ± 5 mm for 300°C Set-Point

Thermocouple	S1	S2	S3	S4	S6
Furnace Zone[1]	Top	Middle	Bottom	Bottom	Top
Max. Temp. / Set-Point[2]	1.063	1.040	1.030	1.030	1.060
Ave. Temp. / Set-Point[3]	1.004	0.992	0.983	0.981	1.002
Min. Temp. / Set-Point[4]	0.990	0.977	0.967	0.963	0.987

[1] heating chamber diameter divided into thirds
[2] a measure of the amount of overshoot observed; ± 0.006
[3] a measure of the amount of control observed over soak duration; ± 0.006
[4] a measure of the amount of droop observed; ± 0.006

Table B.4: Specimen Temperature 100 mm from Centerline ± 5 mm for 300°C Set-Point

Thermocouple	S1	S2	S3	S4	S6
Furnace Zone[1]	Top	Middle	Bottom	Bottom	Top
Max. Temp. / Set-Point[2]	1.043	1.020	1.003	1.003	1.043
Ave. Temp. / Set-Point[3]	0.987	0.974	0.958	0.954	0.990
Min. Temp. / Set-Point[4]	0.973	0.957	0.940	0.939	0.973

[1] heating chamber diameter divided into thirds
[2] a measure of the amount of overshoot observed; ± 0.006
[3] a measure of the amount of control observed over soak duration; ± 0.006
[4] a measure of the amount of droop observed; ± 0.006

Table B.5: Specimen Temperature at Centerline ± 5 mm for 400°C Set-Point

Thermocouple	S1	S2	S3	S4	S6
Furnace Zone[1]	Top	Middle	Bottom	Bottom	Top
Max. Temp. / Set-Point[2]	1.034	1.026	1.015	1.013	1.031
Ave. Temp. / Set-Point[3]	1.002	1.000	0.989	0.986	1.000
Min. Temp. / Set-Point[4]	0.994	0.992	0.980	0.977	0.991

[1] heating chamber diameter divided into thirds
[2] a measure of the amount of overshoot observed; ± 0.004
[3] a measure of the amount of control observed over soak duration; ± 0.004
[4] a measure of the amount of droop observed; ± 0.004

Table B.6: Specimen Temperature 100 mm from Centerline ± 5 mm for 400°C Set-Point

Thermocouple	S1	S2	S3	S4	S6
Furnace Zone[1]	Top	Middle	Bottom	Bottom	Top
Max. Temp. / Set-Point[2]	1.022	1.013	0.999	0.997	1.018
Ave. Temp. / Set-Point[3]	0.987	0.983	0.973	0.970	0.986
Min. Temp. / Set-Point[4]	0.981	0.976	0.965	0.962	0.981

[1] heating chamber diameter divided into thirds
[2] a measure of the amount of overshoot observed; ± 0.004
[3] a measure of the amount of control observed over soak duration; ± 0.004
[4] a measure of the amount of droop observed; ± 0.004

Table B.7: Specimen Temperature at Centerline ± 5 mm for 500°C Set-Point

Thermocouple	S1	S2	S3	S4	S6
Furnace Zone[1]	Top	Middle	Bottom	Bottom	Top
Max. Temp. / Set-Point[2]	1.023	1.018	1.015	1.009	1.020
Ave. Temp. / Set-Point[3]	1.000	0.997	0.994	0.990	0.999
Min. Temp. / Set-Point[4]	0.992	0.989	0.985	0.981	0.991

[1] heating chamber diameter divided into thirds
[2] a measure of the amount of overshoot observed; ± 0.003
[3] a measure of the amount of control observed over soak duration; ± 0.003
[4] a measure of the amount of droop observed; ± 0.003

Table B.8: Specimen Temperature 100 mm from Centerline ± 5 mm for 500°C Set-Point

Thermocouple	S1	S2	S3	S4	S6
Furnace Zone[1]	Top	Middle	Bottom	Bottom	Top
Max. Temp. / Set-Point[2]	1.013	1.004	0.996	0.991	1.010
Ave. Temp. / Set-Point[3]	0.991	0.985	0.977	0.974	0.991
Min. Temp. / Set-Point[4]	0.982	0.976	0.966	0.964	0.981

[1] heating chamber diameter divided into thirds
[2] a measure of the amount of overshoot observed; ± 0.003
[3] a measure of the amount of control observed over soak duration; ± 0.003
[4] a measure of the amount of droop observed; ± 0.003

Table B.9: Specimen Temperature at Centerline ± 5 mm for 600°C Set-Point

Thermocouple	S1	S2	S3	S4	S6
Furnace Zone[1]	Top	Middle	Bottom	Bottom	Top
Max. Temp. / Set-Point[2]	1.004	1.004	1.001	0.993	1.004
Ave. Temp. / Set-Point[3]	1.002	1.001	0.998	0.991	1.001
Min. Temp. / Set-Point[4]	0.973	0.974	0.970	0.963	0.974

[1] heating chamber diameter divided into thirds
[2] a measure of the amount of overshoot observed; ± 0.003
[3] a measure of the amount of control observed over soak duration; ± 0.003
[4] a measure of the amount of droop observed; ± 0.003

Table B.10: Specimen Temperature 100 mm from Centerline ± 5 mm for 600°C Set-Point

Thermocouple	S1	S2	S3	S4	S6
Furnace Zone[1]	Top	Middle	Bottom	Bottom	Top
Max. Temp. / Set-Point[2]	0.999	0.999	0.995	0.994	1.000
Ave. Temp. / Set-Point[3]	0.995	0.995	0.990	0.990	0.996
Min. Temp. / Set-Point[4]	0.968	0.970	0.963	0.963	0.969

[1] heating chamber diameter divided into thirds
[2] a measure of the amount of overshoot observed; ± 0.003
[3] a measure of the amount of control observed over soak duration; ± 0.003
[4] a measure of the amount of droop observed; ± 0.003

Table B.11: Specimen Temperature at Centerline ± 5 mm for 700°C Set-Point

Thermocouple	S1	S2	S3	S4	S6
Furnace Zone[1]	Top	Middle	Bottom	Bottom	Top
Max. Temp. / Set-Point[2]	1.000	1.003	0.999	0.997	1.000
Ave. Temp. / Set-Point[3]	0.998	1.001	0.997	0.994	0.998
Min. Temp. / Set-Point[4]	0.971	0.975	0.970	0.967	0.972

[1] heating chamber diameter divided into thirds
[2] a measure of the amount of overshoot observed; ±s 0.002
[3] a measure of the amount of control observed over soak duration; ± 0.002
[4] a measure of the amount of droop observed; ± 0.002

Table B.12: Specimen Temperature 100 mm from Centerline ± 5 mm for 700°C Set-Point

Thermocouple	S1	S2	S3	S4	S6
Furnace Zone[1]	Top	Middle	Bottom	Bottom	Top
Max. Temp. / Set-Point[2]	-	0.993	0.986	0.985	0.991
Ave. Temp. / Set-Point[3]	-	0.990	0.983	0.982	0.989
Min. Temp. / Set-Point[4]	-	0.965	0.959	0.957	0.964

[1] heating chamber diameter divided into thirds
[2] a measure of the amount of overshoot observed; ± 0.002
[3] a measure of the amount of control observed over soak duration; ± 0.002
[4] a measure of the amount of droop observed; ± 0.002

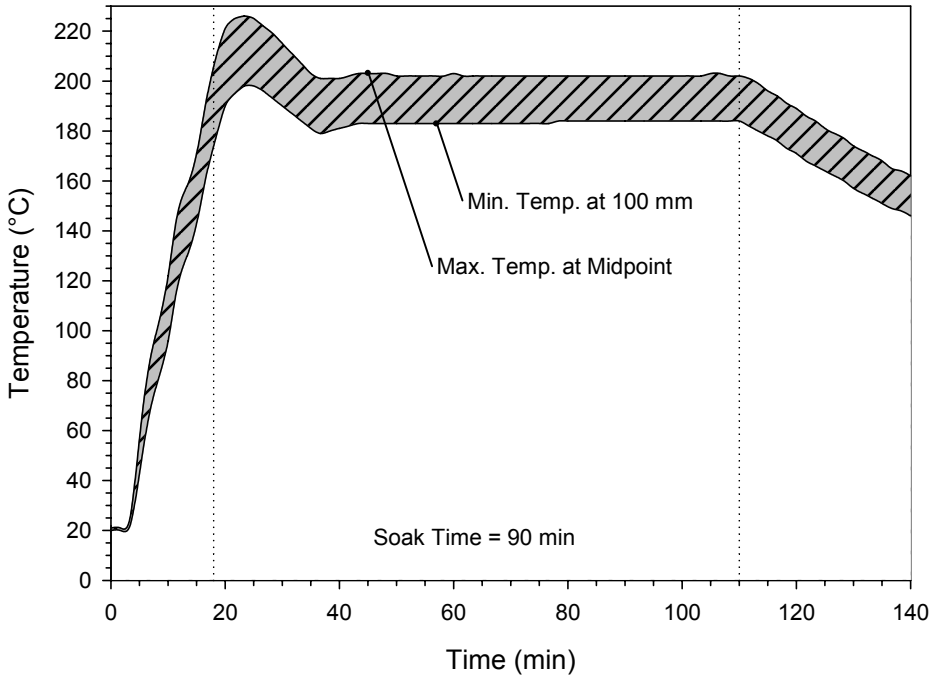

Figure B.1: Maximum Deviation in Temperature for 200°C Set-Point, Over Middle 200 mm of Furnace Length for all Specimens

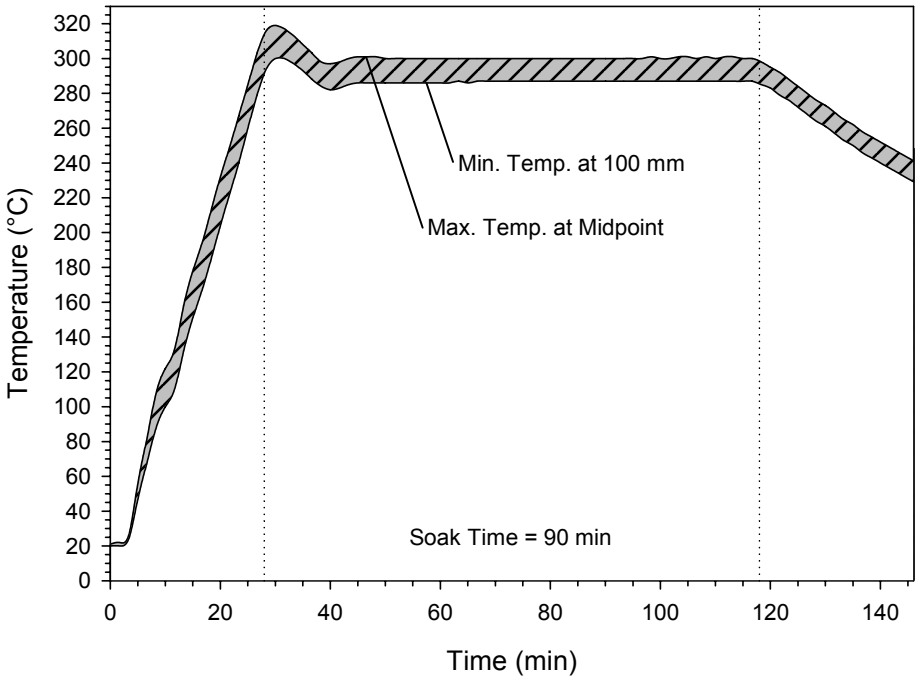

Figure B.2: Maximum Deviation in Temperature for 300°C Set-Point, Over Middle 200 mm of Furnace Length for all Specimens

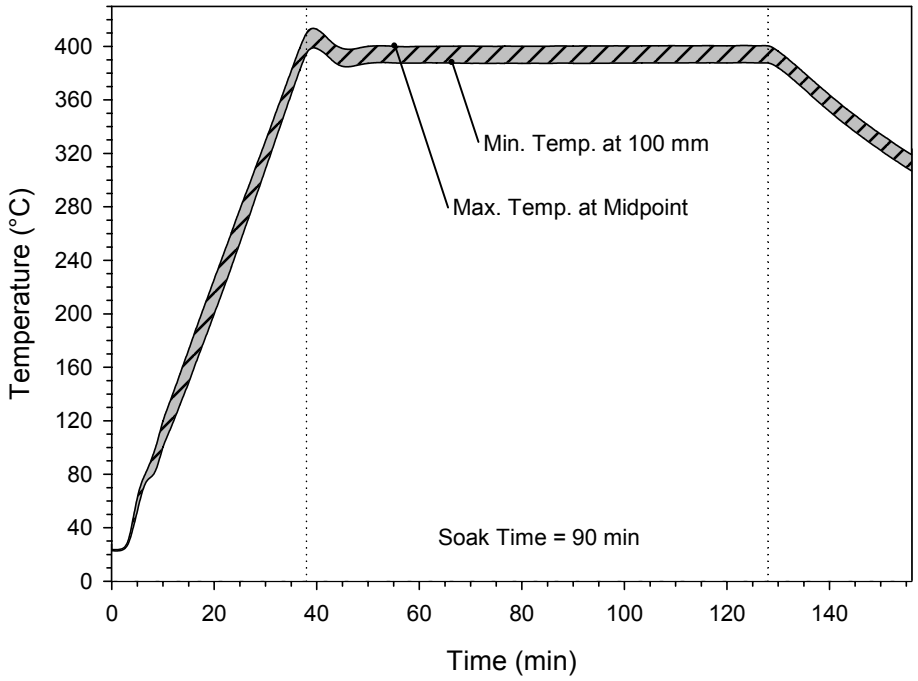

Figure B.3: Maximum Deviation in Temperature for 400°C Set-Point, Over Middle 200 mm of Furnace Length for all Specimens

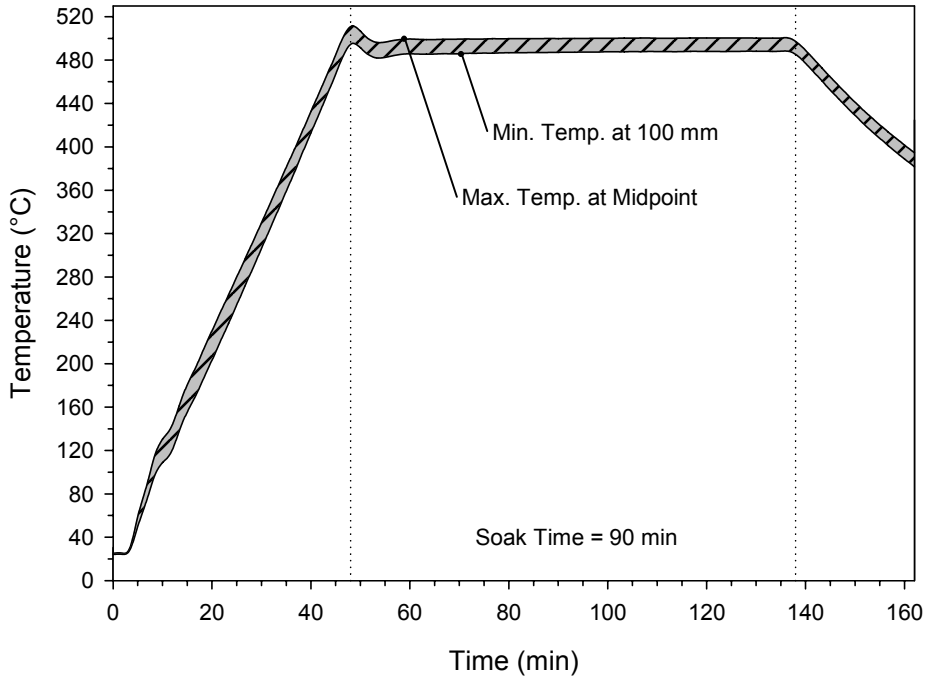

Figure B.4: Maximum Deviation in Temperature for 500°C Set-Point, Over Middle 200 mm of Furnace Length for all Specimens

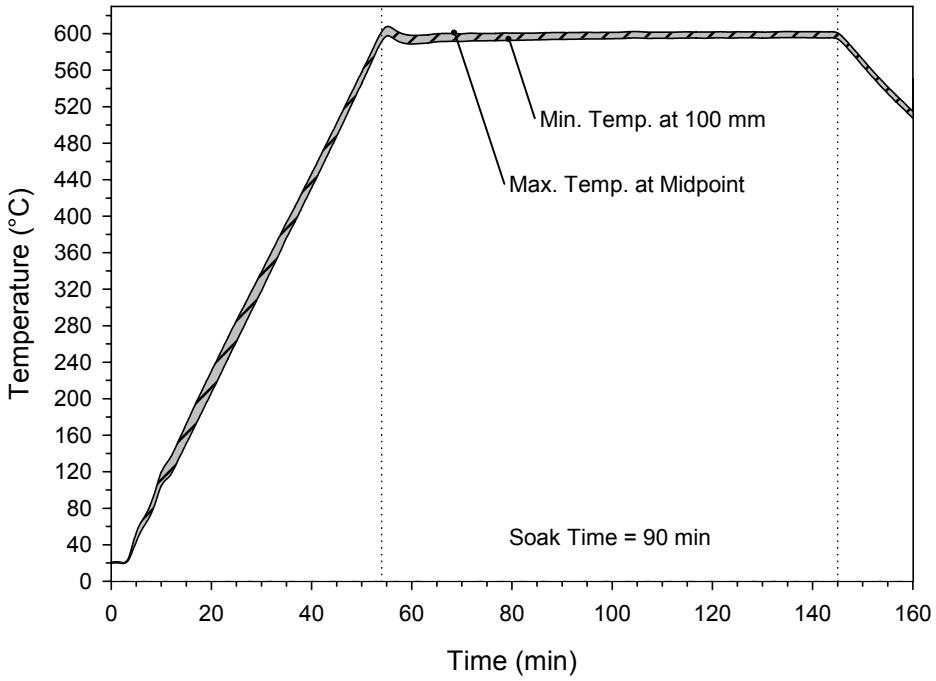

Figure B.5: Maximum Deviation in Temperature for 600°C Set-Point, Over Middle 200 mm of Furnace Length for all Specimens

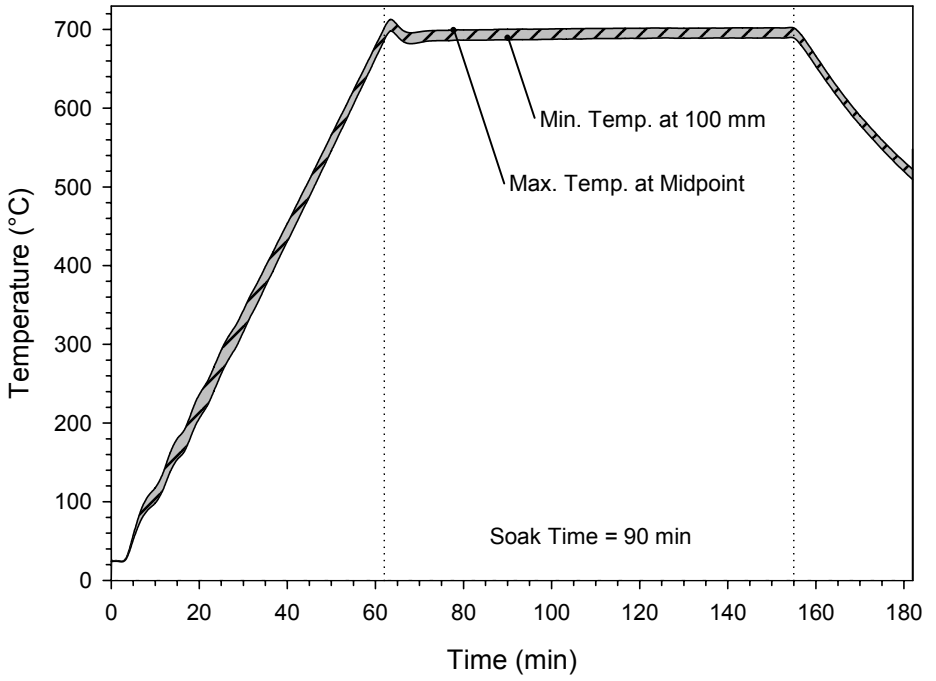

Figure B.6: Maximum Deviation in Temperature for 700°C Set-Point, Over Middle 200 mm of Furnace Length for all Specimens

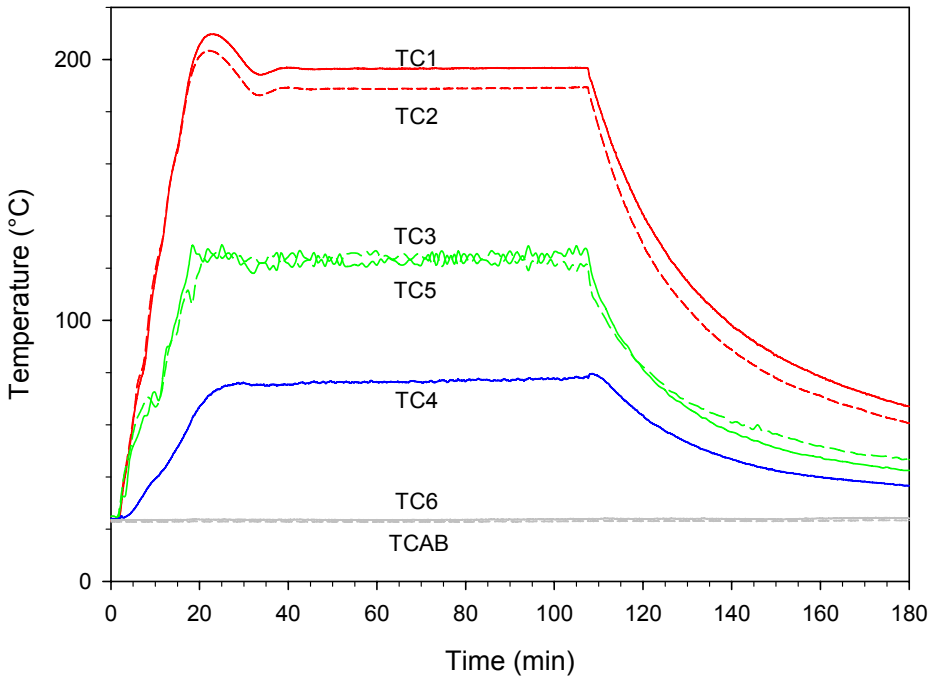

Figure B.7: Experimental Temperature-Time Profiles RLX-90-200

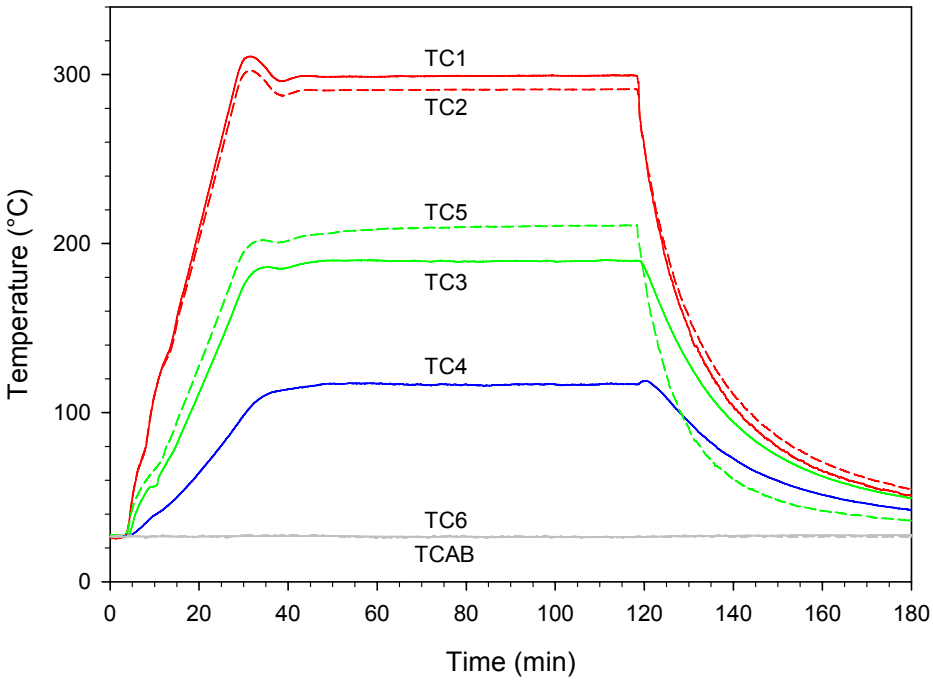

Figure B.8: Experimental Temperature-Time Profiles RLX-90-300

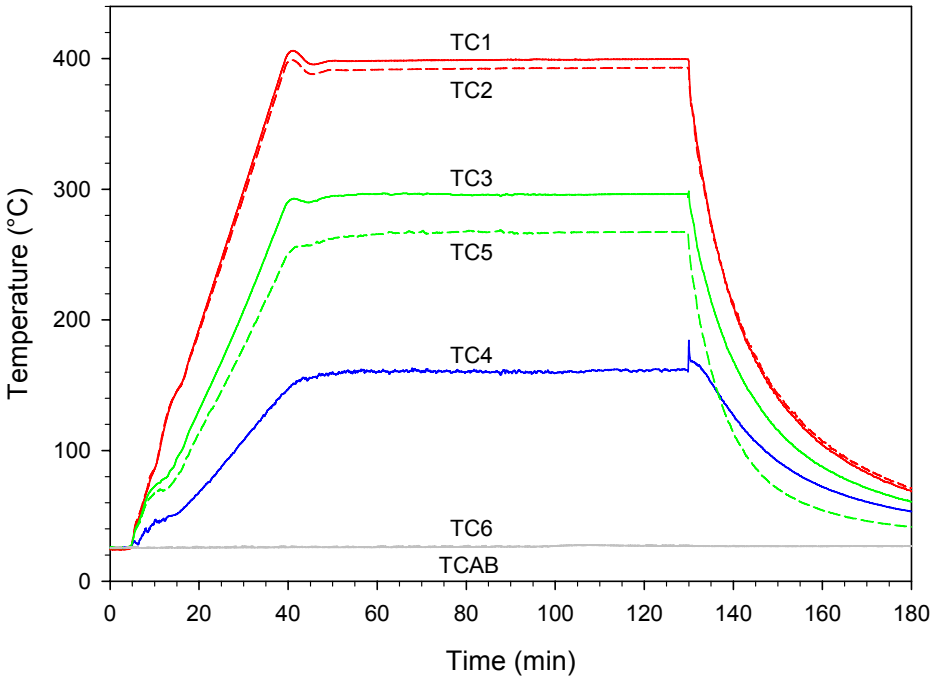

Figure B.9: Experimental Temperature-Time Profiles RLX-90-400

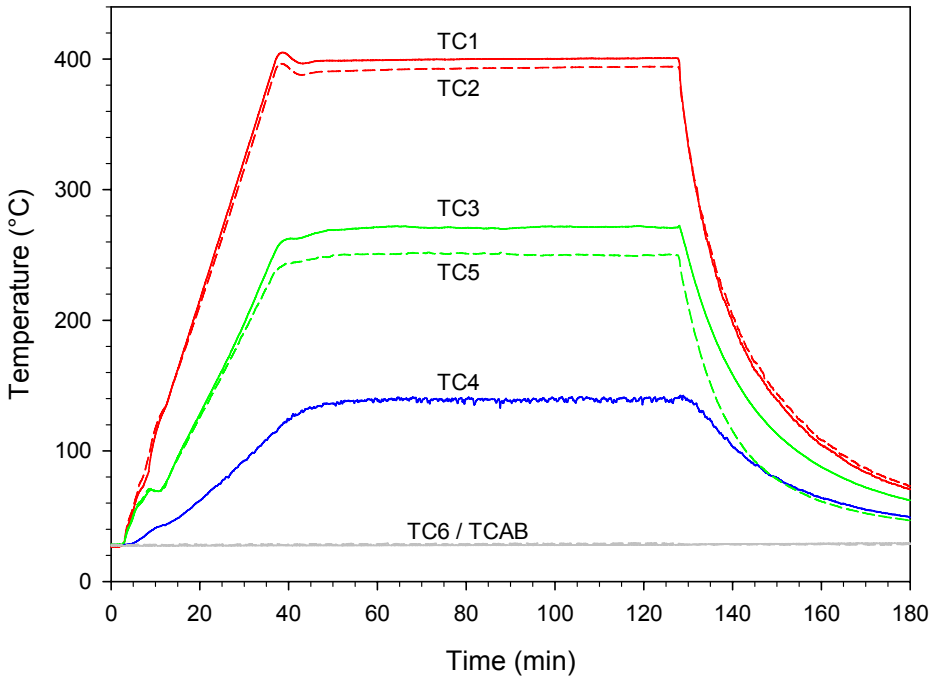

Figure B.10: Experimental Temperature-Time Profiles RLX-90-400A

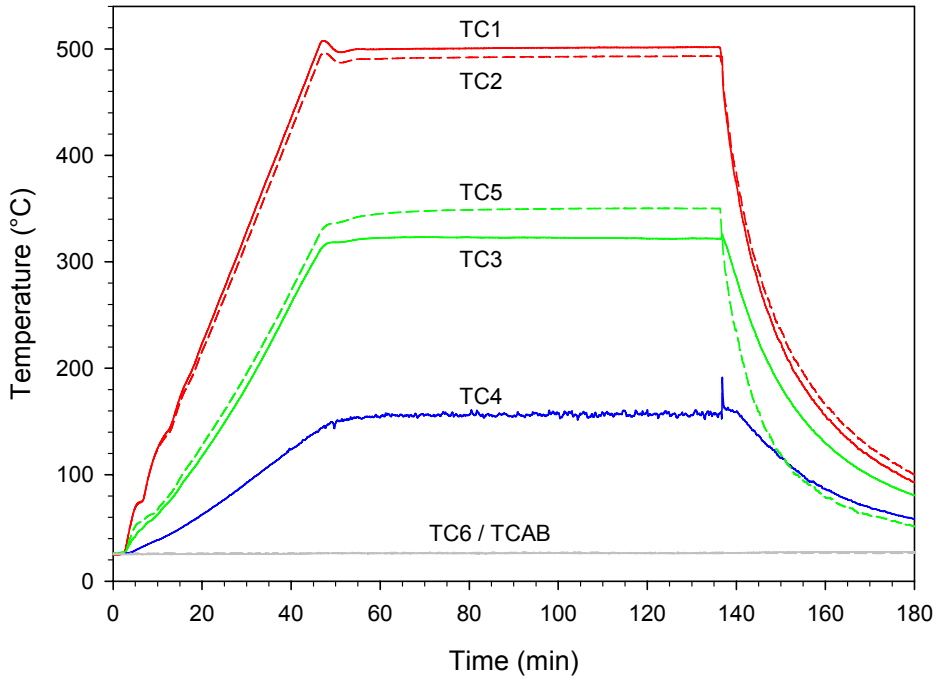

Figure B.11: Experimental Temperature-Time Profiles RLX-90-500

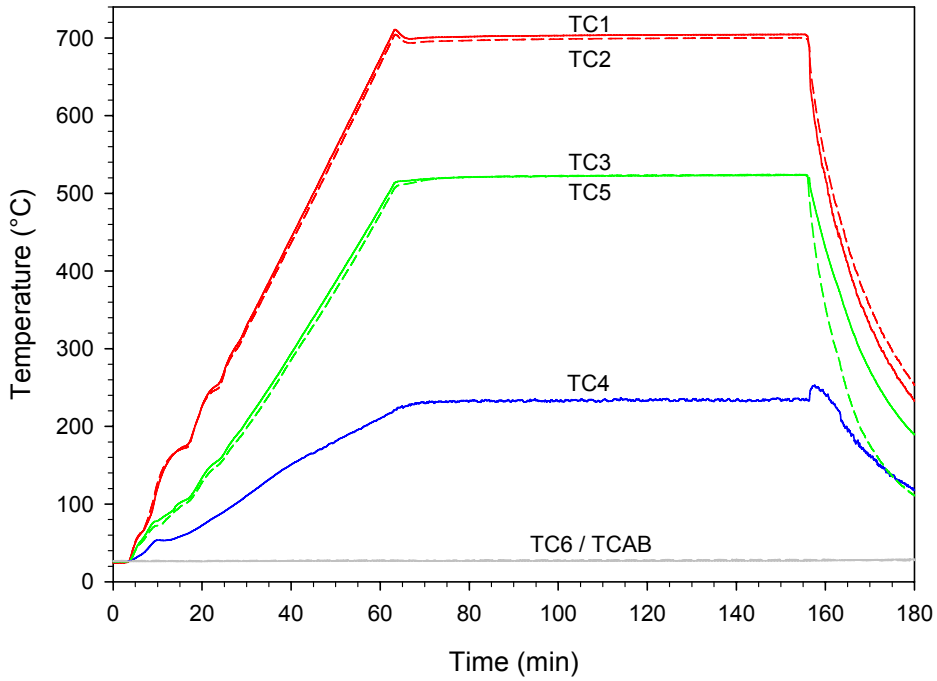

Figure B.12: Experimental Temperature-Time Profiles RLX-90-700

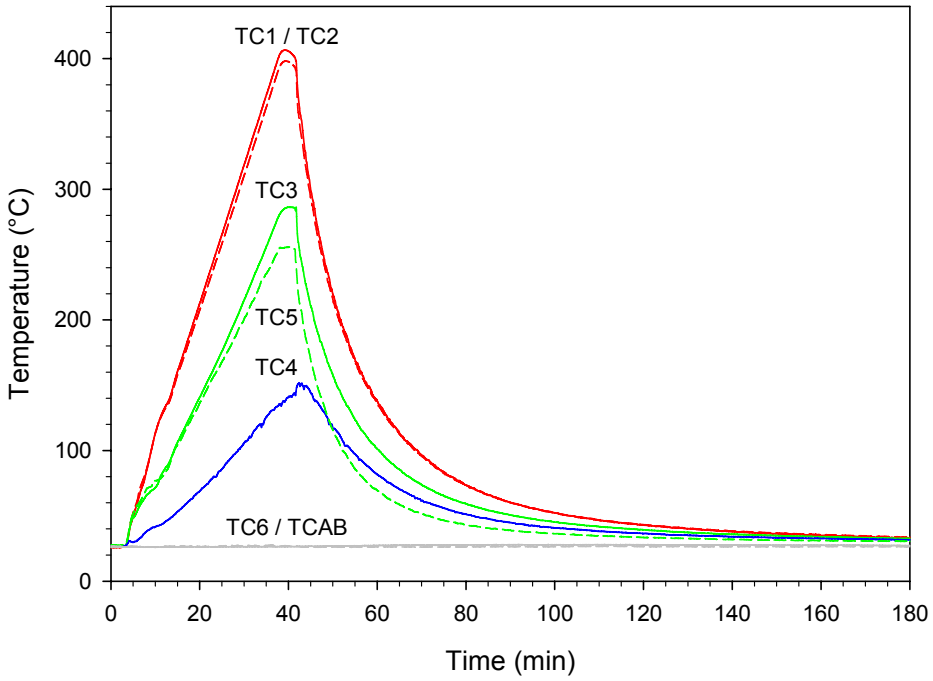

Figure B.13: Experimental Temperature-Time Profiles RLX-5-400

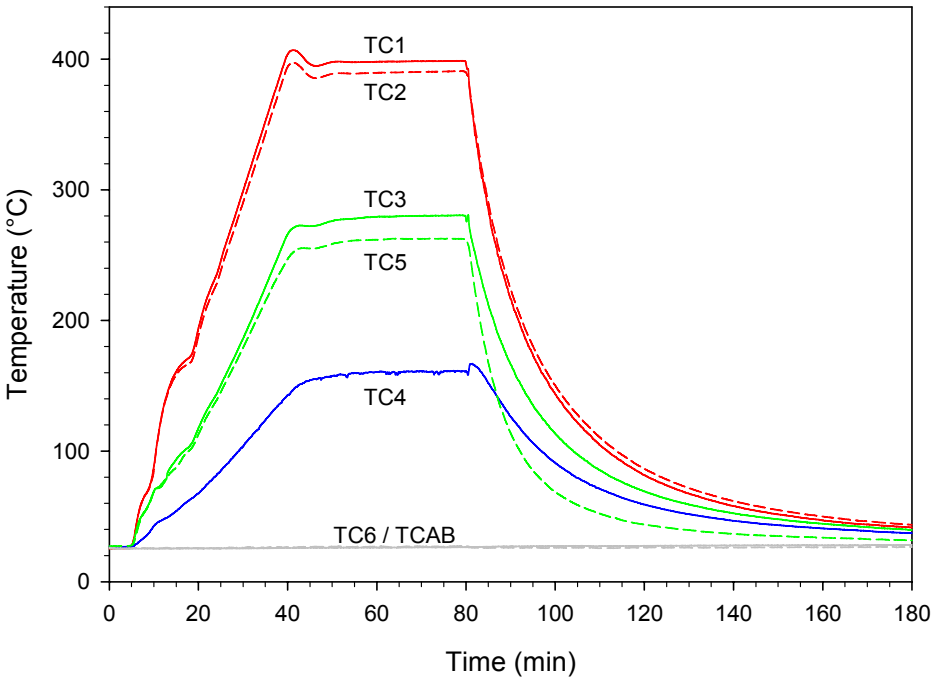

Figure B.14: Experimental Temperature-Time Profiles RLX-45-400

APPENDIX C – Experimental Determination of Mechanical Properties

C.1 General

Mechanical properties (residual and unheated) of cold-drawn prestressing steel were determined experimentally through a series of standard tension tests in accordance with ASTM A370-01 Annex 4 (ASTM 2001a). The analysis of data obtained from these tests and the computation of corresponding uncertainties (denoted ε_{exp}) are outlined herein. A numeric summary of all mechanical properties obtained is presented in Tables C3.1 to C3.8.

C.2 Data Preparation

During tension testing the outputs from a load cell having a known precision of ± 1.0% in the range of 0 kN to 45 kN, a 200 mm MTS series 632 electronic extensometer having an accuracy of ± 0.05 mm, and a Novotechnik model TRS 100 linear potentiometer having an accuracy of ± 0.08 mm were continuously recorded using a Vishay Measurements Group System 5000 16-bit digital data acquisition system sampling data at a frequency of 1 Hz.

Upon completing each test, these recorded data were exported to Microsoft™ Excel spreadsheets using Vishay Measurements Group Strain Smart™ Software for computation of mechanical properties by the Author, and the raw data were archived within the Strain Smart system.

C.3 Determination of Ultimate Tensile Strength (f_{pu})

Because the cold-drawn wires tested in the current research study were extracted from a continuous length of prestressing strand, it was assumed that the 4.4 mm diameter of the core wire was constant for each test performed.

The maximum load recorded for each specimen was determined within an Excel spreadsheet and the stress at rupture was computed from this load using an area of 15.2 mm^2 for a 4.4 mm nominal diameter wire (see Tables C1 to C8). A corresponding uncertainty for each group of specimens was computed by applying the known load cell precision of ± 1.0% to the mean of each group. For ease of discussion the *maximum experimental uncertainty*, ± 1.0% applied to the largest mean of any group of specimens, is often used within the body of this thesis.

C.4 Computation of Elastic Modulus (E)

Load cell and extensometer data were used to define an experimental stress-strain curve for each of the specimens tested (see Figures C1 to C43). The elastic modulus was computed for each specimen by performing linear least-squares regression analysis on data points constituting the middle 70% of the linear elastic portion of the stress-strain curve. Using an estimated modulus of 200 GPa, the 0.2% offset yield (f_{py}) was determined graphically. The upper and lower bounds of data points used in linear regression were subsequently defined as $0.85f_{py}$ and $0.15f_{py}$ respectively. This range was selected to maximize the precision of regression analysis by maximizing the number of data points in each set, yet avoiding nonlinearities caused by grip setting (at low stress) or early plastic deformation (at high stress).

As the computation of elastic modulus requires readings from both the load cell and extensometer, each having their own associated accuracy of measurement, propagation of uncertainty occurs. As both sets of readings are independent of one another, a first order Taylor series expansion was used to determine uncertainty. As there were only two variables used in the computation of elastic modulus, the propagation of uncertainty reduces to the vector sum of each individual instrument. As all strain values used in the determination of elastic modulus are less than 0.2% (0.4 mm on 200 mm gauge length) the associated percentage uncertainty for the extensometer used was ± 12.5%. As previously mentioned the associated percentage uncertainty for the load used was ± 1.0%. Therefore, the vector sum of these quantities, representing the uncertainty in elastic modulus is approximately 12.5%. A summary of the parameters used to calculate elastic modulus, and the associated experimental uncertainty are presented in Table C9.

C.5 Determination of Offset Yield (f_{py})

The final determination of 0.2% offset yield was performed using the elastic modulus value calculated as described in the previous section. A linear function having the same slope as the elastic modulus of the material was plotted from 0.2% strain on the horizontal axis of each stress-strain plot, and the point at which this line intersected the experimental stress-strain curve was taken to be the yield strength of the specimen (see Figures C1 to C43). As the slope of the stress-strain curve decreased drastically after the specimens yielded, only the uncertainty associated with the load cell reading was considered important. Therefore the experimental uncertainty in 0.2% offset yield was taken to be ± 1.0%.

C.6 Elongation at Rupture (ε_u)

The initial length of each specimen was measured between two reference marks using mechanical calipers and a standard metric ruler measuring to the nearest millimetre. Once each specimen had failed, its two halves were carefully fitted back together and its length was again measured. The percentage elongation of each specimen was determined by calculating the total change in specimen length and dividing by its initial length. As the initial gauge length of each specimen was constant (approximately 205 mm), and the associated uncertainty in each measurement was taken to be 0.5 mm, therefore the uncertainty in percentage strain for each specimen was also constant and determined to be 0.25%.

Note that reference marks were created using a permanent marker, rather than with an awl, as would commonly be done, to avoid stress concentrations in proximity to the gauge mark locations.

C.7 Normalization of Data

In order to facilitate the used of the data collected herein many of the figures prepared for discussion in Chapters 3 and 4 were normalized against properties determined from tests of unheated specimens extracted from the same continuous length of prestressing steel. This process does not however reduce or negate any experimental uncertainty previously determined.

C.8 Summary

For unstressed specimens heated up to 400°C (including unheated specimens) the maximum standard deviation in ultimate tensile strength, 0.2% offset yield, and elastic

modulus for each set of test data were all found to be less than the calculated uncertainty for each property (see Tables C1 to C4).

For unstressed specimens heated to 500°C the coefficient of variation ($s\,\bar{x}^{-1}$) of ultimate tensile strength was found to 1.02% which is only slightly larger than the computed experimental uncertainty of ± 1.0%. The standard deviations of both 0.2% offset yield and elastic modulus were found to be less than their associated uncertainties.

For unstressed specimens heated to 600°C the standard deviations of ultimate tensile strength, 0.2% offset yield and elastic modulus were all found to be less than, or in the case of yield strength approximately equal to, their respective uncertainties.

Finally, for unstressed specimens heated to 700°C the standard deviations of all mechanical properties computed were less than their respective uncertainties, indicating good control over the testing procedures and experimental uncertainty for unstressed specimens in the range of 20°C to 700°C. In this range, only elongation at rupture consistently had a standard deviation greater than its associated experimental uncertainty, which is neither surprising (nor significant) given the rather crude technique used to obtain these data. Consequently, experimental precision and repeatability were deemed to be sufficient in the calculation of these properties.

The residual mechanical properties of unstressed specimens were assumed to follow a normal distribution, and an analysis of variance (ANOVA) was performed on each temperature exposure group to determine where statistically significant changes occurred to mechanical properties when compared to properties obtained from unheated specimens. Results of analysis of variance for various significance levels are presented in Tables C.10 to C.13. From this it can be seen that residual ultimate tensile strength and

0.2% offset yield strength experience significant changes in value at the 0.01% significance level between 300°C and 400°C. As well, residual elongation at rupture experiences a significant change in value between 500°C and 600°C. Given the large range of experimental uncertainty present no significant change in elastic modulus (as a result of elevated temperature exposure) could be identified.

Finally, as the sample size for specimens stressed-while-heated prior to residual tension testing was small (a maximum of two tests with the same variables isolated) no standard deviation or mean were computed. However, mechanical properties were compared to unstressed specimens in Chapter 4 by assuming the application of stress had no affect on mechanical properties and then using a statistical 'T-test' to determine if the stressed data points constituted an outlier using ASTM E178-01 (ASTM 2001).

Table C.1: Mechanical Properties of 4.4 mm Cold-Drawn Wire – Unheated

	UH1	UH2	UH3	UH4	UH5	$\bar{x}$	s
f_{pu} (MPa)	2022.9	2008.3	2008.4	2031.7	2026.0	2019.5	10.6
f_{py} (MPa)	1839.2	1836.3	1836.3	1857.6	1844.7	1842.8	8.9
f_{py} / f_{pu}	0.91	0.91	0.91	0.91	0.91	0.91	0.00
E (MPa)	212590	213030	214770	215140	214650	214036	1144
ε_u (%)	5.1	-	4.7	4.7	5.3	5.0	0.3

Maximum stress uncertainty for 4.4 mm specimen ± 20.2 MPa
Maximum elastic modulus uncertainty ± 26893 MPa
Maximum elongation at rupture uncertainty ± 0.25%

Table C.2: Mechanical Properties of 4.4 mm Cold-Drawn Wire – 200°C

	200-1	200-2	200-3	200-4	200-6	$\bar{x}$	s
f_{pu} (MPa)	2015.8	1985.9	2001.3	1999.3	2005.0	2001.5	10.8
f_{py} (MPa)	1830.0	1799.5	1806.9	1810.9	1817.5	1813.0	11.5
f_{py} / f_{pu}	0.91	0.91	0.90	0.91	0.91	0.91	0.00
E (MPa)	220460	226430	217680	216650	216830	219610	4106
ε_u (%)	5.3	4.9	5.3	4.4	5.3	5.0	0.4

Maximum stress uncertainty for 4.4 mm specimen ± 20.0 MPa
Maximum elastic modulus uncertainty ± 28304 MPa
Maximum elongation at rupture uncertainty ± 0.25%

Table C.3: Mechanical Properties of 4.4 mm Cold-Drawn Wire – 300°C

	300-1	300-2	300-3	300-4	300-6	$\bar{x}$	s
f_{pu} (MPa)	2015.0	1998.1	2027.2	1996.4	1994.0	2006.1	14.4
f_{py} (MPa)	1878.4	1849.7	1888.0	1852.3	1849.4	1863.6	18.3
f_{py} / f_{pu}	0.93	0.93	0.93	0.93	0.93	0.93	0.00
E (MPa)	217730	217600	217120	218180	218040	217734	415
ε_u (%)	4.7	5.1	5.4	5.1	4.7	5.0	0.3

Maximum stress uncertainty for 4.4 mm specimen ± 20.1 MPa
Maximum elastic modulus uncertainty ± 27273 MPa
Maximum elongation at rupture uncertainty ± 0.25%

Table C.4: Mechanical Properties of 4.4 mm Cold-Drawn Wire – 400°C

	400-1	400-2	400-3	400-4	400-6	$\bar{x}$	s
f_{pu} (MPa)	1879.3	1887.9	1918.3	1903.2	1884.0	1894.5	16.0
f_{py} (MPa)	1666.0	1668.2	1703.1	1684.5	1662.0	1676.8	17.0
f_{py} / f_{pu}	0.89	0.88	0.89	0.89	0.88	0.89	0.00
E (MPa)	218780	230810	224310	218240	218780	222184	5423
ε_u (%)	4.7	5.1	4.9	4.9	4.9	4.9	0.1

Maximum stress uncertainty for 4.4 mm specimen ± 18.9 MPa
Maximum elastic modulus uncertainty ± 28851 MPa
Maximum elongation at rupture uncertainty ± 0.25%

Table C.5: Mechanical Properties of 4.4 mm Cold-Drawn Wire – 500°C

	500-1	500-2	500-3	500-4	500-6	$\bar{x}$	s
f_{pu} (MPa)	1538.4	1539.7	1570.0	1571.4	1553.0	1554.5	15.9
f_{py} (MPa)	1406.5	1404.4	1428.9	1427.2	1418.8	1417.2	11.4
f_{py} / f_{pu}	0.91	0.91	0.91	0.91	0.91	0.91	0.00
E (MPa)	219940	220090	220300	220700	220160	220238	289
ε_u (%)	5.1	4.7	4.4	5.3	4.9	4.9	0.3

Maximum stress uncertainty for 4.4 mm specimen ± 15.5 MPa
Maximum elastic modulus uncertainty ± 27588 MPa
Maximum elongation at rupture uncertainty ± 0.25%

Table C.6: Mechanical Properties of 4.4 mm Cold-Drawn Wire – 600°C

	600-1	600-2	600-3	600-4	600-6	$\bar{x}$	s
f_{pu} (MPa)	1132.6	1137.6	1154.5	1162.5	1137.9	1145.0	12.8
f_{py} (MPa)	1082.6	1094.3	1102.9	1108.7	1083.4	1094.4	11.6
f_{py} / f_{pu}	0.96	0.96	0.96	0.95	0.95	0.96	0.00
E (MPa)	222860	222610	221080	223570	222840	222592	919
ε_u (%)	6.0	5.6	5.1	5.6	5.6	5.6	0.3

Maximum stress uncertainty for 4.4 mm specimen ± 11.5 MPa
Maximum elastic modulus uncertainty ± 27946 MPa
Maximum elongation at rupture uncertainty ± 0.25%

Table C.7: Mechanical Properties of 4.4 mm Cold-Drawn Wire – 700°C

	700-1	700-2	700-3	700-4	700-6	$\bar{x}$	s
f_{pu} (MPa)	763.4	763.3	773.8	774.9	760.1	767.1	6.8
f_{py} (MPa)	692.8	691.4	704.7	706.1	690.7	697.1	7.6
f_{py} / f_{pu}	0.91	0.91	0.91	0.91	0.91	0.91	0.00
E (MPa)	219600	225700	224710	218730	225640	222876	3424
ε_u (%)	11.1	11.3	10.9	11.3	11.1	11.1	0.2

Maximum stress uncertainty for 4.4 mm specimen ± 7.8 MPa
Maximum elastic modulus uncertainty ± 28213 MPa
Maximum elongation at rupture uncertainty ± 0.25%

Table C.8: Residual Properties of Cold-Drawn Wire – Stressed while Heated (RLX)

	RLX-90-200	RLX-90-300	RLX-90-400	RLX-90-400A	RLX-45-400	RLX-5-400	RLX-90-500	RLX-90-700
T (°C)	200	300	400	400	400	400	500	700
t (min.)	90	90	90	90	45	5	90	90
f_{pu} (MPa)	2010.1	2020.3	1852.5	1830.4	1885.4	1956.8	1402.6	714.7
f_{py} (MPa)	1853.2	1865.1	1606.2	1581.7	1651.3	1738.4	1274.2	633.7
f_{py} / f_{pu}	0.92	0.92	0.87	0.86	0.88	0.89	0.91	0.89
E (MPa)	215200	215140	213570	212250	213340	213720	206400	200990
ε_u (%)	4.8	5.0	4.9	5.1	4.7	5.3	5.1	10.5

Experimental uncertainty ± 1.0%, ± 1.0%, ± 12.5%, and ± 0.25% for f_{pu}, f_{py}, E, and ε_u

Table C.9: Experimental Uncertainty in Elastic Modulus

Specimen	stress range	E (MPa)	± (MPa)	R^2	f_{py}
UH-1	276-1563	212590	26574	0.9997	1839.2
UH-2	275-1561	213030	26629	0.9998	1836.3
UH-3	275-1561	214770	26846	0.9998	1836.3
UH-4	279-1579	215140	26893	0.9999	1857.6
UH-5	277-1568	214650	26831	0.9999	1844.7
200-1	275-1556	220460	27558	1.0000	1830.0
200-2	270-1530	226430	28304	0.9999	1799.5
200-3	271-1536	217680	27210	0.9999	1806.9
200-4	272-1539	216650	27081	1.0000	1810.9
200-6	273-1545	216830	27104	1.0000	1817.5
RLX-90-200	278-1575	215200	26900	1.0000	1853.2
300-1	282-1597	217730	27216	1.0000	1878.4
300-2	277-1572	217600	27200	1.0000	1849.7
300-3	283-1605	217120	27140	1.0000	1888.0
300-4	278-1574	218180	27273	1.0000	1852.3
300-6	277-1572	218040	27255	1.0000	1849.4
RLX-90-300	280-1585	215140	26893	1.0000	1865.1
400-1	250-1416	218780	27348	1.0000	1666.0
400-2	250-1418	230810	28851	0.9999	1668.2
400-3	255-1448	224310	28039	0.9999	1703.1
400-4	253-1432	218240	27280	1.0000	1684.5
400-6	249-1413	218780	27348	1.0000	1662.0
RLX-90-400	241-1365	213570	26696	1.0000	1606.2
RLX-90-400A	237-1344	212250	26531	1.0000	1581.7
RLX-45-400	248-1404	213340	26668	0.9999	1651.3
RLX-5-400	261-1478	213720	26715	1.0000	1738.4
500-1	211-1196	219940	27493	1.0000	1406.5
500-2	211-1194	220090	27511	1.0000	1404.4
500-3	214-1215	220300	27538	1.0000	1428.9
500-4	214-1213	220700	27588	1.0000	1427.2
500-6	213-1206	220160	27520	1.0000	1418.8
RLX-90-500	191-1083	206400	25800	0.9999	1274.2
600-1	162-920	222860	27858	1.0000	1082.6
600-2	164-930	222610	27826	1.0000	1094.3
600-3	165-937	221080	27635	1.0000	1102.9
600-4	166-942	223570	27946	1.0000	1108.7
600-6	163-921	222840	27855	1.0000	1083.4
700-1	104-589	219600	27450	0.9999	692.8
700-2	104-588	225700	28213	0.9999	691.4
700-3	106-599	224710	28089	0.9999	704.7
700-4	106-600	218730	27341	0.9999	706.1
700-6	104-587	225640	28205	0.9999	690.7
RLX-90-700	107-607	200990	25124	1.0000	633.7

Table C.10: ANOVA Residual Ultimate Tensile Strength (f_{pu})

Comparison	F	F_{crit} ($\alpha = 0.01$)	F_{crit} ($\alpha = 0.05$)
200°C to 20°C	7.072	11.259	5.318
300°C to 20°C	2.772	11.259	5.318
400°C to 20°C	211.126	11.259	5.318
500°C to 20°C	2966.247	11.259	5.318
600°C to 20°C	13818.225	11.259	5.318
700°C to 20°C	49464.657	11.259	5.318
400°C to 300°C	134.217	11.259	5.318

Table C.11: ANOVA Residual Elastic Modulus (E)

Comparison	F	F_{crit} ($\alpha = 0.01$)	F_{crit} ($\alpha = 0.05$)
200°C to 20°C	8.549	11.259	5.318
300°C to 20°C	46.161	11.259	5.318
400°C to 20°C	10.804	11.259	5.318
500°C to 20°C	138.075	11.259	5.318
600°C to 20°C	169.972	11.259	5.318
700°C to 20°C	29.977	11.259	5.318

Table C.12: ANOVA Residual 0.2% Offset Yield (f_{py})

Comparison	F	F_{crit} ($\alpha = 0.01$)	F_{crit} ($\alpha = 0.05$)
200°C to 20°C	10.900	11.259	5.318
300°C to 20°C	5.192	11.259	5.318
400°C to 20°C	372.466	11.259	5.318
500°C to 20°C	4324.878	11.259	5.318
600°C to 20°C	13071.171	11.259	5.318
700°C to 20°C	47660.954	11.259	5.318
400°C to 300°C	279.428	11.259	5.318

Table C.13: ANOVA Residual Elongation at Rupture (ε_u)

Comparison	F	F_{crit} ($\alpha = 0.01$)	F_{crit} ($\alpha = 0.05$)
200°C to 20°C	0.412	11.259	5.318
300°C to 20°C	0.294	11.259	5.318
400°C to 20°C	0.000	11.259	5.318
500°C to 20°C	0.010	11.259	5.318
600°C to 20°C	12.703	11.259	5.318
700°C to 20°C	1802.667	11.259	5.318
600°C to 500°C	12.938	11.259	5.318

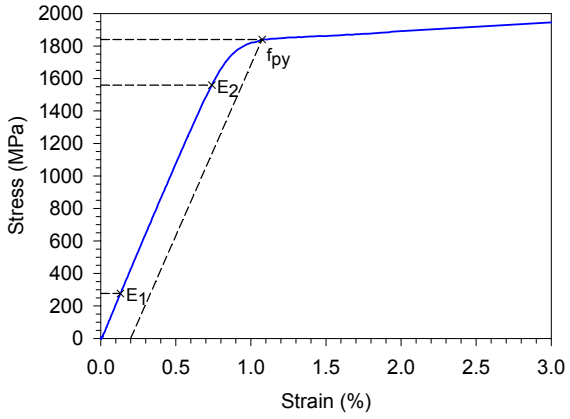

Figure C.1: Specimen UH-1
Experimental Stress-Strain Curve

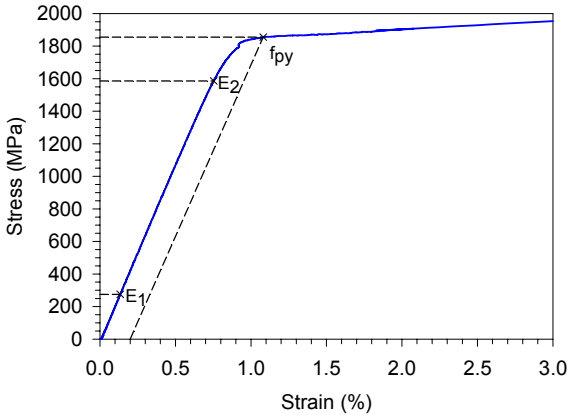

Figure C.4: Specimen UH-4
Experimental Stress-Strain Curve

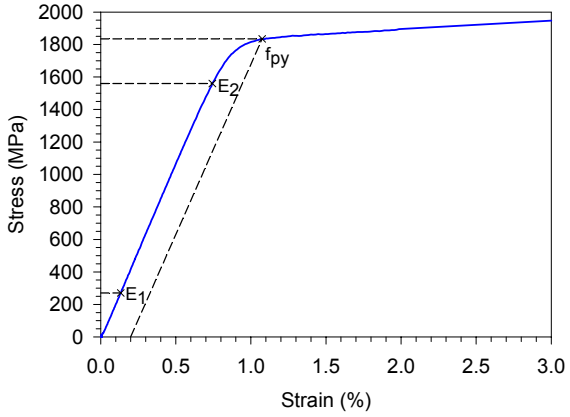

Figure C.2: Specimen UH-2
Experimental Stress-Strain Curve

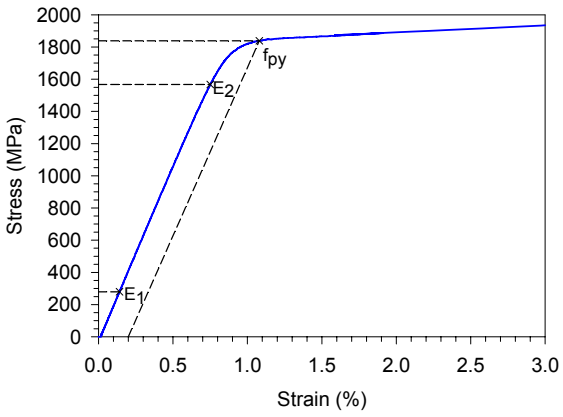

Figure C.5: Specimen UH-5
Experimental Stress-Strain Curve

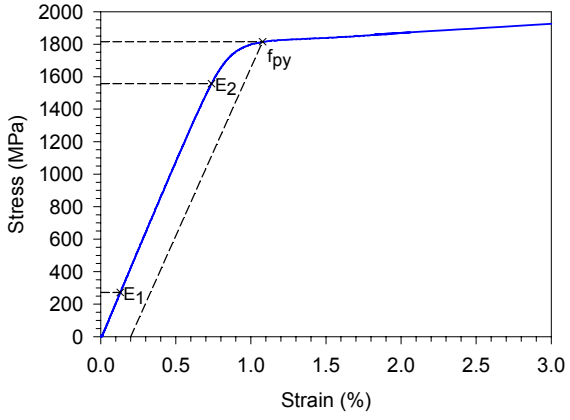

Figure C.3: Specimen UH-3
Experimental Stress-Strain Curve

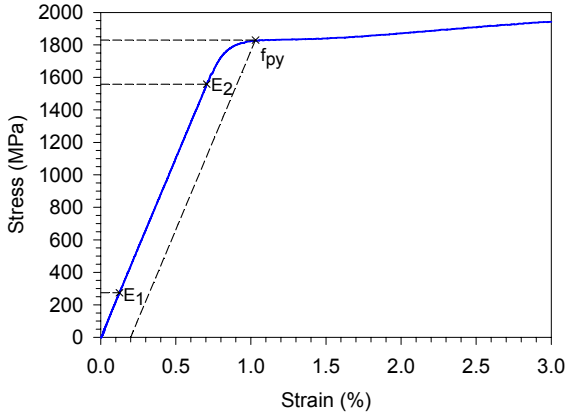

Figure C.6: Specimen 200-1
Heated at 200°C for 90 min.

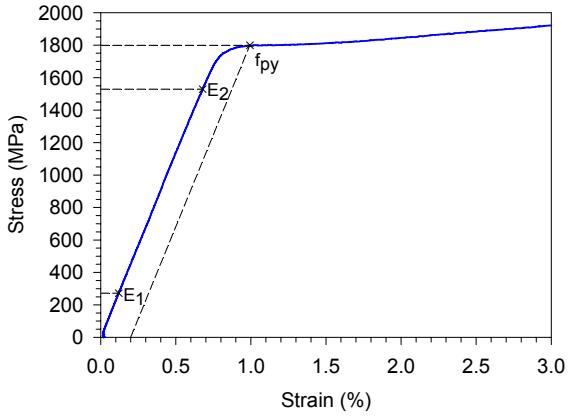

Figure C.7: Specimen 200-2
Heated at 200°C for 90 min.

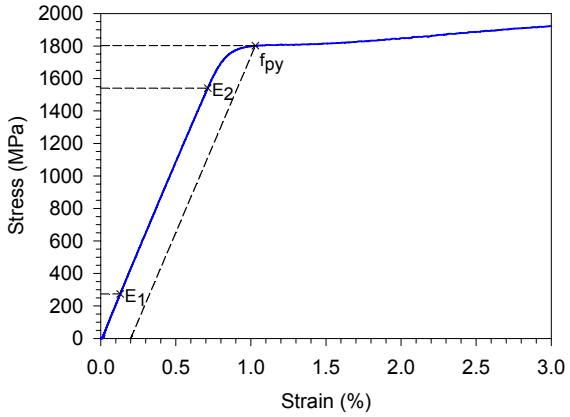

Figure C.8: Specimen 200-3
Heated at 200°C for 90 min.

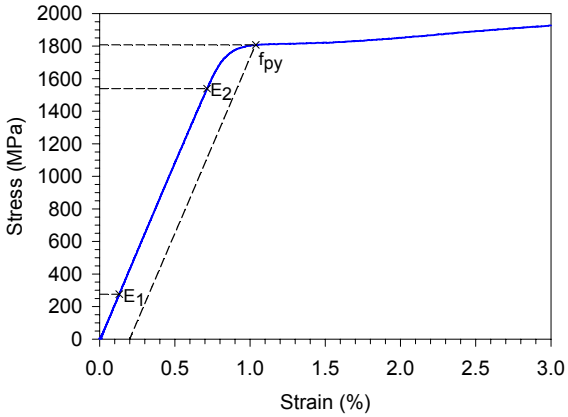

Figure C.9: Specimen 200-4
Heated at 200°C for 90 min.

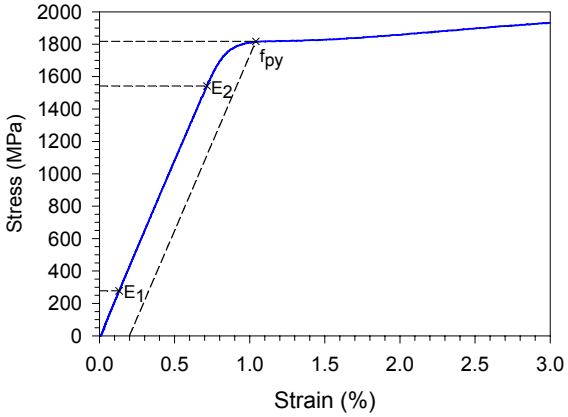

Figure C.10: Specimen 200-6
Heated at 200°C for 90 min.

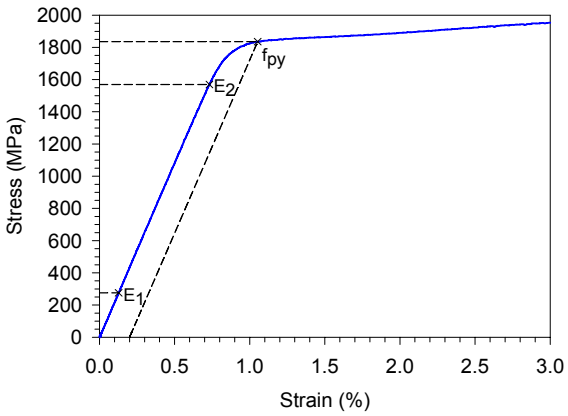

Figure C.11: Stressed Specimen
RLX-90-200

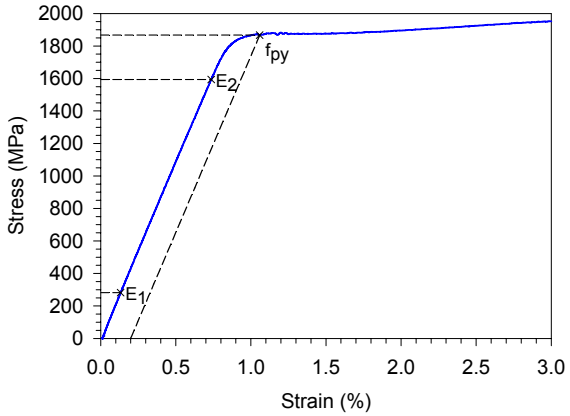

Figure C.12: Specimen 300-1
Heated at 300°C for 90 min.

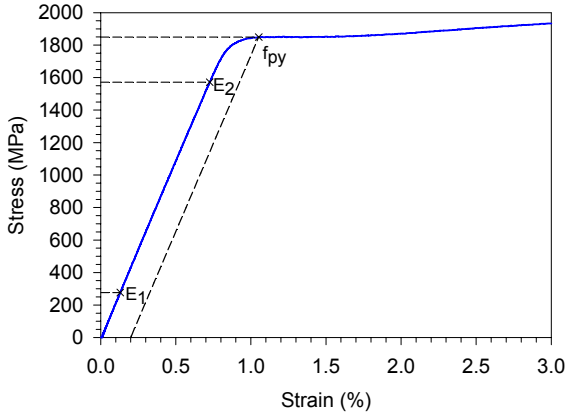

Figure C.13: Specimen 300-2
Heated at 300°C for 90 min.

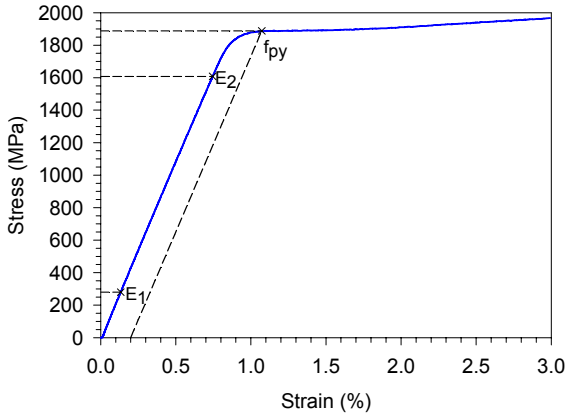

Figure C.14: Specimen 300-3
Heated at 300°C for 90 min.

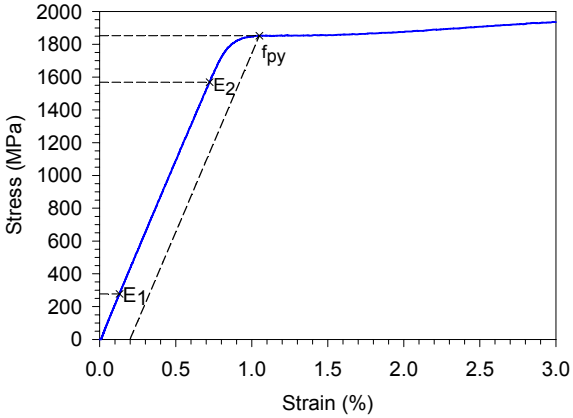

Figure C.15: Specimen 300-4
Heated at 300°C for 90 min.

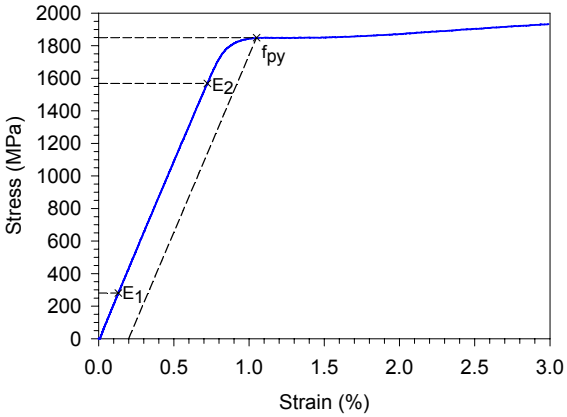

Figure C.16: Specimen 300-6
Heated at 300°C for 90 min.

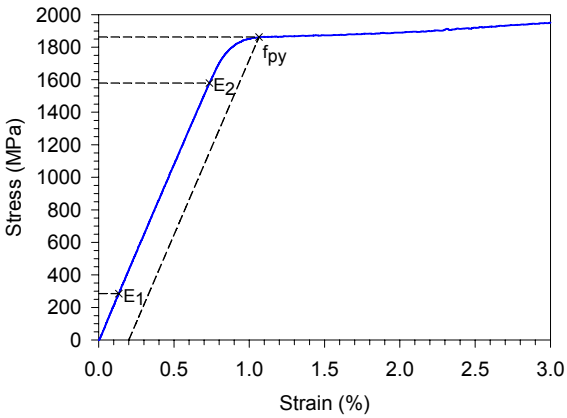

Figure C.17: Stressed Specimen
RLX-90-300

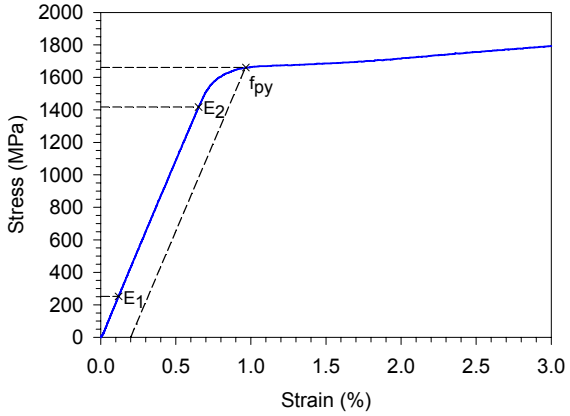

Figure C.18: Specimen 400-1
Heated at 400°C for 90 min.

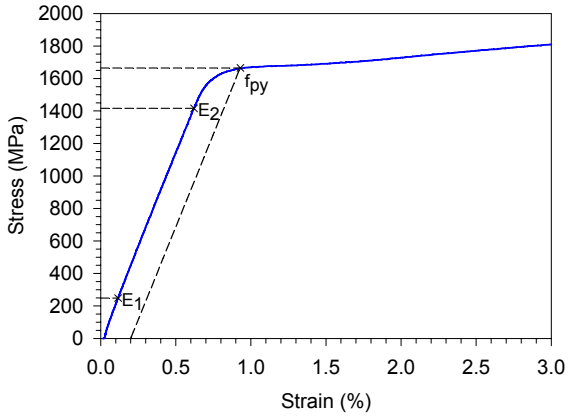

Figure C.19: Specimen 400-2
Heated at 400°C for 90 min.

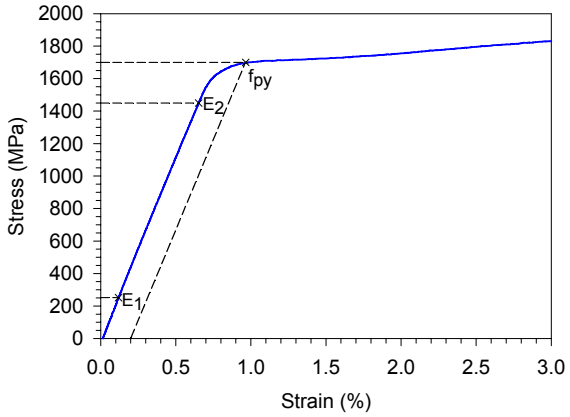

Figure C.20: Specimen 400-3
Heated at 400°C for 90 min.

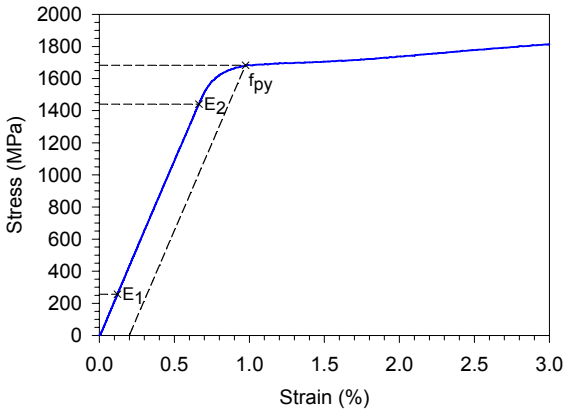

Figure C.21: Specimen 400-4
Heated at 400°C for 90 min.

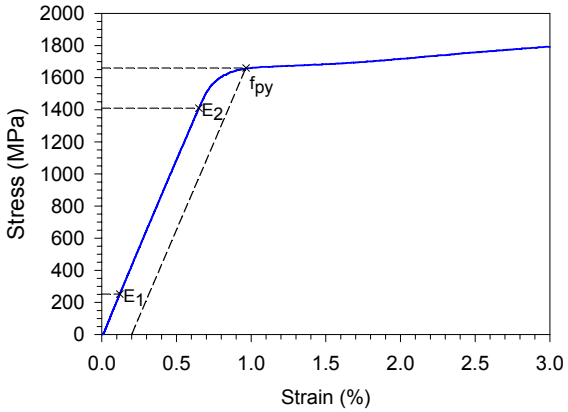

Figure C.22: Specimen 400-6
Heated at 400°C for 90 min.

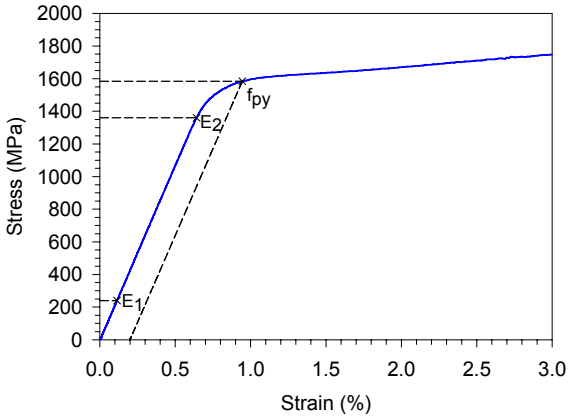

Figure C.23: Stressed Specimen
RLX-90-400

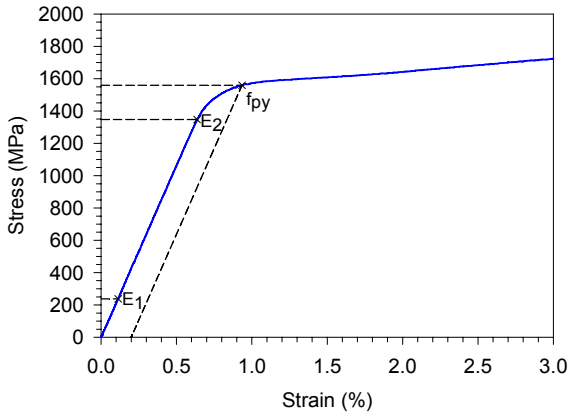

Figure C.24: Stressed Specimen
RLX-90-400A

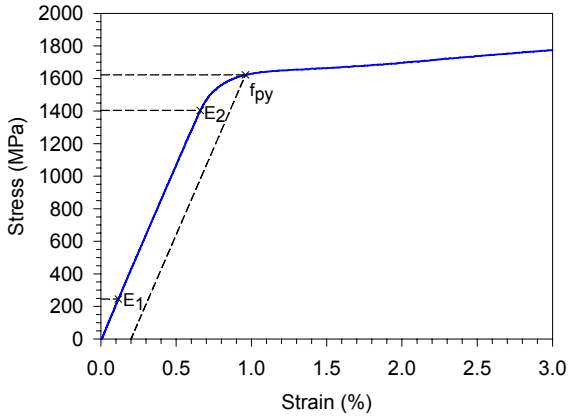

Figure C.25: Stressed Specimen
RLX-45-400

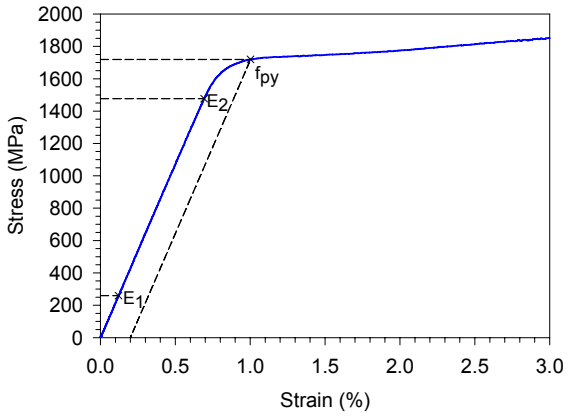

Figure C.26: Stressed Specimen
RLX-5-400

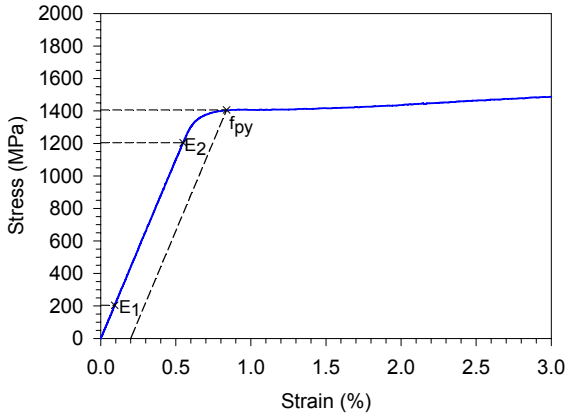

Figure C.27: Specimen 500-1
Heated at 500°C for 90 min.

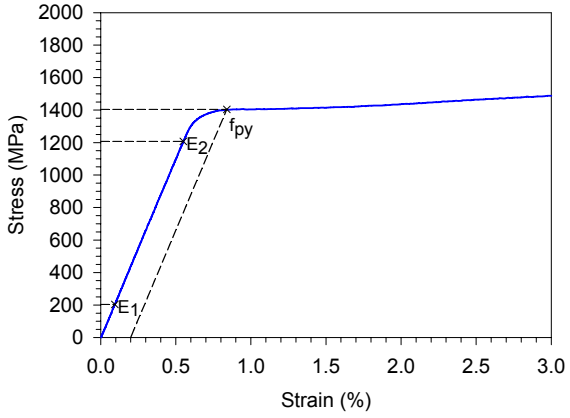

Figure C.28: Specimen 500-2
Heated at 500°C for 90 min.

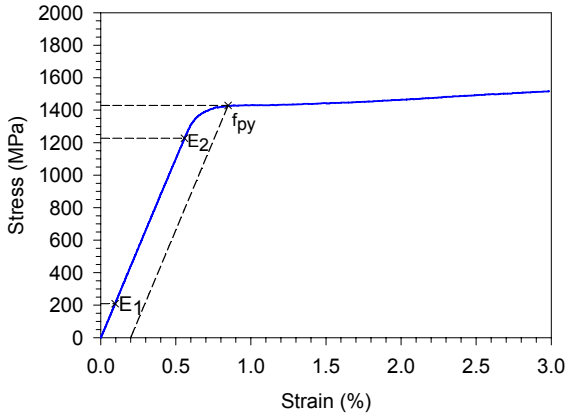

Figure C.29: Specimen 500-3
Heated at 500°C for 90 min.

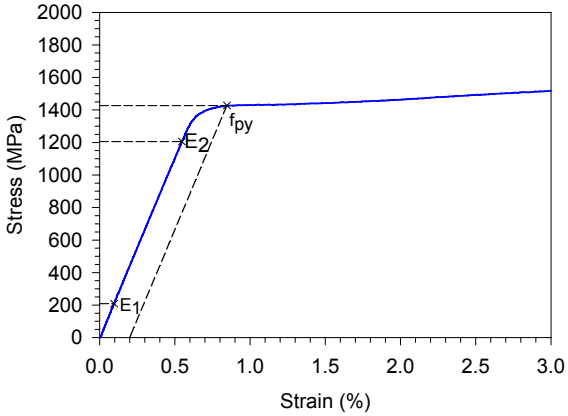

Figure C.30: Specimen 500-4
Heated at 500°C for 90 min.

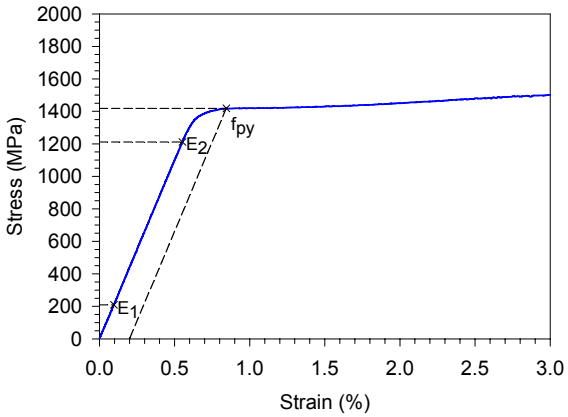

Figure C.31: Specimen 500-6
Heated at 500°C for 90 min.

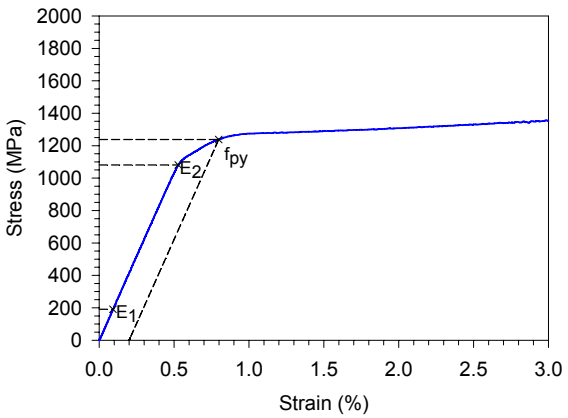

Figure C.32: Stressed Specimen
RLX-90-500

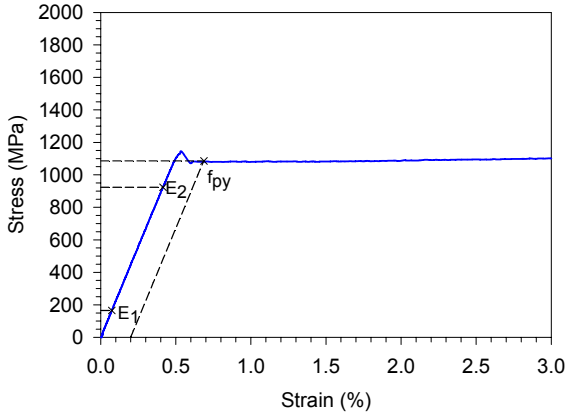

Figure C.33: Specimen 600-1
Heated at 600°C for 90 min.

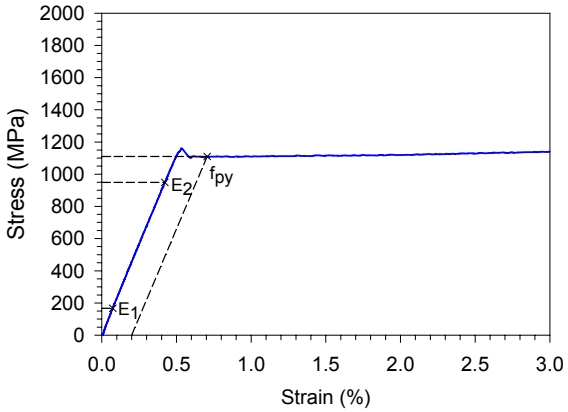

Figure C.36: Specimen 600-4
Heated at 600°C for 90 min.

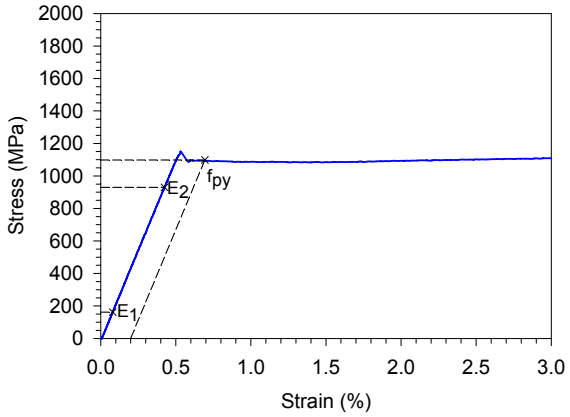

Figure C.34: Specimen 600-2
Heated at 600°C for 90 min.

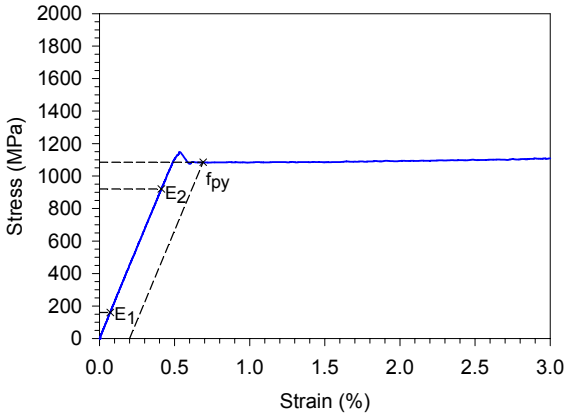

Figure C.37: Specimen 600-6
Heated at 600°C for 90 min.

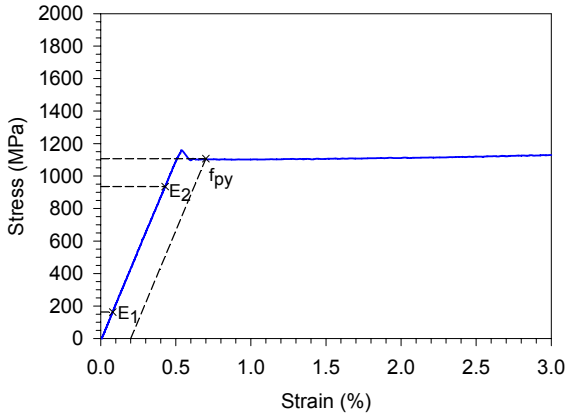

Figure C.35: Specimen 600-3
Heated at 600°C for 90 min.

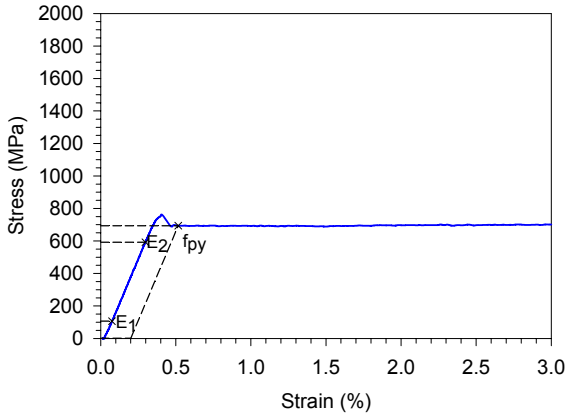

Figure C.38: Specimen 700-1
Heated at 700°C for 90 min.

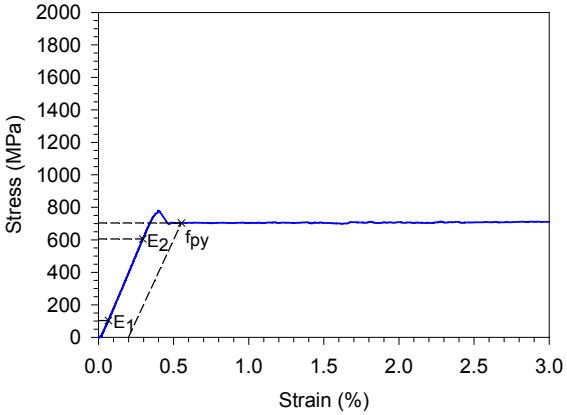

Figure C.41: Specimen 700-4
Heated at 700°C for 90 min.

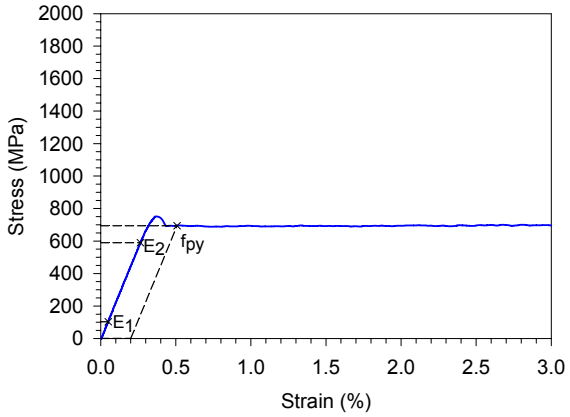

Figure C.39: Specimen 700-2
Heated at 700°C for 90 min.

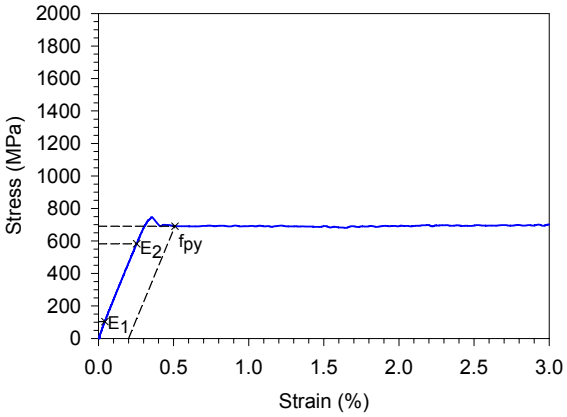

Figure C.42: Specimen 700-6
Heated at 700°C for 90 min.

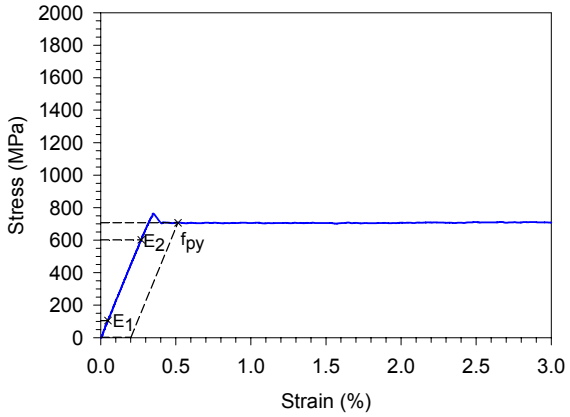

Figure C.40: Specimen 700-3
Heated at 700°C for 90 min.

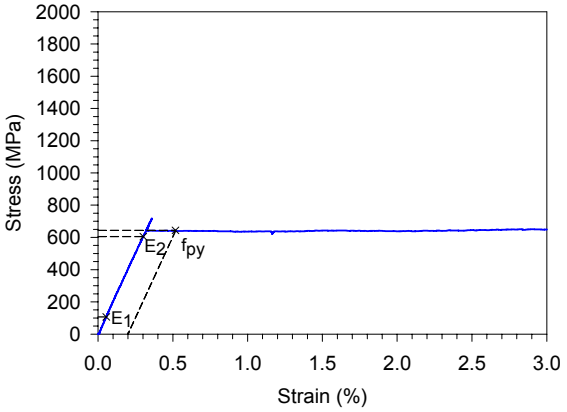

Figure C.43: Stressed Specimen
RLX-90-700